Kinetic Modeling and Simulation of an Industrial Diesel Hydroprocessing Plant

by

Ayşe Dilan Çelebi

A Thesis Submitted to the
Graduate School of Sicences and Engineering
in Partial Fulfillment of the Requirements for
the Degree of

Master of Science
in
Chemical and Biological Engineering

Koc University

August 2014

Koc University

Graduate School of Sciences and Engineering

This is to certify that I have examined this copy of a master's thesis by

Ayşe Dilan Çelebi

and have found that it is complete and satisfactory in all respects,
and that any and all revisions required by the final
examining committee have been made.

Committee Members:

_____

Yaman Arkun, Ph. D. (Advisor)

_____

Alper Uzun, Ph. D.

_____

Murat Sözer, Ph. D.

Date: _____

ABSTRACT

In refineries, hydroprocessing is a vital technology for upgrading the quality of petroleum. For example hydrotreating is used to remove impurities like sulfur, nitrogen and metals from feedstocks and hydrocracking is used to crack the larger molecules into valuable products.

Sulfur removal is a very important issue since governments mandate lower sulfur content fuels because of air pollution by SO_x which is produced during combustion of petroleum products.

This study focuses on kinetic modeling of an industrial diesel hydroprocessing (DHP) process which consists of three catalytic reactor beds that carry out hydrodesulfurization and hydrocracking. Steady-state non-isothermal, pseudo-homogeneous plug flow models for the catalytic hydrodesulfurization and hydrocracking reactors are separately developed. Continuous lumping approach is used to characterize the complex reaction mixture. Three adjustable hydrodesulfurization parameters and one adjustable hydrocracking parameter are fine-tuned using available industrial data. The main purpose of developing the reactor models is to be able to do simulations under different scenarios and to predict the best operating conditions for the DHP process.

Simulations show that the developed model is able to accurately predict temperature profiles in each bed, sulfur content of the product and the product distribution in the hydrocracker.

ÖZET

Hidro-işleme, rafinerilerde petrolün kalitesini iyileştimek için kullanılan çok önemli bir teknolojidir. Örneğin, hidrojenle muamele teknolojisi besleme akımındaki kükürt, azot ve metaller gibi safsızlıkları gidermek için kullanılırken, hidrokraking büyük molekülleri kırınıma uğratıp daha değerli ürünlerin oluşturulması için kullanılır.

Petrol ürünlerinin yanması sonucu oluşan SO_x hava kirliliğine sebep olduğundan düşük kükürt içerikli yakıtların kullanımı şart koşulmaktadır, bu yüzden kükürt giderimi çok önem taşıyan bir konudur.

Bu çalışma içinde hidrojenle kükürt giderme ve hidrokraking işlemlerinin gerçekleştiği üç katalitik reaktör yatağından oluşan endüstriyel dizel hidro işleme prosesinin kinetik olarak modellenmesi üzerine odaklanmıştır. Katalitik hidrojenle kükürt giderme ve hidrokraking reaktörleri için yatışkın durumda izotermal olmayan, sözde homojen tapa akış modelleri ayrı ayrı geliştirilmiştir. Kompleks reaksiyon karışımını karakterize etmek için sürekli yığılma yaklaşımı kullanılmıştır. Üç ayarlanabilir hidrojenle kükürt giderme modeli parametreleri ve bir ayarlanabilir hidrokraking modeli parametresi mevcut endüstriyel veriler kullanılarak ince ayarlanmıştır. Reaktör modellerinin geliştirlmesinin başlıca amacı farklı senaryolar altında simülasyonlar yapabilmek ve dizel hidro-işleme prosesi için en iyi işletme koşullarını tahmine edebilmektir.

Yapılan simülasyonlar, geliştirilmiş olan modelin her bir yataktaki sıcaklık profillerini, ürünün içindeki kükürt içeriğini ve hidrokrakerdeki ürün dağılımını doğru olarak öngördüğünü göstermiştir.

ACKNOWLEDGEMENTS

I remember the first day that I decided to pursue a master's degree in the area of process systems engineering. Professor Yaman Arkun, with his expertise in this area, shared my interests and a new era has started in my life. I would like to express my sincere gratitude to my advisor Prof. Yaman Arkun for every second that he invested in supporting and guiding me in every step of my thesis work and I wish to thank him for his valuable comments and suggestions, being patient and helpful.

I would like to extend my gratitudes to Asst. Prof. Dr. Alper Uzun for being my dissertation committee member and I want to thank him for being a source of encouragement and inspiration to improve my academic skills. He always answered my questions and gave me valuable suggestions that shapes my future academic life. I would like to thank to Assoc. Prof. Dr. Murat Sözer for being such generous and kind since he accepted to be involved in my thesis committee member in his limited time. I am grateful to my thesis committee members for their time and valuable suggestions.

I acknowledge financial assistance from TUPRAS for my thesis.

I sincerely thank to my collagues Hasan Şıldır and Erdal Aydın for their supports and friendship. Hasan deserves my deepest gratitudes for his contributions and invaluable suggestions throughout planning and execution of my thesis work. I was lucky to be in the same group with such great individuals.

My warmest thanks go to my friends. My homemates Yaprak Özbakır and Selma Bulut deserves my limitless love for their endless supports and unconditional friendships. I feel peaceful, happy and completed when I am with them. I would like to sincerely thank to Volkan Balci, Sinan Yücetürk and Fatih Rahim for being such close friends to me and making this a fun journey. I am really grateful to Yeliz Gürdal for her intimate friendship

and support. She is always in my heart even she is miles away. I always think that I have a second family in Koc University.

I would like to express my special thanks to Aybüke Deringöz for being such a great friend for over nine years. I have first learned the meaning of being close friends from her and she is always near me to witness my life with her unconditional love, trust and moral support.

Above all, I wholeheartedly thank to my precious family Hatice-Cemalettin-Serdar Çelebi for their limitless support and enormous love throughout my entire life. I could not achieve all these without help of my family. They always believe in me and trust me all the way. My dear aunt Nilüfer Veli deserves my special thanks for always supporting and encouraging me. My great thanks go to Yasemin Veli Kara for being such a wonderful sister and being my role model. She always couraged my decisions with her endless love and I feel safe and happy with the existence of her in my life. I owe her too much. I want to thank to Adil Kara for his supports and keeping his eyes on me like a big brother. My little nephew Mete Kara occupies an important place in my life by giving me hope, peace and power to achieve things with his pure love.

I want to dedicate this thesis to my beloved mother Hatice Çelebi who is the most beautiful person in my life and she is the reason behind everything I do. I am very proud and happy to be daughter of her.

TABLE OF CONTENTS

List of Tables **x**

List of Figures **xii**

Nomenclature **xvi**

Chapter 1: Introduction **1**

Chapter 2: Literature Review **4**

2.1 Overview. 4
2.2 Chemistry of HDS Reactions. 8
2.2.1 Hydrodesulfurization Mechanism. 11
2.3 Chemistry of Hydrocracking Reactions. 15
2.4 Process Modeling 16
2.5 Kinetic Modeling Approaches 17
2.5.1 Discrete Lumping Approach 18
2.5.2 Continuous Lumping Approach. 19
2.5.3 Structure-Oriented Lumping (SOL) Approach. 20
2.6 Reviews on Hydrotreating Modeling. 22
2.7 Reviews on Hydrocracking Modeling. 28

Chapter 3: DHP Plant and Characterization of Petroleum Fractions 33

3.1 DHP Process Configuration. 33
3.2 Characterization of Petroleum Fractions. 35
3.3 Pseudocomponent Generation and Properties Estimation. 38

Chapter 4: Modeling of Hydrodesulfurization Reactor 44

4.1 Introduction. 44
4.2 Generation of Feed Sulfur Curve. 44
4.3 Hydrodesulfurization Reactor Model (Beds 1 and 2). 62
4.3.1 Mass Balance 63
4.3.2 Energy Balance 67
4.4 Parameter Estimation. 69
4.4.1 Objective Function and Algorithm. 70
4.4.2 Sensitivity Analysis. 71

Chapter 5: Modeling of Hydrocracking Reactor 83

5.1 Introduction. 83
5.2 Hydrocracker Reactor Model. 85
5.2.1 Generation of Feed and Product Mass Fraction Curve 86
5.2.2 Mass Balance 97
5.2.3 Energy Balance 99
5.3 Parameter Estimation. 101
5.3.1 Objective Function and Algorithm. 101

5.3.2 Sensitivity Analysis. 102

Chapter 6: Results and Discussion **111**

6.1 Interface for Simulation and Parameter Update Purposes. 111
6.2 Simulations of Days 120
6.3 Monitoring of Model Parameters 128

Chapter 7: Conclusion **149**

Bibliography **151**

LIST OF TABLES

Table 2.1: Range of Operating Conditions for Different Feedstocks 5
Table 3.1: Plant Assay Example on 07.01.2014 36
Table 3.2: Constants for Daubert's Distillation Curves Interconversion Method 40
Table 3.3: Physical Properties of the Pseudocomponents of Feed (07.01.2014) 42
Table 4.1: Plant Sulfur Distribution Data for Selected Days 50
Table 4.2: Adjustable Parameters for HDS Model 70
Table 4.3: Effects of 10% Perturbation in Parameters of 07.01.2014 79
Table 4.4: Effects of -10% Perturbation in Parameters of 07.01.2014 79
Table 4.5: Sensitivity Matrix S_{ij} for 07.01.2014 80
Table 4.6: Fisher Information Matrix for 07.01.2014 80
Table 4.7: Nominal Values of the Fixed Parameters 81
Table 4.8: Literature Ranges for Parameters of HDS Model 82
Table 5.1: Plant Data of Naphta Product 87
Table 5.2: Plant Data of Diesel Product 88
Table 5.3: TBP versus Liquid Volume Data for Selected Days 90
Table 5.4: Adjustable Parameters for HDS Model 101
Table 5.5: Effects of 10% Perturbation in Parameters of 07.01.2014 106
Table 5.6: Effects of -10% Perturbation in Parameters of 07.01.2014 107
Table 5.7: Sensitivity Matrix S_{ij} for 07.01.2014 107
Table 5.8: Fisher Information Matrix for 07.01.2014 108
Table 5.9: Nominal Values of the Fixed Parameters 108
Table 5.10: Literature Ranges for Parameters of HDS Model 109
Table 6.1: Percent Error of Prediction (07.01.2014 00:00-08:00) 130

Table 6.2: Model Parameters for Shift 1on 07.01.2014 130
Table 6.3: Percent Error of Prediction (07.01.2014 08:00-16:00) 132
Table 6.4: Model Parameters for Shift 2 on 07.01.2014 132
Table 6.5: Percent Error of Prediction (07.01.2014 08:00-16:00) After Updating the Parameters. 132
Table 6.6: Percent Error of Prediction (07.01.2014 16:00-24:00) 134
Table 6.7: Model Parameters for Shift 3 on 07.01.2014 134
Table 6.8: Percent Error of Prediction (09.01.2014 00:00-08:00) 136
Table 6.9: Model Parameters for Shift 1 on 09.01.2014 138
Table 6.10: Percent Error of Prediction (09.01.2014 00:00-08:00) After Updating Parameters. 138
Table 6.11: Model Parameters for Selected Days 140
Table 6.12: Percent Errors of Prediction 145
Table 6.13: Correlated Parameters with Sulfur Mass Flow Rate. 146

LIST OF FIGURES

Figure 2.1: Illustration of the trickle-flow regime in a trickle-bed reactor 6
Figure 2.2: Examples of some hydrotreating reactions 7
Figure 2.3: Sulfur-containing molecules in petroleum 9
Figure 2.4: Impact of sulfur species 10
Figure 2.5: Desulfurization reactions of typical sulfur compounds 11
Figure 2.6: HDS reaction network of thiophenes 12
Figure 2.7: HDS reaction network of benzothiophenes 13
Figure 2.8: Pathways for the HDS of DBT in the presence of $CoMo/Al_2O_3$ 14
Figure 2.9: An example of Continuous Lumping 19
Figure 2.10: An example to Structure-Oriented Lumping 21
Figure 3.1: Simplified DHP plant flowsheet 34
Figure 3.2: TBP Distillation Curve on 07.01.2014 38
Figure 4.1: Impact of sulfur species 46
Figure 4.2: Hydrodesulfurization rate constant versus TBP. 48
Figure 4.3: Examples of beta probability distribution functions 51
Figure 4.4: Examples of beta cumulative distribution functions 52
Figure 4.5: Normalized beta sulfur distribution of feed on 07.01.2014 53
Figure 4.6: Normalized beta sulfur distribution of feed on 09.01.2014 54
Figure 4.7: Normalized beta sulfur distribution of feed on 14.01.2014 54
Figure 4.8: Normalized beta sulfur distribution of feed on 16.01.2014 55
Figure 4.9: Normalized beta sulfur distribution of feed on 23.01.2014 55
Figure 4.10: Normalized beta sulfur distribution of feed on 30.01.2014 56
Figure 4.11: Standard uniform distribution 57

Figure 4.12: Cumulative standard uniform distribution 58
Figure 4.13: Uniform sulfur distribution of feed on 07.01.2014 59
Figure 4.14: Uniform sulfur distribution of feed on 09.01.2014 59
Figure 4.15: Uniform sulfur distribution of feed on 14.01.2014 60
Figure 4.16: Uniform sulfur distribution of feed on 16.01.2014 60
Figure 4.17: Uniform sulfur distribution of feed on 23.01.2014 61
Figure 4.18: Uniform sulfur distribution of feed on 30.01.2014 61
Figure 4.19: Effect of k_{min1} on model outputs for a perturbation of ±10 % 75
Figure 4.20: Effect of k_{max} on model outputs for a perturbation of ±10 % 75
Figure 4.21: Effect of β on model outputs for a perturbation of ±10 % 76
Figure 4.22: Effect of k_{min2} on model outputs for a perturbation of ±10% 76
Figure 4.23: Effect of E_{a1} on model outputs for a perturbation of ±10 % 77
Figure 4.24: Effect of E_{a2} on model outputs for a perturbation of ±10 % 77
Figure 4.25: Effect of ΔH_1 on model outputs for a perturbation of ±10 % 78
Figure 4.26: Effect of ΔH_2 on model outputs for a perturbation of ±10 % 78
Figure 5.1: Product TBP curve for 07.01.2014 in ASPEN HYSYS 89
Figure 5.2: Cumulative mass fraction curves for product, naphta and diesel 91
Figure 5.3: Cumulative feed mass fractions of pseudocomponents versus normalized TBP for four days. 93
Figure 5.4: Cumulative product mass fractions of pseudocomponents versus normalized TBP for four days. 94
Figure 5.5: Feed mass fraction distributions of pseudocomponents versus normalized TBP for four days. 95
Figure 5.6: Product mass fraction distributions of pseudocomponents versus normalized TBP for four days. 96

Figure 5.7: Superimposed plots of feed and product cumulative mass fraction curves for 07.01.2014 97
Figure 5.8: Effect of k_{max} on model outputs for a perturbation of ±10 % 103
Figure 5.9: Effect of α on model outputs for a perturbation of ±10 % 103
Figure 5.10: Effect of a_0 on model outputs for a perturbation of ±10 % 104
Figure 5.11: Effect of a_1 on model outputs for a perturbation of ±10 % 104
Figure 5.12: Effect of E_a on model outputs for a perturbation of ±10 % 105
Figure 5.13: Effect of c on model outputs for a perturbation of ±10 % 105
Figure 5.14: Effect of m on model outputs for a perturbation of ±10 % 106
Figure 6.1: Plant data for temperature difference in bed 1 112
Figure 6.2: Plant data for temperature difference in bed 2 113
Figure 6.3: Plant data for temperature difference in bed 3 114
Figure 6.4: Plant data for sulfur mass flow rate measurements of feed 115
Figure 6.5: Plant data for sulfur ppmwt in product 116
Figure 6.6: Plant data naphta wt% in product 117
Figure 6.7: Interface window for inputs of simulation 119
Figure 6.8: Interface window for input parameters of simulation 120
Figure 6.9: Simulation results of HDS reactor 121
Figure 6.10: Remaining sulfur at the HDS reactor exit 122
Figure 6.11: Remaining sulfur at the HDS reactor exit 123
Figure 6.12: HDS reactor temperature profile 124
Figure 6.13: Results of HC simulations 125
Figure 6.14: Temperature profile for HC reactor 126
Figure 6.15: Overall performance of the HDS and HC models for 30.01.2014 127
Figure 6.16: Overall performance of the HDS and HC models for shift 1 on 07.01.2014 129

Figure 6.17: Overall performance of the HDS and HC models for shift 2 on 07.01.2014 131
Figure 6.18: Overall performance of the HDS and HC models for shift 2 on 07.01.2014 after udpating parameters. 133
Figure 6.19: Overall performance of the HDS and HC models for shift 3 on 07.01.2014 135
Figure 6.20: Overall performance of the HDS and HC models for shift 1 on 09.01.2014 137
Figure 6.21: Overall performance of the HDS and HC models for shift 1 on 09.01.2014 after updating the parameters. 139
Figure 6.22: Change of $k_{min1,HDS}$ for a period of time 141
Figure 6.23: Change of $k_{min1,HDS}$ for a period of time 142
Figure 6.24: Change of $\Delta H_{2,HDS}$ for a period of time 143
Figure 6.25: Change of $k_{max,HC}$ for a period of time 144
Figure 6.26: Relationship between mass flow rate of sulfur in feed and $k_{min1,HDS}$ 147
Figure 6.27: Relationship between mass flow rate of sulfur in feed and $\Delta H_{2,HDS}$ 148

NOMENCLATURE

$T_{b,i}$	Nomal boiling point of the pseudocomponent i
SG_i	Specific gravity 60 °F/60 °F of the pseudocomponent i
K_W	Watson characterization factor
SG_{avg}	Average (bulk) specific gravity 60 °F/60 °F of the petroleum fraction
T_{avg}	Average boiling temperature of the petroleum fraction
w_i	Mass fraction of the pseudocomponent i
v_i	Volume fraction of the pseudocomponent i
θ	Normalized boiling point
TBP	True boiling point
min(TBP)	Lowest TBP (Initial Boiling Point) in the fraction
max(TBP)	Highest TBP (Final Boiling Point) in the fraction
$P(x)$	Probability density function
$B(p,q)$	Beta distribution function
p, q	Shape parameters of the beta distribution function
$I_x(p,q)$	Cumulative distribution function of beta distribution
k	Reactivity (rate constant)
$c_s(k,z)$	Normalized sulfur weight percent of fraction with reactivity k at axial position z
v	mass average velocity
k'	Ratio of reactivity k to mass velocity, *v*
E_a	Activation energy

k_0	Reactivity at some reference temperature T_0
R	Gas constant
m_{oil}	Mass flow-rate of the feed
$C_{p,oil}$	Heat capacity of the feed
m_s	Mass flow-rate of sulfur in the feed
ΔH_r^0	Heat of reaction
m_{H_2}	Mass flow-rate of the hydrogen consumed
MW_{H_2}	molecular weight of hydrogen
MW_S	molecular weight of sulfur
γ^{H_2}	Stoichiometric coefficient of H_2 in hydrodesulfurization reactions
$k_{min1,HDS}$	Minimum reactivity of sulfur species in Bed 1
$k_{max,HDS}$	Maximum reactivity of sulfur species
β	parameter in HDS reactivity equation
$k_{min2,HDS}$	Minimum reactivity of sulfur species in Bed 2
Ea_1	Activation energy of the reactions in Bed 1
Ea_2	Activation energy of the reactions in Bed 2
ΔH_1	Heat of Reaction in HDS Bed 1
ΔH_2	Heat of Reaction in HDS Bed 2
ΔT	Difference between inlet and outlet temperatures of each bed
w_s	Total (bulk) sulfur weight fraction at the reactor exit
S_n^{ij}	Normalized sensitivity matrix
F_n	Normalized Fisher matrix
$D(k)$	Species-type distribution function
$k_{max,HC}$	Reactivity of the species with highest boiling point

$TBP_{cut\text{-}point}$	Cut-point temperature
FBP_L	Final boiling point of the light fraction
IBP_H	Initial boiling point of adjacent the heavy fraction
$c(k, z)$	Weight fraction of species with reactivity k at axial position z
$p(k,K)$	Yield function
m, c	Parameters in the equation of heat of reaction of hydrocracking
a	Parameter in reactivity equation of HC
a_0, a_1	Parameters in yield function
C_i	Weight fraction of i^{th} pseudocomponent at the reactor exit.
x_{naphta}	Weight fraction of naphta in the product

Chapter 1

INTRODUCTION

Crude oil which is a complex mixture of organic liquids, sulfur, nitrogen, oxygen and some metallic compounds is the largest source of energy. In a refinery, crude oil is converted to higher value products after different physical and chemical processes such as distillation, extraction, reforming, blending and cracking. Liquid petroleum gas, gasoline, jet fuel, diesel fuel, wax, lubricants, bitumen and petrochemicals are the major products of a refinery [1].

Consumption of transportation fuels increases day by day and the pollution from exhaust gas continues to grow at alarming rates. The major pollutants include SOx, CO, NOx, particulates, olefins and aromatic hydrocarbons. The most important and the most costly issues are the environmental restrictions regarding the quality of the fuels and emissions from refinery [2].

The rising demand for transportation fuels and the stringent environmental restrictions have resulted in increased attention to refinery processes such as hydroprocessing [3]. Hydroprocessing is a broad term that includes processes such as hydrotreating and hydrocracking [4]. Hydrotreating (HDT) includes a variety of hydrogenation processes that operate at high temperatures and pressures to produce higher-value hydrocarbon products with lower level of pollutants [5]. Catalytic hydrotreaters are used to remove the contaminants such as sulfur, nitrogen, oxygen and metallic compounds like nickel,

vanadium, iron and copper to improve the quality of the products and to eliminate the adverse effects on the refining equipments and catalysts used [6].

One of the common hydrotreating processes is hydrodesulfurization (HDS) in which the organic sulfur compounds are converted to hydrogen sulfide. Another hydrotreatment process is hydrodenitrogenation (HDN) in which the organic nitrogen compounds are converted to ammonia. HDM refers to hydrodemetallation or hydrodemetallization, in which the organo-metals are converted to the respective metal sulfides before hydrocracking to avoid catalyst poisoning. Other treatments are removal of oxygen by converting the organic oxygen compounds to water, olefin saturation by converting organic compounds containing double bonds to saturated compounds, aromatic saturation which decreases the aromatic content referred as hydrodearomatization saturation (HDA) in which some of the aromatic compounds are converted to naphthenes and halides removal, in which the organic halides are converted to hydrogen halides [7, 8].

In many refining systems, the most important hydrotreating process is hydrodesulfurization since sulfur is the third most abundant element in crude oil and combustion of sulfur containing compounds emits sulfur oxides into atmosphere, which can cause detrimental effects on human health and environment [6]. As a result, many countries around the world have cut down the sulfur content of the diesel fuel to ultra low levels (<10 ppm) and demand for ultra-low sulfur diesel (ULSD) has been steadily increasing. This calls for more investment and revamping of hydrodesulfurization processes and research on this area has gained enormous interest in scientific community worldwide [9].

In petroleum refineries, process models are necessary to predict the optimal operation to guarantee profitability. These models are used to do simulations under different scenarios and to predict the best operating conditions along with real time process optimization and control of the unit.

In this thesis, a steady-state model is presented for an industrial diesel hydoprocessing plant that includes hydrodesulfurization and hydrocracking reactors. In this process, after hydrodesulfurization, higher molecular weight compounds in the diesel feedstock are cracked and saturated with hydrogen to form distillate fractions which are naphtha and diesel with higher hydrogen/carbon ratio and lower content of contaminants.

Necessary background and literature review on reaction kinetics and process modeling of the hydrodesulfurization and hydrocracking reactions are presented in Chapter 2. Chemistry of the hydrodesulfurization and hydrocracking reactions is also reviewed briefly.

Chapter 3 describes the diesel hydroprocessing plant in detail and discusses the characterization of the fractions by using the concept of pseudocomponents presented.

Chapter 4 and chapter 5 give kinetic modeling studies for HDS and HC, respectively. Generation of the sulfur curve for the modeling of hydrodesulfurization reactor is presented in Chapter 4. In both chapters, model formulation is given in detail mass and energy balance equations. The parameter estimation procedure and sensitivity analysis are also described.

The results obtained via simulation of the reactor models are given in Chapter 6 and the overall performance of the model is discussed in the light of these results. The user-friendly interface that is developed for simulation of the reactors is also presented. Monitoring of the model parameters is given.

The thesis is concluded with a brief summary of the research highlighting what has been achieved and future research work is explained shortly in Chapter 7.

Chapter 2

LITERATURE REVIEW

2.1. Overview

The main purpose of the hydrotreating reactions is removal of the impurities or to saturate olefins without any change in the boiling range of the feedstock. In contrast hydrocracking reactions yield products that have boiling point range less than of the feedstock [10].

The type and the amount of impurities present in feedstocks can vary. Generally, light feeds (e.g. naphtha) contain lighter impurities, while heavy feeds (e.g. residua) have a high concentration of heavy compounds. Also the impurities in heavy feeds are more complex and refractory than those present in light feeds. This explains why hydrotreating of light feeds is operated at less severe reaction conditions and heavy oils needs higher reaction pressures and temperatures [11].

The operating conditions for hydrotreating can vary from feedstock to feedstock and depend on the required products, and the availability of hydrogen. Typical process conditions for various hydrotreatment operations can be summarized in Table 2.1.

Table 2.1: Range of Operating Conditions for Different Feedstocks [5]

Feedstock	Temperature (K)	Pressure (atm)	LHSV (hr^{-1})
Naphtha	593	15-30	3-8
Kerosene	603	30-45	2-5
Atmospheric gas oil	613	38-60	1.5-4
Vacuum gas oil	633	75-135	1-2
Atmospheric residue	643-683	120-195	0.2-0.5
Vacuum residue	673-713	150-225	0.2-0.5

The hydrotreating operations have four most important process variables reported in the literature: reaction temperature, liquid hourly space velocity (LHSV), hydrogen partial pressure and hydrogen to oil ratio (H_2/Oil) ratio. Generally, the degree of impurities removal and conversion increases with increasing severity of the reaction; that is, increasing pressure, temperature, or H_2/Oil ratio, and decreasing the space velocity for a specific feedstock and catalyst [12-15].

Hydrotreating reactions are carried out in trickle-bed reactors (TBR) which are three phase reactors (gas-liquid-solid). These reactors are commonly operated at temperatures in the range 300–450 $^{\circ}$C, and at H_2 pressures of 3.0–5.0 MPa, usually with $CoMo/Al_2O_3$ or $NiMo/Al_2O_3$ catalysts [16, 17].

A TBR is a cylindirical column reactor which consists of a gas phase (hydrogen) and a liquid phase (oil) that flow cocurrently downward through a fixed bed of solid catalyst particles [18].

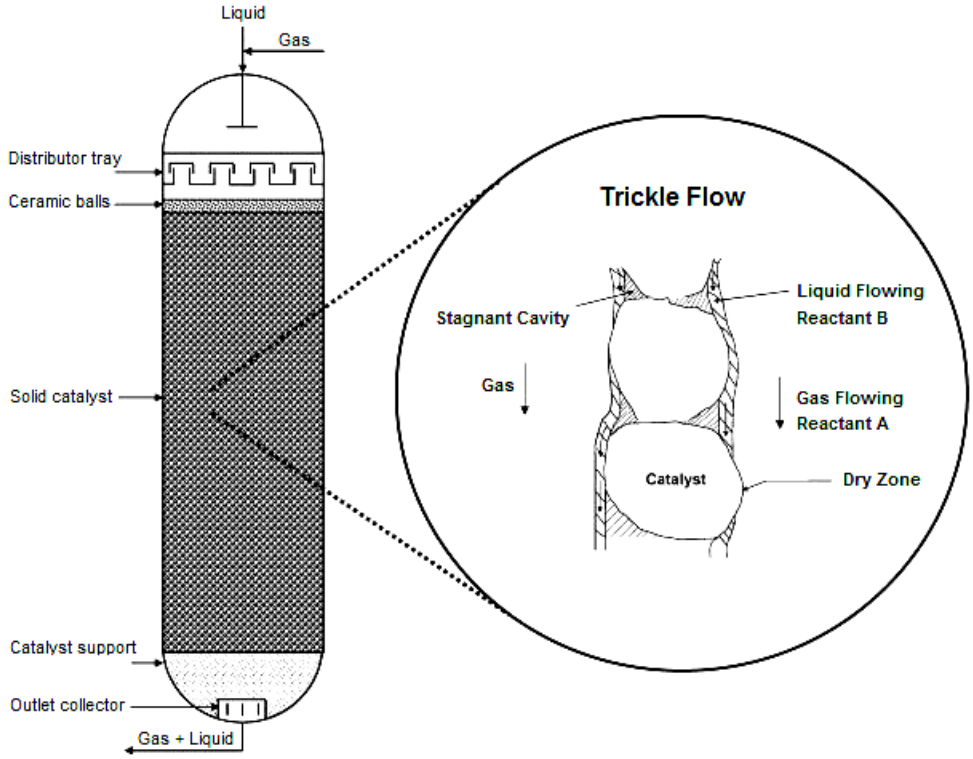

Figure 2.1: Illustration of the trickle-flow regime in a trickle-bed reactor [19]

There are two types of reactions that occur during catalytic hydrotreating: hydrogenolysis and hydrogenation. In hydrogenolysis reactions, cleavage of carbon-heteroatom (e.g sulfur, nitrogen, oxygen, metals) single bond occurs by the addition of hydrogen. Hydrodesulfurization (HDS), hydrodenitrogenation (HDN), hydrodeoxygenation (HDO) and hydrodemetallization (HDM) are the principal hydrogenolysis reactions in catalytic hydrotreating. In hydrogenation reactions, hydrogen is added to the molecule without breaking its bonds. Saturation of olefins and hydrodearomatization are the principal hydrogenation reactions [11].

Some general reactions which occur during hydrotreating are in Figure 2.2.

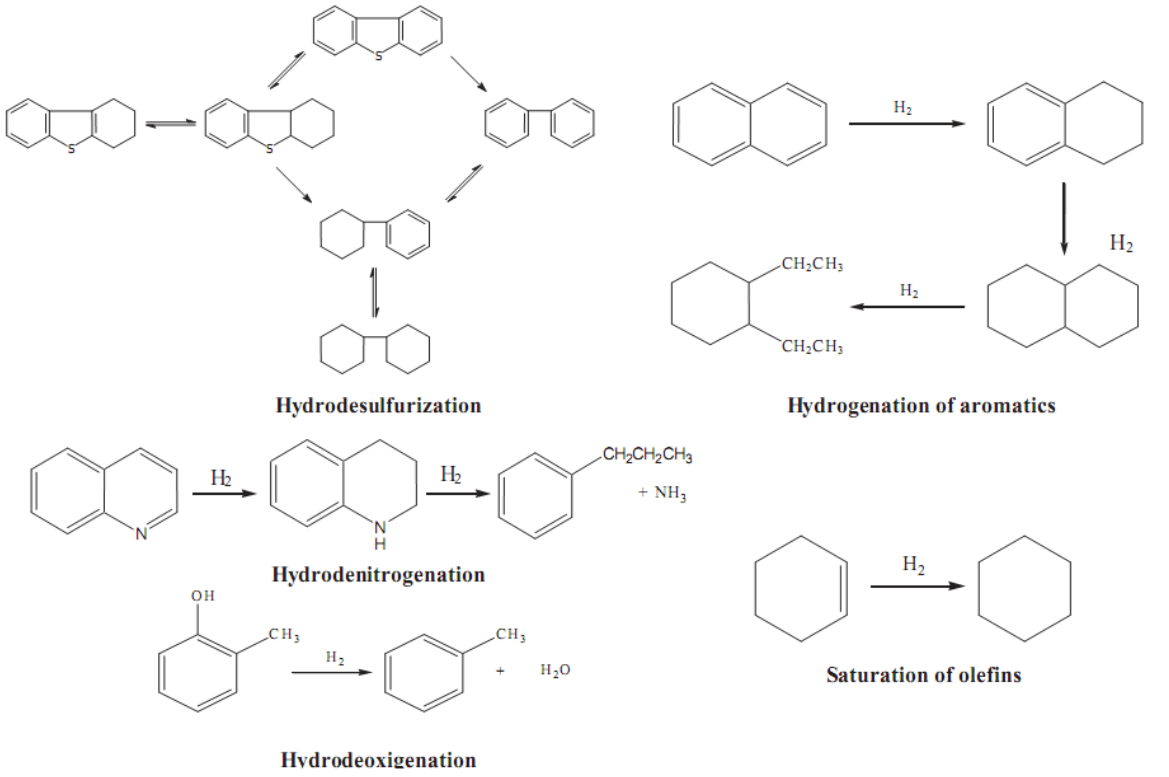

Figure 2.2: Examples of some hydrotreating reactions [11]

Hydrocracking is the most important and widely used conversion process in a refinery to upgrade heavy feedstocks like heavy vacuum gas oil into more valuable middle distillates like diesel and kerosene in hydrogen-rich atmosphere at elevated temperature and pressure. After hydrocracking, the desired products have lower molecular weights than feedstocks. Hydrocracking is the best source of low-sulfur and low-aromatics diesel fuel in the environmentally aware 1990s [20].

2.2. Chemistry of HDS Reactions

As mentioned in the introduction, hydrodesulfurization is the most important hydrotreatment process since the sulfur content has a great influence on the value of the petroleum product. Sulfur content is defined as a percent sulfur by weight and varies from less than 0.1% to bigger than 5% depending on the type and source of crude oils [1].

In refinery sulfur compounds are undesirable as they poison catalysts and cause corrosion problems in pipeline, pumping, and refining equipments. Furthermore, emitted sulfur oxide gases react with water in the atmosphere to form sulfates and acid rain which damages buildings, acidifies soil, and leads to loss of forests and various other ecosystems. Sulfur emissions also cause respiratory illnesses, aggravate heart disease, trigger asthma, and contribute to formation of atmospheric particulates [1, 3].

HDS reactions are generally hydrogenolysis reactions that occur in the presence of catalysts which are usually $CoMo/Al_2O_3$ or $NiMo/Al_2O_3$ catalysts and can be written in the general form below;

$$R-S+H_2 \rightarrow R+H_2S$$

where R represents the hydrocarbon molecule. Also, HDS reactions are highly exothermic and irreversible.

The sulfur compounds exist in various forms and can be classified as mercaptans, sulfides, disulfides, thiophenes, benzothiophenes, dibenzothiophenes, and substituted dibenzothiophenes. Mercaptans are the easiest molecules to remove and dibenzothiophenes are the most difficult. Sulfur removal difficulty increases in the following order: paraffins < naphthenes < aromatics [11]. Some of these compounds are shown in Figure 2.3.

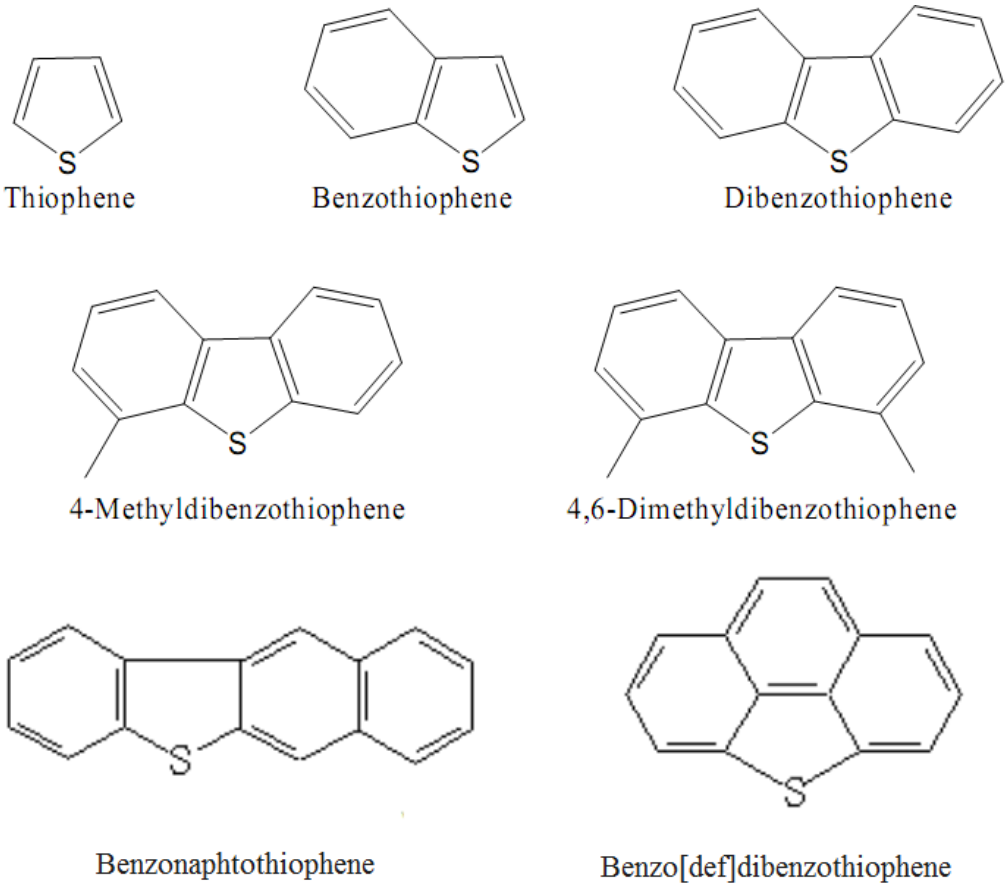

Figure 2.3: Sulfur-containing molecules in petroleum [2, 21]

For treating oil to lower sulfur levels, it is necessary to remove sulfur from the compounds that are the most difficult to desulfurize. Higher molecular weight dibenzothiophenes are the most refractive sulfur compounds that contain side chains in positions close to the sulfur atom (Figure 2.4). Two such sterically hindered compounds that have been identified as most difficult to desulfurize are 4-methyl dibenzothiophene (4-MDBT) and 4,6-dimethyl dibenzothiophene (4,6-DMDBT) [22].

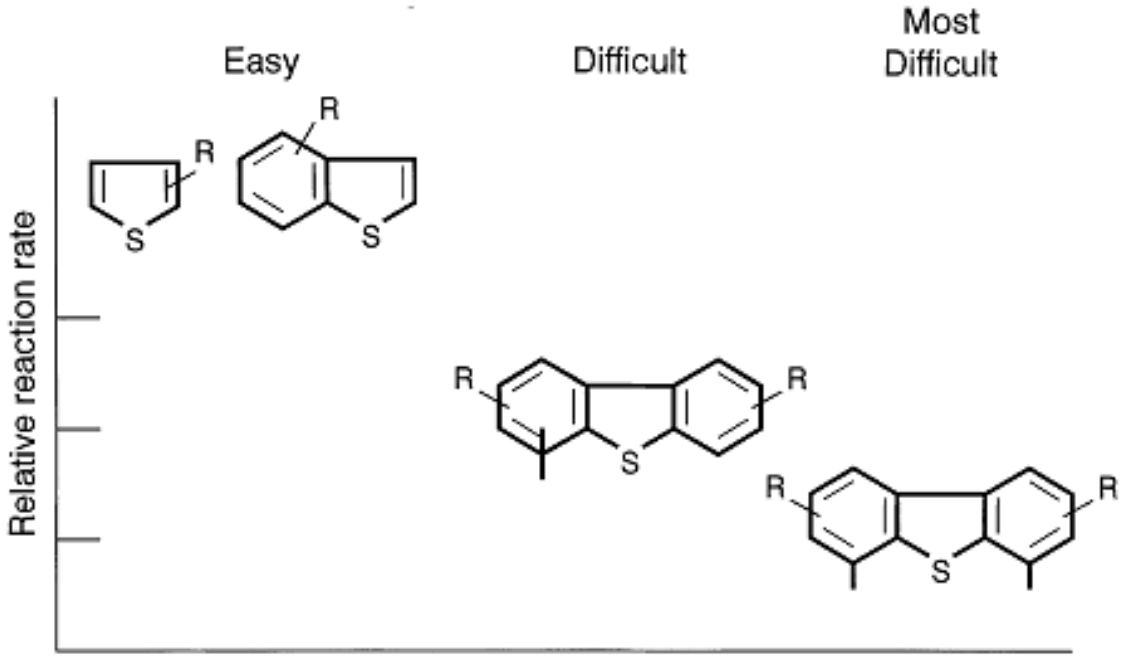

Figure 2.4: Impact of sulfur species [22]

Sulfur is removed by the conversion of the organic sulfur compounds to H_2S. Typical reactions for different sulfur compounds are shown below in Figure 2.5.

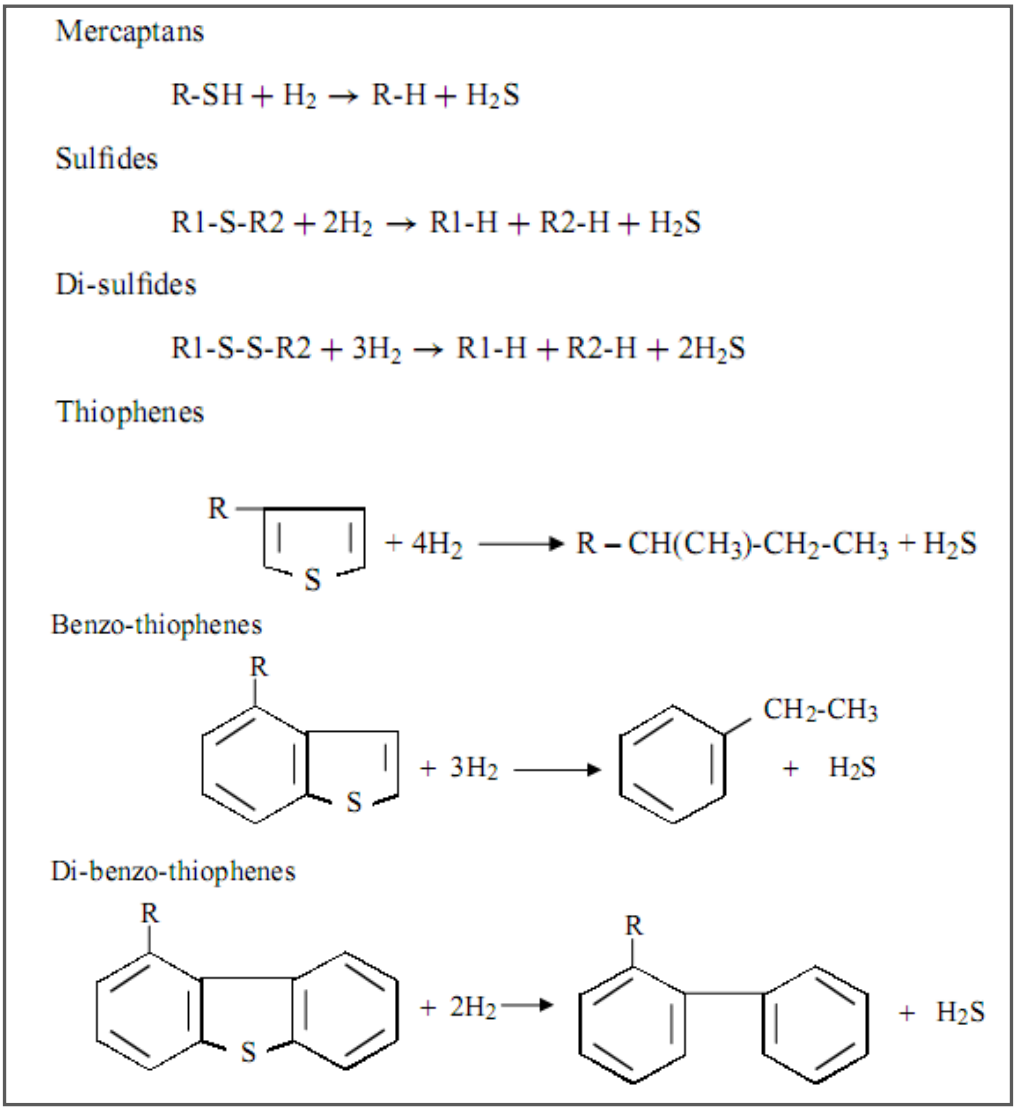

Figure 2.5: Desulfurization reactions of typical sulfur compounds [8]

2.2.1. Hydrodesulfurization Mechanism

In HDS, the reaction mechanism of sulfur compounds may follow two main pathways and the preferred pathway depends on the structure of the organo-sulfur compound. One is

DDS (direct desulfurization) or hydrogenolysis pathway where sulfur is removed directly from the aromatic rings. Sulfur is replaced by hydrogen in the compound without hydrogenation of any C=C bonds. Other pathway is a hydrogenation desulfurization (HYD) pathway, in which aromatic rings of sulfur compounds are preferentially hydrogenated to intermediates and are subsequently desulfurized. In the second pathway there is higher hydrogen consumption than the first pathway [1, 23, 24].

The kinetics of hydrodesulfurization is complex since the diesel feedstock which is under interest in this study contains a variety of sulfur compounds.

The reaction mechanism for the HDS of thiophenes is not totally clear but common idea is that first hydrogenolysis of C-S bond occurs to produce butadiene, then this intermediate is hydrogenated to produce butene and butene hydrogenates to produce butane at last (Figure 2.6) [21].

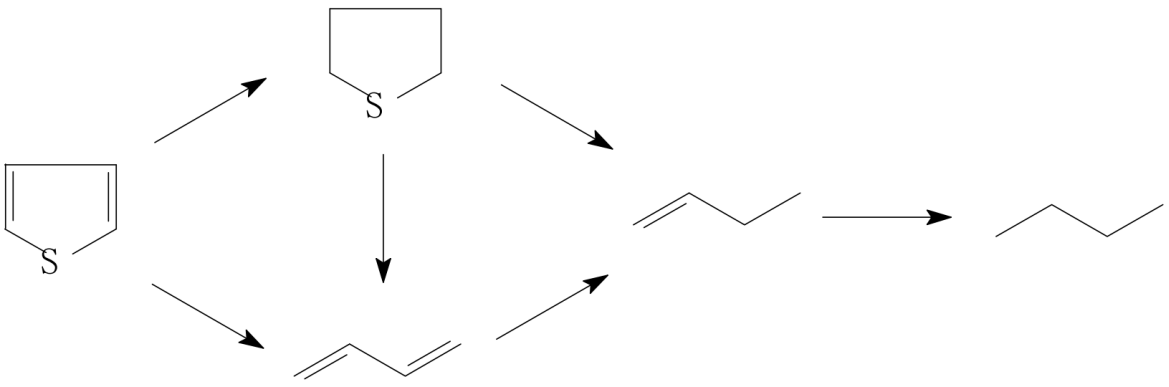

Figure 2.6: HDS reaction network of thiophenes

The reaction network proposed for benzothiophenes is similar to the mechanism of thiophene. The reaction scheme is a triangular network due to the production of

dihydrobenzothiophene which is intermediate and it reacts to produce ethylbenzene (Figure 2.7) [21].

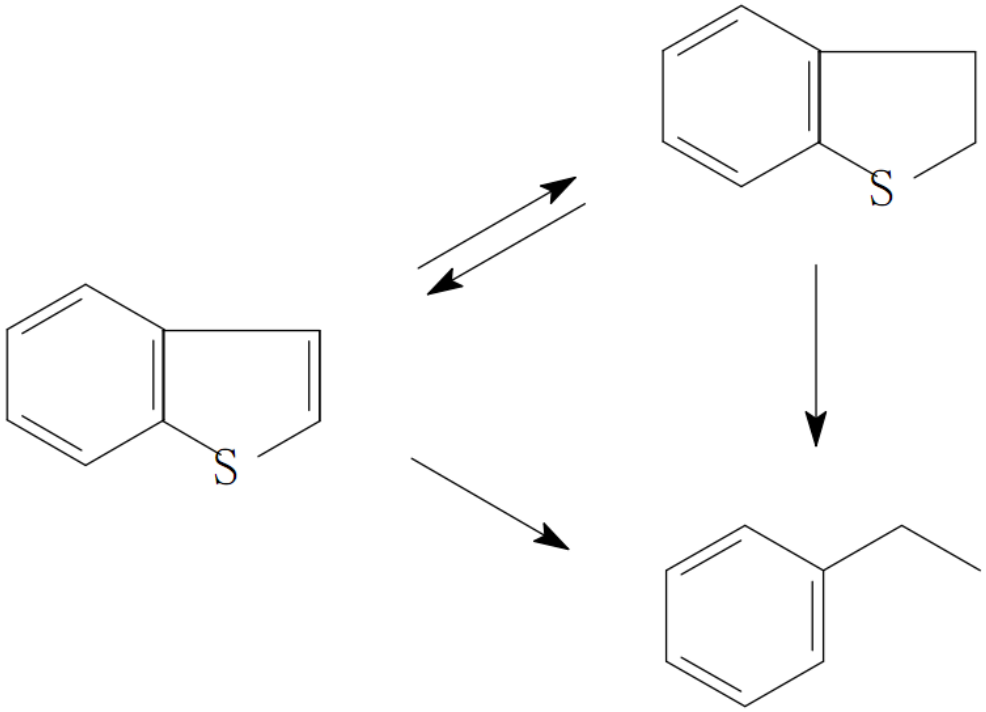

Figure 2.7: HDS reaction network of benzothiophenes

The reactions of individual sulfur compounds such as thiophene, benzothiophene and dibenzothiophene are very fast and can be described as first-order reactions. But, substituted-dibenzothiophenes have equilibrium limitations depending on the operating temperature [21].

The reaction mechanism for the HDS of DBT at 300 °C and 102 atm is shown in Figure 2.8 [21]. Biphenyl (BiPh) is the predominant organic product in reaction of hydrogen with

DBT. Tetrahydrodibenzothiophene (THDBT) and/or hexahydrodibenzothiophene (HHDBT) are the primary products formed in the HYD pathway mechanism. Cyclohexylbenzene (CHB) is the secondary product after desulfurization. This pathway is referred to as HYD pathway since the sulfur compound is hydrogenated prior to desulfurization. Direct C–S bond hydrogenolysis of DBT gives biphenyl via DDS pathway [1].

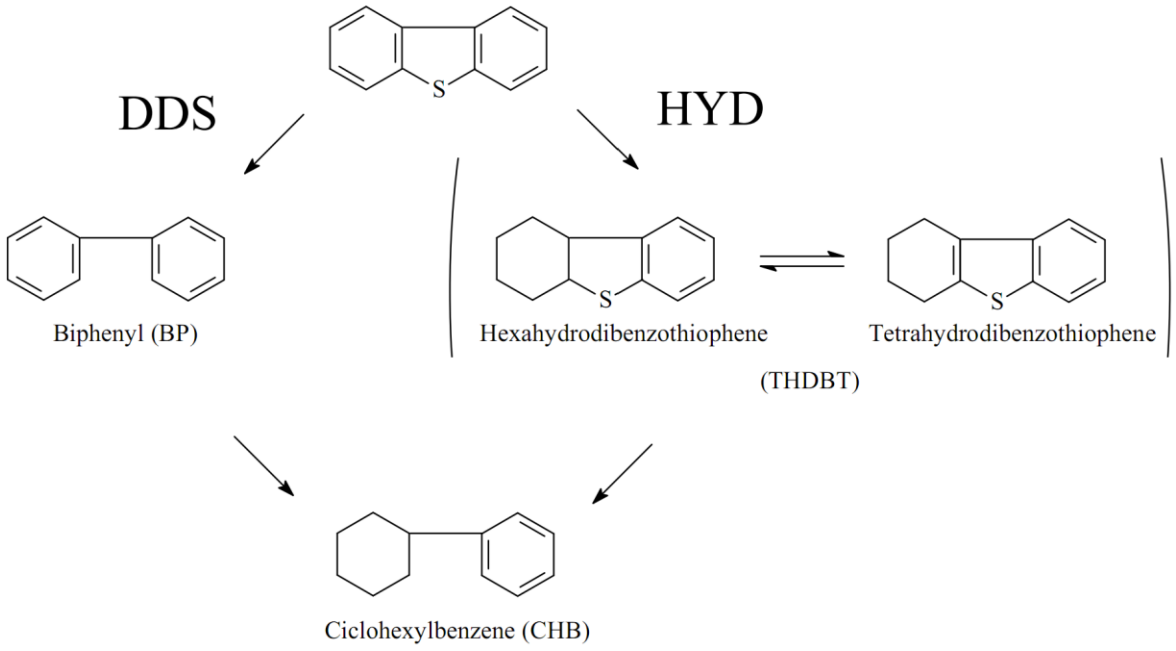

Figure 2.8: Pathways for the HDS of DBT in the presence of $CoMo/Al_2O_3$

2.3. Chemistry of Hydrocracking Reactions

In hydrocracking reactions, cleavage of C-C bonds is most likely to occur. Molecules with high molecular weight crack into low molecular weight compounds. Olefins, aromatics, sulfur, nitrogen and oxygen compounds are hydrogenated to some extent in a hydrogen-rich environment. The overall hydrocracking process is exothermic in nature since the hydrogenation reactions are highly exothermic although the cracking reactions are somewhat endothermic.

Hydrocracking reactions occur in the presence of a catalyst and since the reactions involve both cracking and hydrogenation, dual functional catalysts are required. These catalysts consist of a hydrogenation component spread on a porous acidic support for providing cracking activity. A typical catalyst consists of molybdenum supported on high surface area carrier like amorphous silica-alumina (or zeolites) promoted by cobalt or nickel. Dispersed metals such as cobalt, nickel, molybdenum, platinum, palladium and tungsten carry out for hydrogenation reactions while silica-alumina and zeolites serves for cracking [20].

An example of hydrocracking reactions is as follows [5];

$$RCH_2CH_2R + H_2 \rightarrow RCH_3 + RCH_3$$

or

$$C_{10}H_{22} + H_2 \rightarrow C_4H_{10} + C_6H_{14}$$

2.4. Process Modeling

In petroleum refineries, process models are necessary to predict the optimal operation to guarantee profitability. These models are used to do simulations under different scenarios and to predict the best operating conditions along with real time process optimization and control of the unit. New process units can be designed and suitable catalysts can be chosen in the light of the information obtained from simulations of the model. Effect of operating parameters such as reactor temperature, space velocity on product yield can be understood and product yield can be predicted as well [25].

Using a process model has many advantages. Firstly, it is cheaper to simulate a model instead of running the real plant to see the effects of any changes in the process conditions..

A mathematical process model consists of a set of variables which describes some properties of the process and a set of equations that builds relationships between variables to explain the behavior of the system. For complex systems found in many chemical and petrochemical industry, the models present mostly nonlinear equations like reaction rate expressions in mass and energy balances [5].

There are three types of models [5, 20]:

1. The model can be derived from industrial process data (data-driven black box models) when no physical insight is available. These models are obtained by system identification methods and are in the form of empirical input-output models

2. The model can be derived from first principles (knowledge driven white box models or mechanistic models) including mass and energy balances, and thermo-physical properties of the process. These models are in the form of nonlinear differential and algebraic equations (DAE). Some assumptions are usually made to simplify the complexity of such models.

3. The model can be a combination of input-output and first principles models (hybrid grey box models).

Development of mathematical models for hydrotreating and hydrocracking reactions is a challenging task since petroleum feedstocks are complex mixtures whos reactivity can vary widely from feedstock to feedstock. The crude oil contains a lot of compounds with different structures. It is very important to develop kinetic models that can accurately predict the product yields under different scenarios with accurately estimated parameters. For the hydrotreating case, most models only take into consideration the hydrodesulfurization reactions because of the complexity of the system. However, hydrodesulfurization (HDS) of crude oil has not been reported widely in the literature [5, 26, 27].

In this thesis, a white–box model (first principles model) is used for the modeling of hydodesulfurization and hydrocracking reactors.

2.5. Kinetic Modeling Approaches

The petroleum mixture consists of a huge number of hydrocarbons. Therefore it is difficult to perform kinetic studies which take into account each compound and all possible reactions. Complexity of reactions and computational limitations make the development of a detailed mechanistic model difficult when considering real feedstocks [11]. Instead, simpler kinetic and reactor models can be used with some confidence.

It is obvious that as the number of the compounds increases, more kinetic parameters will be needed and estimation of these parameters will be more demanding and less reliable. Alternatively, it is possible to simplify the problem by considering partitioning of the species into a few classes which are called lumps, and then assuming that each class is

an independent entity [28]. This technique is called as lumping technique. Lumping approach is the most widely used technique because of its simplicity.

The kinetic modeling techniques reported in the literature can be classified as (1) the traditional lumping (discrete lumping) approach, (2) continuous lumping approach, and (3) structure-oriented lumping approach [11].

2.5.1. Discrete Lumping Approach

In this approach, the reaction mixture is divided into discrete pseudocompounds (lumps) based on their boiling range, molecular weight or C-number distribution [29].

Weekman's 10-lump model [30] to model fluid catalytic cracking (FCC) reactions is one of the classical examples of discrete lumping approach. There is a need of increasing the number of lumps to obtain more accurate model in discrete lumping approach. However this increases the number of model parameters and the amount of experimental data [29].

The disadvantages of the discrete lumping are as follows:

(a) need to perform extensive experimental work to calculate a number of rate constants,

(b) inability to extrapolate different feedstocks because of compositional differences within the same defined lumps,

(c) variations of composition of lumps as conversion changes,

(d) inability to predict changes in product properties [27, 29].

2.5.2. Continuous Lumping Approach

Oil fractions contain extremely large numbers of components such as organosulfur, organonitrogen or aromatic species, and their concentration and reactivity vary widely from feedstock to feedstock, so they can be treated as a continuum [27].

The continuous lumping approach takes the reactive mixture to form a continuum mixture that consists of infinite number of components with respect to its species type, boiling point, molecular weight, etc. While formulating the model, an intrinsic property is chosen to characterize the reaction mixture. This parameter is usually true boiling point (TBP) [29, 31].

An example of dividing into pseudocomponents to form a continuous mixture is given in Figure 2.9 [27]:

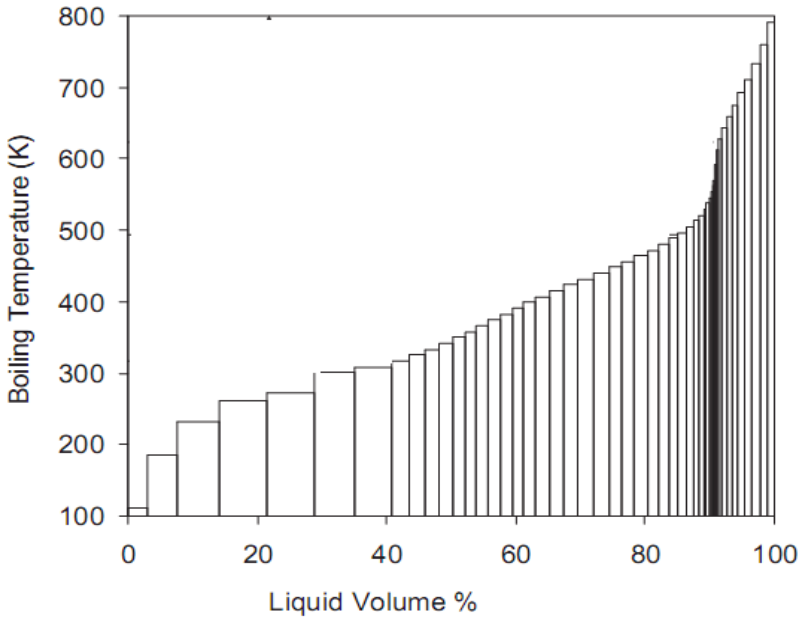

Figure 2.9: An example of Continuous Lumping [27]

Aris [32] studied first applying continuum theory of lumping to treat complicated mixtures. After his study, number of other groups including his group, have employed this approach for various systems (Aris [33] ; Astarita [34]; Astarita and Nigam [35]; Astarita and Ocone [36]; Chou and Ho [37] ; Ho et al. [38] ; Ho [39] [40]; Ho and Aris [41] ; Laxminarasimhan et al. [42]; Prasad et al. [43]).

For simulating the different reactions occuring during hydrotreatment, the continuous kinetic model is a suitable approach. Continuum theory of lumping can make accurate predictions with few parameters and thus it overcomes the shortcomings of the discrete approach.

Some of the advantages of using continuous kinetic model are summarized below:

(a) prediction of the entire boiling point curve by using few model parameters,

(b) easy way to calculate any fraction with arbitrary initial and final boiling points,

(c) easy adaptation to kinetics of heavy and extra-heavy oils,

(d) a limited number of kinetics parameters are required [27].

2.5.3. Structure-Oriented Lumping (SOL) Approach

Structure - oriented lumping approach uses most of the information obtained through modern analytical techniques for model reaction modeling. This is a detailed technique at molecular level [11]. SOL is a molecular- based modeling technique.

Quann and Jaffe [44] proposed a procedure for structure-oriented lumping (SOL) by representing individual hydrocarbon molecules as a vector of structural features, and the lumps were defined according to the structure of the compounds. Different molecules with the same set of structural groups, i.e., certain isomers, are lumped and represented by the same vector. The reacting mixture was represented as a set of these vectors, each with an

associated weight percent. But this approach would require large experimental data bank and computational power to build a reasonable model.

An example to structure-oriented lumping was represented as follows:

a =	[A6	A4	A2	N6	N5	N4	N3	N2	N1	R	br	me	IH	AA	NS	RS	AN	NN	RN	NO	RO	KO]
S:																						
carbon	6	4	2	6	5	4	3	2	1	1	0	0	0	0	-1	0	-1	-1	0	-1	0	0
hydrogen	6	2	0	12	10	6	4	2	1	1	0	0	2	-2	-2	0	-1	-1	1	-2	0	0
sulfur	0	0	0	0	0	0	0	0	0	0	0	0	0	0	1	1	0	0	0	0	0	0
nitrogen	0	0	0	0	0	0	0	0	0	0	0	0	0	0	0	0	1	1	1	0	0	0
oxygen	0	0	0	0	0	0	0	0	0	0	0	0	0	0	0	0	0	0	0	1	1	1

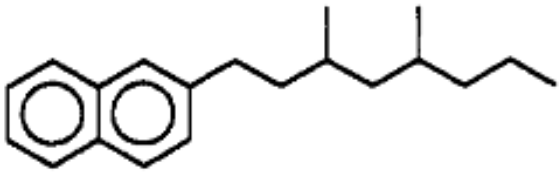

A6	A4	A2	N6	N5	N4	N3	N2	N1	R	br	me	IH	AA	NS	RS	AN	NN	RN	NO	RO	KO
1	1	0	0	0	0	0	0	0	10	2	0	0	0	0	0	0	0	0	0	0	0

Figure 2.10: An example to Structure-Oriented Lumping [44]

Single - event approach was studied by Froment [45] starting from the elementary steps of carbenium ion chemistry. This approach is a detailed approximation and keeps the full details of the reaction pathways of the individual feed components and reaction intermediates. In Froment's study, methanol-to-olefins and catalytic cracking of oil fraction reactions were illustrated.

2.6. Reviews on Hydrotreating Modeling

Different classifications of reactor models have been reported in the literature. Because of the complexity of the system, most TBR models only take into consideration the HDS reaction. Most of the reports describe pseudo-homogeneous and heterogeneous steady state models. A pseudo-homogeneous model generally assumes no gradients of mass or temperature between two adjacent phases [46]. The heterogeneous models distinguish the phases in a trickle-bed reactor.

Froment et al. [47] developed a one–dimensional heterogeneous non-isothermal model by using rate equations to simulate the hydrotreatment of diesel oil. The kinetic model was built on a feed mixture that consists of dibenzothiophene and alkyl-substituted DBTs.

A three-phase reactor model was developed by Korsten and Hoffmann [48] to simulate a pilot trickle-bed reactor in which the hydrotreating reaction of vacuum gas oil took place under high–pressure and isothermal conditions. The model assumed two–film theory where mass transfer phenomena at gas–liquid and liquid–solid interfaces were integrated and mass transfer coefficients, gas solubilities, pressure drop and the physical properties were estimated by correlations. The simulation results showed reasonably good agreement with experimental results.

Sau et al. [49] proposed a pseudo-homogeneous plug-flow model and simulated a commercial kero-HDS reactor by applying the continuum lumping theory. They grouped organic sulfur compounds into different classes: mercaptans, sulfides, disulfides, and thiophenes. The reactivity equation was formed by assuming a monotonically decreasing relationship between the reactivity of sulfur compounds within each group and true boiling point (TBP). The rate equation was built by using Langmuir-Hinshelwood kinetics which takes into account the inhibiting effect of hydrogen sulfide. Pressure and temperature

effects and reaction heat were included into the model. The simulated results were very satisfactory.

A kinetic model for HDS in a trickle bed reactor with different catalysts was investigated by Tsamatsoulis and Papayannakos [50]. A real feed, vacuum gas oil was employed. A plug-flow and a non-ideal liquid flow model were used for the liquid phase.

Differences in reaction rates in hydrodesulfurization were discussed and sulfur concentration and hydrogen consumption were predicted by the models to fit the experimental data. The authors observed that the plug-flow model succeeded in simulation of HDS and hydrogen consumption predictions at low conversions; otherwise, axial dispersion effects should be incorporated in the plug–flow model.

Ho and co-workers [40] have investigated HDS modeling of diesel fuels with a so-called distribution function model by using a gamma function to explain the distribution of sulfur concentrations as a function of their rate constants. Continuous lumping approach was employed. The model consisted of two simple parameters. The results were successful in prediction of HDS over a wide reaction range down to 20 ppm.

A computer model was developed by Van Hasselt et al. [51] for hydrodesulfurization of vacuum gas oil and the aim was to compare two different configurations of non-isothermal co-current trickle–bed reactor: counter-current and semi–counter current configurations. It was observed that the countercurrent flow configuration results in a significant increase of impurities conversion.

Cotta et al. [52] simulated an adiabatic diesel hydrotreating trickle-bed reactor with and applied a one-dimensional homogeneous model. HDS and HDN reactions were investigated by applying the power law model. It is shown that using the most rigorous conditions increases the HDN conversion and they concluded with that a larger reactor length is required for the nitrogen conversion.

An isothermal reactor with co-current upflow was modeled by Matos and Guirardello

[53] to simulate heavy oil hydrodesulfurization and hydrodemetallization.

A co-ccurrent downflow trickle bed reactor was modeled by Kumar et al. [54] and the case study was hydrodesulfurization of diesel oil using two types of catalysts. The reaction rate equation was a power law model to estimate the kinetic parameters.

Bhaskar et al. [55] developed a three phase heterogeneous model and applied to a pilot plant trickle–bed hydrodesulfurization reactor which had a feed of atmospheric gas oil. They operated the pilot plant under different operating conditions and they observed the effects of effects of hydrodynamic parameters and reaction rates on reactor performance. The experimental observations agreed well with the simulated data.

A two phase flow reactor model was developed for desulfurization and dearomatization of diesel oil in an experimental trickle- bed reactor by Chowdhury et al. [46]. They considered both mass transfer and chemical reaction in the isothermal reactor. Hydrodesulfurization and hydrogenation kinetics of three types of aromatics were established. The results from the model were in good agreement with the experimental results.

Avraam and Vasalos [56] built a steady–state model for a trickle bed reactor by assuming the plug-flow conditions and they simulated the model for hydroprocessing of light oil feedstocks containing volatile compounds. Hydrodesulfurization (HDS), hydrodenitrogenation (HDN), olefins saturation (HTO) and hydrogenation of aromatics (HTA) processes were described by using Langmuir–Hinshelwood mechanism and they has taken into account aromatic hydrogenation equilibrium and inhibition by hydrogen sulfide, ammonia, and aromatics. The experimental pilot plant results showed satisfactory match with the data obtained from the mathematical model.

The effect of the oil fractions compositions on the conversion of sulfur compounds in laboratory-scale TBR was investigated by Perdernera et al. [57]. They extended the model which was studied by Chowdhury et al. [46]. The model was built in Aspen Plus and the

results showed good agreement with experimental results.

A continuous kinetic model for an industrial hydrocracking reactor was developed by Basak et al. [29]. The hydrogen consumption and bed temperature profiled were monitored by simulating the model developed.

A one-dimensional three phase heterogeneous reactor model based on two film theory was studied by Bhaskar et al. [58] to simulate the performance of pilot plant and industrial trickle bed reactors in which the feedstock was diesel cuts. HDS, HDN, HDA, HGO, and HCR reactions were modelled. The authors reported that simulation results showed good agreement with the experimental results. Also, a three phase non–isothermal heterogeneous model was simulated to describe the effect of different operating conditions on product in a commercial reactor using the kinetic parameters of the pilot plant experiments.

The model studied by Rodriguez and Ancheyta [59] is an extension of the model which was studied by Korsten and Hoffman [48]. The authors developed mathematical correlations for the rate of hydrodesulfurization, hydrodenitrogenation and aromatics hydrogenation reactions. The rate equation was a Langmuir–Hinshelwood kinetics type for HDS reaction. The model simulations were validated with experimental data generated at a pilot plant which operates under isothermal conditions and the feed of the pilot plant was vacuum gas oil. The kinetic parameters were found by least-squares criterion with nonlinear regression. The results of the simulations agreed well with the experimental ones. The model was also studied for non-isothermal operation.

The model developed by Korsten and Hoffman [48] was used by Yamada and Goto [60] for pilot and industrial scale simulation of HDS of the vacuum gas oil. The reactor was a trickle bed reactor and both countercurrent and co-current flow regimes were studied.

Jimenez et al. [61] studied a steady–state one–dimensional heterogeneous model to

describe the performance of a pilot plant hydrotreating reactor for feed of VGO and the model covered hydrodesulfurization, hydrodenitrogenation and hydrogenation of aromatics reactions. Also, physical and chemical properties were related to operating conditions and estimated as function of these conditions. A comparison between experimental and predicted results showed insignificant error.

Sertic-Bionda et al. [62] developed a simple steady-state pseudo-homogeneous plug-flow model to simulate a trickle bed reactor for prediction HDS and to observe how some reaction factors affect hydrotreating of atmospheric gas oil and light cyclic oil.

The mechanisms of asphaltene conversion during hydrotreatment of Maya heavy oil was investigated by Trejo and Ancheyta [63] by employing a power law model. A pilot plant under different operating conditions was simulated and the kinetic model results showed good agreement with insignificant error when compared to experimental results.

In the literature, kinetic models for the hydrotreating of bitumen-derived heavy gas oil from Athabasca over a commercial $NiMo/Al_2O_3$ catalyst in a trickle-bed reactor was investigated by Botchwey et al. [64] for short-range temperature regimes by using discrete lumping approach. The oil samples are grouped as four lumps according to their boiling cuts with five kinetic parameters. Gas chromatography simulated distillation results were used in derivation of the distribution of boiling-point.

Mederos et al. [65] studied a heterogeneous one-dimensional model of TBR for hydrotreating of oil fractions by employing two film theory. HDS, HDN and HDA reactions were investigated under isothermal and non-isothermal conditions. Heat and mass transfer coefficients, gases solubilities, and oil and gases properties were calculated by the correlations developed. The validation of the results of model with experimental results was good.

A one–dimensional heterogeneous model for simulating an industrial trickle bed reactor was developed by Jimenez et al. [66]. The case study was HDS, HDN and HDA

reactions of feedstock of VGO and heavy oil fractions. The theoretical and experimental results agreed well.

Mederos and Ancheyta [67] developed a one–dimensional heterogeneous plug flow model for oil fractions. The model was built to predict the behavior of trickle bed reactors under co-current and countercurrent operations for HDS, HDN and HDA reactions. The performance of pilot plant and commercial trickle bed reactors was simulated.

Shokri et al. [68] used a trickle bed reactor with two film theory for describing the HDS of gas oil. They developed a plug-flow one-dimensional heterogeneous model that was validated with pilot data to estimate the optimal operating conditions. The reaction rate equations were described by the kinetics suggested by Vanrysseiberghe and Froment [69].

A three phase heterogeneous plug flow reactor model was investigated by Alvarez and Ancheyta [70] to simulate the residue hydrotreating in a multi–fixed bed reactor system. The kinetic rate equation for HDS reaction was Langmuir–Hinshelwood kinetics and power law kinetics were employed for HDN, HDM, HDAs and HDC. The simulated model's predictions agreed with experimental results obtained from the lab–scale.

Alvarez and Ancheyta [71] desribed a one dimensional heterogeneous trickle bed reactor for industrial vacuum gas oil taking the HDS, HDN and HDA reactions into account. The trickle bed reactor model was employed from the studies of Korsten and Hoffmann [48] and Rodriguez and Ancheyta [59].

A mathematical model for atmospheric residue HDS in a pilot plant reactor was developed by Bahzad and Kam [72] . The feed to reactor was Al–Kuwait heavy crude. They observed that there were some mismatches between the experimental and model results which may be occurred because of the catalyst used.

Chen et al. [73] built a steady-state adiabatic trickle bed reactor model which is one dimensional and has plug flow characteristics for an industrial gas oil hydrotreater taking HDS and HDA reactions into account. The performance on impurities removal was investigated under different operating conditions and it was observed that as the pressure increased, the temperature also increased and the oil is hydrotreated better.

Farahani and Shahhosseini developed a heterogeneous trickle bed reactor model for the hydrodesulfurization of heavy gas oil and non-isothermal conditions were employed by taking the Langmuir-Hingshelwood kinetics. The results of the simulations agreed satisfactorily with the experimental data [74].

2.7. Reviews on Hydrocracking Modeling

Since hydrocracking technology occupies very important place in a refinery, many researchers have studied hydrocracking processes.

The first experimental study seems to be conducted by Qader and Hill [75] and they developed a kinetic model of a continuous fixed bed reactor for the hydrocracking of gas oil. Gasoline, middle distillate and diesel were the products.

A model for conversion of vacuum gas oil in terms of a relatively large number of pseudocomponents was developed by Liguras and Allen [76] based on the nature of carbon centers in the pseudocomponents. They employed group contribution methods by using data on the catalytic reactions of model compounds.

A three-parameter kinetic model was developed to observe the yield of a hydrocracker by Stangeland [77] and discrete lumping approach was employed. This study is known a classical example to discrete lumping approach. He divided the feed into pseudocomponents by assuming that heavier cuts crack into lighter cuts by a first order

reaction. Best kinetic parameters were found and used for similar feeds although they have different boiling point ranges.

A kinetic model for the hydrocracking of a residue feedstock was investigated by Mosby et al. [78]. Lumped first order kinetics was employed. The products of the process were naphtha, middle distillates, gas oil and residue. Optimal process parameters were found by using the results of the experiments.

Krishna and Saxena [79] studied on the development of a detailed kinetic model of hydrocracking of vacuum gas oil. Seven lumps was generated according to temperature ranges and these lumps are sulfur compounds which are assumed to be a heavy lump, heavy and light aromatics, naphthenes, and paraffins.

A kinetic model of a trickle bed reactor for a first order hydrocracking reactions was developed by Yui and Sanford [80] and simulated under different operating conditions. The feedstock was heavy oil and feed and liquid products were distilled into naphtha, LGO, and HGO.

An industrial pseudo-homogeneous hydrocracking reactor model for a feedstock of vacuum gas oil was investigated by Mohanty et al. [81] by lumping into 23 pseudocomponents. Each pseudocomponent was described by its boiling range and specific gravity and the reaction order was taken as first order. The estimated parameters were evaluated against the literature data and plant data. It was observed that the results of the simulation of the model were satisfactorily well when validated with plant data.

Laxminarasimhan, Verma and co-workers have modeled hydrocracking reactions by using continuous lumping theory [42]. They derived yield distribution function from literature data and they presented the yield distribution function in skewed Gaussian form. They reported good agreement between experimental and model yields.

First-order kinetic models were investigated for Maya residue hydrocracking by Callejas and Martínez [82]. The models included atmospheric residuum (AR), light oils (LO), and gases as lumps.

A model for the hydrocracking of hydrogenated vacuum gas oil in which the reaction mechanism was described by a set of single events was developed by Martens and Marin [83]. Computational tools were used to write the algorithm for generating the reaction networks.

A single-lumped kinetic model of hydrotreating and hydrocracking was studied by Aoyagi et al. [84] to investigate the influence of feed specifications on product yield by using discrete lumping approach. The case studies were feedstocks with different properties which were prepared from gas oils, coker gas oils, and gas oils derived from Athabasca bitumen. In this system, there were two reactors in series, the first reactor was assumed to be hydrotreater and hydrocracking is the main reaction in the second reactor.

A kinetic model for hydrocracking of heavy oils was studied by Sanchez et al. [85] and they successfully applied lumping technique which consists of five lumps: unconverted residue, vacuum gas oil, distillates, naphtha and gases. Maya heavy oil was studied in a fixed-bed reactor to obtain experimental results and these results were used to calculate model parameters.

The continuous hydrocracking model developed by Laxminarasimhan and co-workers [42] was extended by Khorasheh et al. and Ashuri et al. [86, 87] to model hydrocracking, hydrodesulfurization and hydrodenitrogenation. And Arrhenius equation was employed to observe the effect of temperature on model parameters.

Bhutani et al. [20] developed a kinetic model for an industrial hydrocracking reactor by applying discrete lumping approach and using the available industrial data. He divided the feedstock and products into pseudocomponents in HYSYS and he aimed to find a range of optimal solutions by multi-objective optimization.

Another kinetic model for a pilot trickle bed reactor hydrocracking of heavy oils was studied by Sanchez and Ancheyta [88] which consists of five lumps: gases naphtha, middle distillates, vacuum gas oil and residue. The reactions were assumed to be second order. Various operating conditions were employed to collect experimental data. The error between the estimations and the model were insignificant and a good agreement was concluded.

A method to describe the hydrocracking feedstock as a continuous mixture was developed by Govindhakannan and Riggs [89]. The results observed from the study were successful.

Elizalde et al. [31] developed a kinetic model for a moderate hydrocracking reactor of heavy oil by applying continuous lumping approach. An isothermal fixed bed hydrocracking reactor was simulated under different operating conditions to gather experimental data. The results obtained by simulating the reactor with optimized parameters were in a good agreement with the experimental data.

A kinetic model of a pilot reactor for the hydrocracking of vacuum gas oil was investigated by Sadighi et al. [90] and different operating conditions were employed. Discrete lumping approach was applied and five lumps were generated to describe the yield of hydrocracking reactions.

Sildir et al. [91] developed a kinetic model for an industrial hydrocracking unit by applying continuous lumping approach. The model was simulated for non-isothermal operation and steady-state and dynamic simulations were investigated to predict product yields and reactor temperatures in addition to hydrogen consumption. The model predictions were in a good agreement with the plant data.

In this study, we propose a pseudo-homogeneous steady-state non-isothermal model for hydrodesulfurization and hydrocracking reactions in industrial trickle-bed hydroprocessing reactors. The feedstock is blended diesel and reaction mixture is treated as a single-

phase(liquid) continuous mixture by applying continuous lumping approach for both hydrodesulfurization and hydrocracking reactions. The initial sulfur distribution is assumed to be uniform distribution differently from the studies in the literature. The first principle HDS and HC models include adjustable parameters and these parameters are estimated by plant data. The results of the model agreed well with the plant data.

Chapter 3

DHP PLANT AND CHARACTERIZATION OF PETROLEUM FRACTIONS

3.1. DHP Process Configuration

The industrial diesel hydroprocessing (DHP) plant of interest in this study is shown in Figure 3.1.

The diesel hydrotreater unit is designed to process 4500 cubic meters per day of diesel feedstock. The process consists of a blending system followed by four catalytic reactor beds; two hydrodesulfurization beds followed by a hydrocracking bed and the last bed is designed for dewaxing processes. The feed to the first bed of reactors is obtained by blending four streams: HD (straight run heavy diesel), LD (straight run light diesel), LVGO (light vacuum gas oil) and a diesel from a tank. HD and LD streams are derived from crude distillation unit and LVGO stream is derived from vacuum distillation unit. These streams are blended to maintain a certain T95 value and flow rate (4500 cubic meters per day) for the reactor charge and sent to feed drum. The blended feed from the feed drum is then mixed with recycle hydrogen gas (Treat gas) and finally the feed enters the furnace where the feed is heated to the required temperature for the reactor inlet. Hydrodesulfurization occurs at high temperatures in the presence of hydrogen to produce higher-value hydrocarbon products with lower sulfur levels. In the first two HDS beds, the organic sulfur compounds are converted to hydrogen sulfide. Reactions are exothermic due to hydrogenation and products are cooled by hydrogen quench between beds. Hydrocracking

(HC) occurs in the third bed. The presented model covers the days of operation when the last bed was inactive. The reactor product is next separated into useful products such as diesel and naphta that meet certain specifications including sulfur, density, distillation (ASTM D86 95 Vol.%) and polycyclic aromatics.

The main operational objective is to meet the product specifications especially specification of 10 weight ppm sulfur in the diesel product by running the reactor under optimal operating conditions.

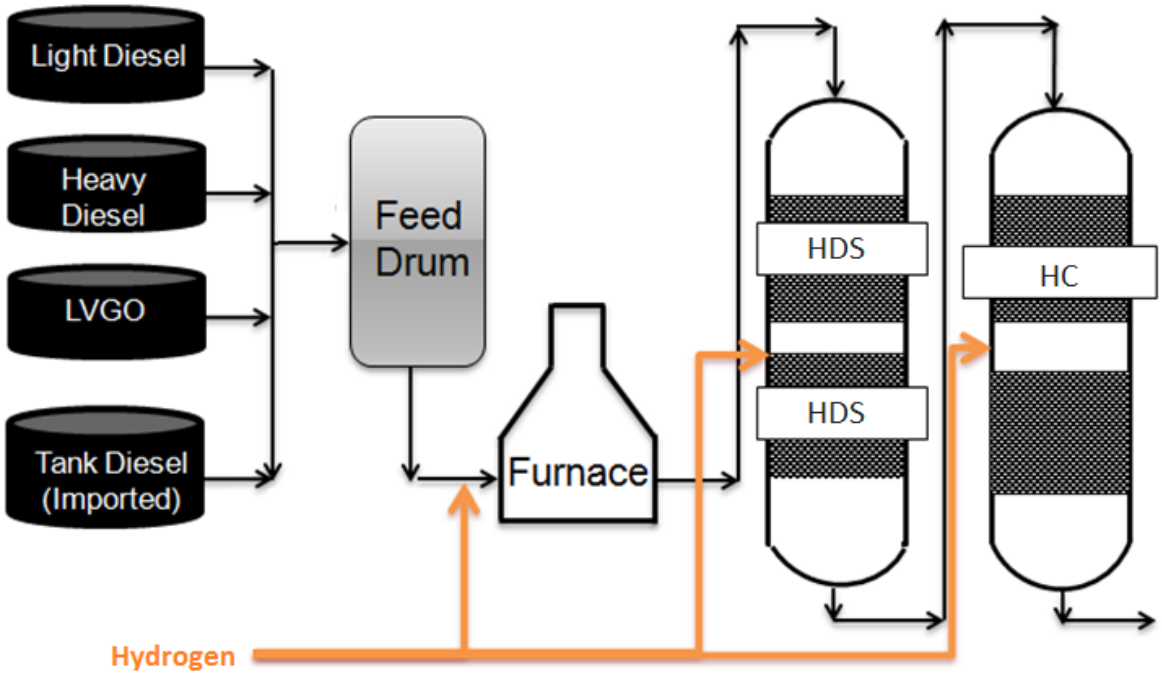

Figure 3.1: Simplified DHP plant flowsheet

In this research, we present a steady-state DHP model that includes the first two HDS beds and the last HC bed developed by applying continuum lumping approach. The model can be easily changed to accommodate the last bed when it is needed.

3.2. Characterization of Petroleum Fractions

In refinery operations, it is very important to understand the compositions and thermophysical properties of crude oil and petroleum fractions. Since it is difficult to determine each individual component, crude assay is used to characterize the petroleum. In general, the properties given are the boiling temperatures as a function of fractions distilled and bulk properties such as specific gravity, sulfur content, nitrogen content, metal content, C/H ratio, pour point, flash point, freeze point, smoke point, aniline point, viscosity and refractive index [92].

A typical assay example from industrial data used in this study is given in the Table 3.1 below;

Table 3.1: Plant Assay Example on 07.01.2014

	DHP FEED DRUM
API	34.0
S (w%)	1.31
distillation type	**D86**
ASTM IBP , ˚C	205
5 vol% , ˚C	227
10 vol% , ˚C	247
30 vol% , ˚C	278
50 vol% , ˚C	303
70 vol% , ˚C	328
90 vol% , ˚C	365
95 vol% , ˚C	386
ASTM FBP , ˚C	401

API (American Petroleum Institute) gravity is used to define the specific gravity (SG) of the crude oil as API = (141.5/SG) – 131.5. Specific gravity is the ratio of the density of the crude oil to the density of water both at 15.6 °C (60 °F). Heavier the crude is smaller the API. Very heavy crudes have API less than 10 and light crudes have API bigger than 40 [92].

Sulfur content is defined as a percent sulfur by weight and varies from less than 0.1% to bigger than 5% depending on the type and source of crude oils [92].

True boiling point (TBP) curve is one of the most common ways to approximate the composition of crude oil. For this method, a batch distillation column is used with a specified number of plates and reflux amount. The TBP curve is temperature versus liquid

volume distilled and any temperature on this curve represents the temperature of the hydrocarbon component which has the true boiling point at given volume percent distilled.

The initial boiling point (IBP) is the temperature at which the first drop of liquid leaves the condenser tube of the distillation apparatus while the final boiling point (FBP) is the highest temperature observed [92].

Since TBP distillation method is time consuming and requires labor, a faster distillation method which employs a batch distillation procedure with no trays or reflux developed by the American Society for Testing and Materials (ASTM). ASTM distillation is a standard test method for distillation of petroleum products at atmospheric pressure. ASTM distillation tests are conducted instead of TBP distillation tests and ASTM boiling point curve is converted into TBP curve by using correlations in the API technical data book-petroleum refining [93].

The most common ASTM test methods are ASTM D86, ASTM D1160 (atmospheric distillation), ASTM D1160 (vacuum distillation) and ASTM D2887 (chromatographic simulation). The ASTM D86 distillation of an oil fraction takes place at laboratory room temperature and pressure.

An example of a TBP curve which is derived from the industrial ASTM distillation data is given in Figure 3.2.

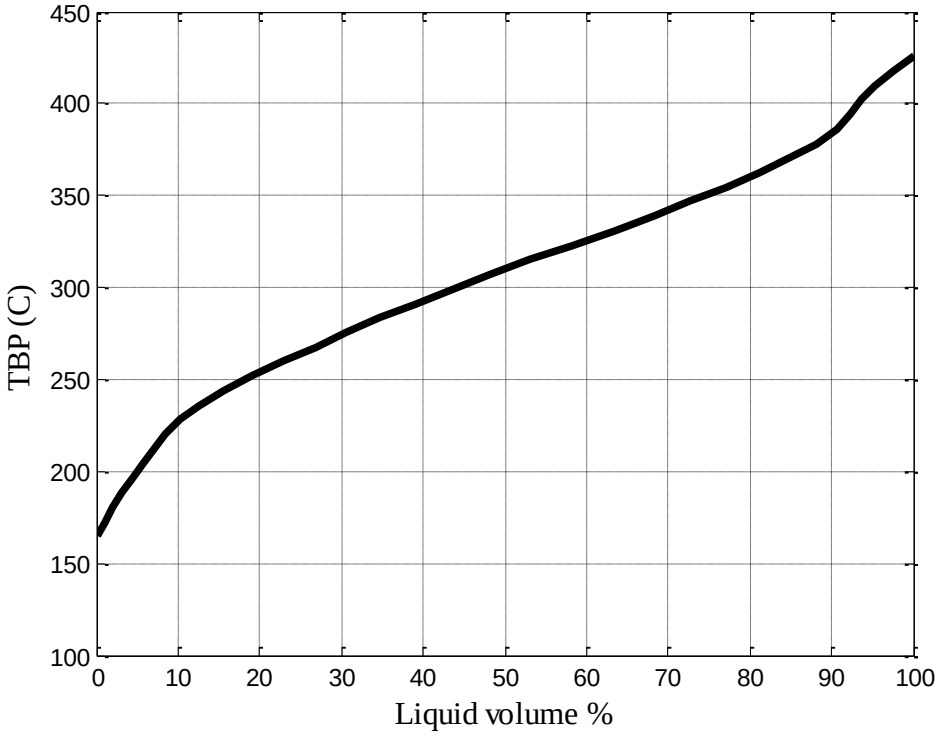

Figure 3.2: TBP Distillation Curve on 07.01.2014

3.2.1. Pseudocomponent Generation and Properties Estimation

Construction of a pseudocomponent scheme is a necessary task to characterize the complex petroleum mixture since a large number of lumps are generated for modeling the unit by continuous lumping approach in this study. These lumps are generated based on boiling point ranges.

ASTM D86 distillation information can be converted into TBP distillation data by ASPEN HYSYS Oil Manager which also uses the interconversion methods published in API Technical Data Book [93]. To do this, a crude assay is created and light ends are

ignored. The necessary boiling point data that corresponds to some specified volume fractions is entered and pseudocomponents are generated automatically. It is also possible to generate a specified number of cuts and specify the range between the cuts e.g. 10 ˚C which means that the first pseudocomponent is between IBP and IBP+10 ˚C.

Alternatively, a MATLAB code is generated which employs one of the interconversion methods between ASTM D86 and TBP distillation data which is published in API Technical Data Book [93]. Furthermore, MATLAB code is extended to a version that generates pseudocomponents with a specified cut range and calculates the properties of the pseudocomponents by using the related correlations which published in API Technical Data Book [93] . Since an interface is developed for simulation purposes, development of MATLAB code is preferred instead of using ASPEN HYSYS in this study.

There are a few methods for conversion of ASTM D86 into TBP distillation and the interconversion method used in the code is known as Daubert's method or API 1994 method since Daubert [94] has developed this method and published in the 1994 API Technical Data Book. The method has the following equations for conversion [95];

$$
\begin{aligned}
&T'_{50} = A_4.(T_{50})^{B_4} \\
&T'_{30} = T'_{50} - \Delta T'_3 \quad \Delta T_3 = T_{50} - T_{30} \\
&T'_{10} = T'_{30} - \Delta T'_2 \quad \Delta T_2 = T_{30} - T_{10} \\
&T'_i = T'_{10} - \Delta T'_1 \quad \Delta T_1 = T_{10} - T_i \\
&T'_{70} = T'_{50} + \Delta T'_5 \quad \Delta T_5 = T_{70} - T_{50} \\
&T'_{90} = T'_{70} + \Delta T'_6 \quad \Delta T_6 = T_{90} - T_{70} \\
&T'_{95} = T'_{90} + \Delta T'_7 \quad \Delta T_7 = T_f - T_{90} \\
&\Delta T'_i = A_i.(\Delta T_i)^{B_i}
\end{aligned}
\tag{3.1}
$$

where

T_i' = TBP temperature at initial point [°F]

T_f' = TBP temperature at final point [°F]

T_n' = TBP temperature at n % volume distilled [°F]

T_n = D86 temperature at n % volume distilled [°F]

A_i and B_i are coefficients given in Table 3.2.

Table 3.2: Constants for Daubert's Distillation Curves Interconversion Method [95]

Index number i	A_i	B_i
1	7.4012	0.6024
2	4.9004	0.7164
3	3.0305	0.8008
4	0.8718	1.0258
5	2.5282	0.8200
6	3.0419	0.7750
7	0.1180	1.6606

After converting the ASTM data into TBP curve, the second step is to cut the entire boiling range into a specified number of cut-point ranges to define pseudocomponents. The number of cuts can be determined arbitrarily and the cuts can be constructed on a specified width basis such as 10˚C.

Normal boiling point temperature is the average boiling temperature of the pseudocomponent and is calculated by

$$T_{b,i} = \frac{ICP_i + FCP_i}{2} \tag{3.2}$$

where ICP_i is the initial boiling point of the pseudocomponent while FCP_i is the final boiling temperature of the pseudocomponent.

Once the petroleum mixture has been divided into pseudo-components, the next step is the estimation of the density distribution of each pseudocomponent to characterize further. For estimation of the densities of each pseudocomponent, bulk density information must be available.

First, Watson-Murphy characterization factor or K factor is assumed to be constant throughout the entire boiling range and the average value of K_W must be determined as [96]:

$$K_w^{avg} = \frac{(1.8T_{avg})^{1/3}}{SG_{avg}} \tag{3.3}$$

where the average specific gravity is given as bulk value. The average boiling temperature of the petroleum fraction can be computed from the equation [96]

$$T_{avg} = \frac{T_{b(10\%v)} + 2T_{b(50\%v)} + T_{b(90\%v)}}{4} \tag{3.4}$$

After calculating the average boiling point of the crude, average Watson factor can be calculated and used to calculate the density distribution of the entire boiling range:

$$SG_i = \frac{(1.8T_{b,i})^{1/3}}{K_w^{avg}} \tag{3.5}$$

where SG_i is the specific gravity 60 °F/60 °F of pseudocomponent i and $T_{b,i}$ is the normal boiling point of pseudocomponent i [96].

Since the mass fractions of the pseudocomponents are also required as a model input, the volume fractions must be converted into mass fractions like below;

$$w_i = v_i \frac{SG_i}{SG_{avg}} \tag{3.6}$$

Estimation of the required properties such as molecular weight, critical temperature and critical pressure distributions can be computed from the correlations in the literature.

An example of feed characterization in MATLAB is given for a selected day in the table below.

Table 3.3: Physical Properties of the Pseudocomponents of Feed (07.01.2014)

pseudocomponent number	TBP	NBP	liquid volume %	SG	weight fraction %
1	164.6907	164.6907	0	0.664139	0
2	172.6044	168.6475	0.009842	0.779591	0.007645
3	180.5181	176.5613	0.01072	0.784218	0.009832
4	188.4318	184.475	0.011492	0.788791	0.010602
5	196.3456	192.3887	0.01216	0.793312	0.011283
6	204.2593	200.3024	0.012564	0.797782	0.011723

7	212.173	208.2162	0.012748	0.802202	0.011961
8	220.0867	216.1299	0.014427	0.806575	0.01361
9	228.0005	224.0436	0.017789	0.8109	0.016872
10	235.9142	231.9573	0.02391	0.81518	0.022797
11	243.8279	239.8711	0.030121	0.819415	0.028868
12	251.7416	247.7848	0.034722	0.823607	0.033448
13	259.6554	255.6985	0.037713	0.827756	0.036511
14	267.5691	263.6122	0.039092	0.831865	0.038035
15	275.4828	271.526	0.038931	0.835933	0.038064
16	283.3966	279.4397	0.040767	0.839962	0.040051
17	291.3103	287.3534	0.043569	0.843953	0.043007
18	299.224	295.2671	0.045519	0.847906	0.045142
19	307.1377	303.1809	0.046616	0.851823	0.046444
20	315.0515	311.0946	0.048031	0.855704	0.048071
21	322.9652	319.0083	0.051645	0.859551	0.051921
22	330.8789	326.922	0.052055	0.863363	0.052565
23	338.7926	334.8358	0.048799	0.867141	0.049492
24	346.7064	342.7495	0.043869	0.870888	0.044685
25	354.6201	350.6632	0.043496	0.874602	0.044494
26	362.5338	358.5769	0.041715	0.878285	0.042852
27	370.4475	366.4907	0.037837	0.881937	0.03903
28	378.3613	374.4044	0.031863	0.885559	0.033002
29	386.275	382.3181	0.023835	0.889152	0.024788
30	394.1887	390.2318	0.016527	0.892716	0.017256
31	402.1024	398.1456	0.014242	0.896252	0.01493
32	410.0162	406.0593	0.01727	0.89976	0.018174
33	417.9299	413.973	0.021671	0.903241	0.022894
34	425.8436	421.8867	0.024444	0.906695	0.025922

Chapter 4

MODELING OF HYDRODESULFURIZATION REACTOR

4.1. Introduction

Hydrotreating and hydrocracking units are trickle bed reactors in which the liquid phase consists of blended gas oil feed; hydrogen is in the gas phase and the catalyst constitutes the solid phase. Pseudo-homogeneous models have been widely reported in the literature due to their reliability and simplicity. A pseudo-homogeneous model assumes that there are no diffusional resistances. We use a single-phase (liquid) pseudo-homogeneous model. We further assume that only hydrodesulfurization occurs in beds 1 and 2 and only hydrocracking occurs in bed 3.

In this chapter, modeling studies for the hydrodesulfurization reactions in the first two beds are presented.

4.2. Generation of Feed Sulfur Curve

As mentioned before, the petroleum mixture is complex mixture which consists of large numbers of components such as organosulfur, organonitrogen or aromatic species. The feedstock under investigation in this study is a blend of gas oils and therefore it is difficult to perform kinetic studies which take into account each compound and all possible reactions. Instead the oil mixture can be treated as a continuum [27].

Since the continuous lumping approach requires an intrinsic property to characterize the reaction mixture as continuum, true boiling point (TBP) is chosen. Normalized TBP defined as follows;

$$\theta = \frac{TBP - \min(TBP)}{\max(TBP) - \min(TBP)} \tag{4.1}$$

where *min(TBP)* is the lowest TBP (Initial Boiling Point) and *max(TBP)* is the highest TBP (Final Boiling Point) in the fraction.

Organo-sulfur compounds exist in various forms and can be classified as

(a) Mercaptans
(b) Sulfides
(c) Disulfides
(d) Thiophenes
(e) Benzothiophenes
(f) Dibenzothiophenes & substituted dibenzothiophenes

and their existence in the oil mixture depends upon boiling range and type of mixture. Diesel fractions contain mainly all the sulfur compounds but mostly benzothiophenes, dibenzothiophenes and substituted dibenzothiophenes [49, 97]. Sulfur removal difficulty increases in the following order: paraffins < naphthenes < aromatics. The reactivity of the sulfur compounds decreases in the same order [11]. Figure 4.1 shows the trend of reactivities and types of sulfur compounds present in different petroleum fractions.

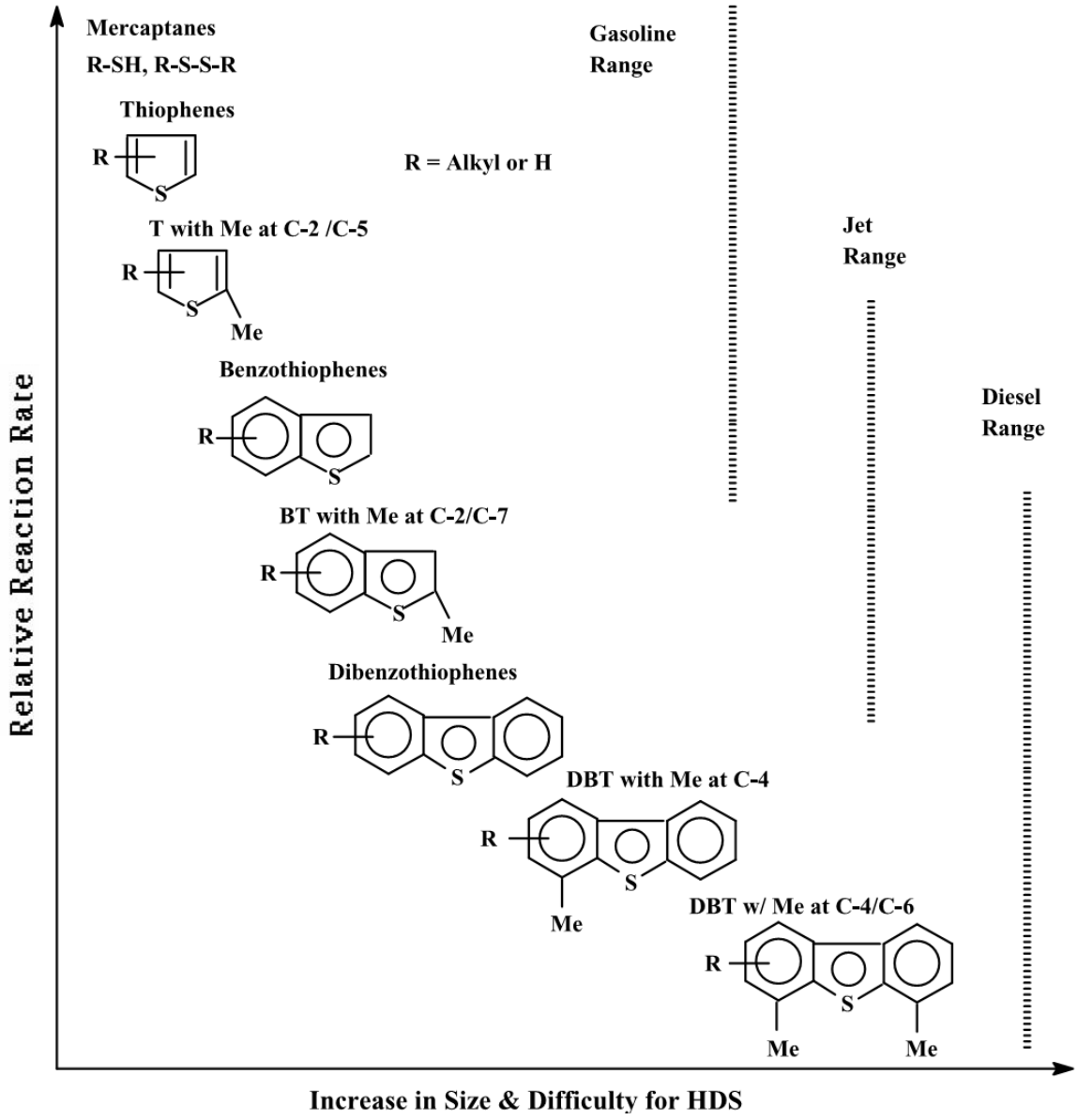

Figure 4.1: Impact of sulfur species [97]

The reactivity can be represented as a function of θ as follows;

$$k=k(\theta) \tag{4.2}$$

In our model the reaction rate constant for hydrodesulfurization is parameterized in terms of the normalized TBP to cover the range of all possible sulfur compounds:

$$k = k_{\min} - k_{\max} \ln[e^{-1} - (e^{-1} - 1)\theta^{\frac{1}{\beta}}] \tag{4.3}$$

where $k_{\min}$, $k_{\max}$ and β are adjustable (to be estimated) parameters. This relationship has been derived by Sau et al. [49] and obtained from experimental information of model compounds. Figure 4.2 shows the change in the reactivity along the boiling point according to the reactivity equation 4.3 above.

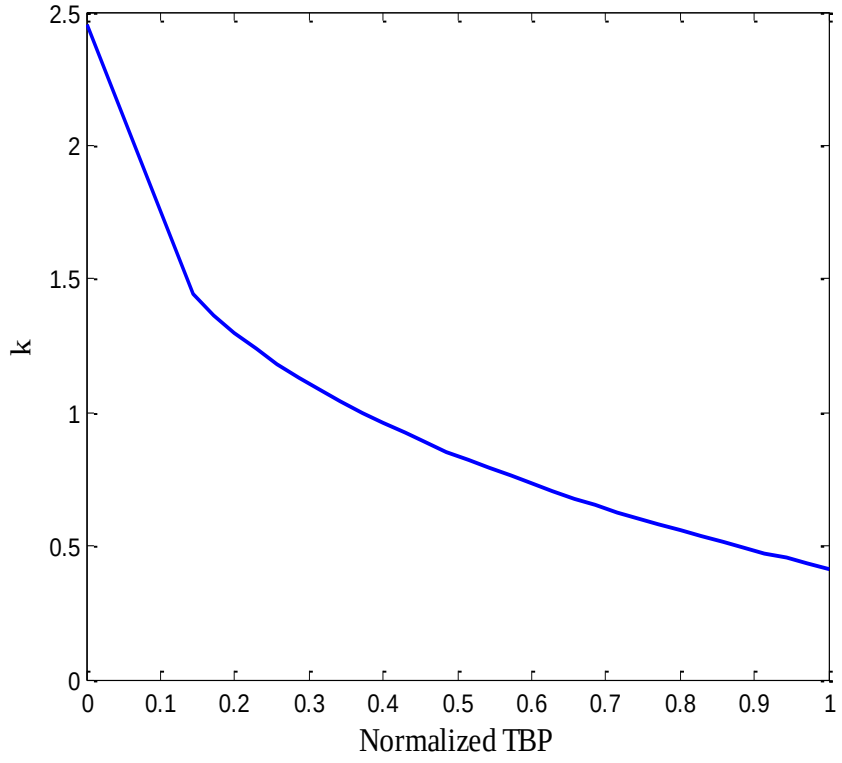

Figure 4.2: Hydrodesulfurization rate constant versus TBP

As seen from the Figure 4.2, equation 4.3 indicates that the reactivity of sulfur compounds decreases monotonically as true boiling point of pseudocomponents increases. This means that the most reactive sulfur compounds present in light fractions and heavy cuts contain the most refractive compounds.

$C_s(\theta, z, t)d\theta$ indicates weight fraction of sulfur compounds present within Θ & Θ+$d\Theta$ at time t and axial position z. The total or bulk sulfur weight percent then becomes [49]:

$$C_s^{total}(z,t) = \int_{k_{min}}^{k_{max}} C_s(\theta,z,t)d\theta \tag{4.4}$$

It would be mathematically consistent to formulate the model equation in k plane rather than θ plane. Therefore [49]

$$C_s(\theta,z,t)d\theta = c_s(k,z,t)D(k)dk \tag{4.5}$$

where D(k) is species type distribution function and D(k)dk describes the number of species between *k* and *k*+*dk*. D(k) for the hydrodesulfurization reactions may be written as give reference

$$D(k) = N.\frac{d\theta}{dk} = N.\left(\frac{\beta}{(1-e^{-1})^{\beta}}\right).\left(e^{-\frac{(k-k_{min})}{k_{max}}} - e^{-1}\right)^{(\beta-1)}.\left(e^{-\frac{(k-k_{min})}{k_{max}}}\right).\left(-\frac{1}{k_{max}}\right) \tag{4.6}$$

Since the total sulfur weight percent at time t and axial position z is defined as,

$$C_s^{total}(z,t) = \int_{k_{min}}^{k_{max}} C_s(\theta,z,t)d\theta \tag{4.7}$$

The equation becomes the following form in k plane;

$$C_s^{total}(z,t) = \int_{k_{min}}^{k_{max}} c_s(k,z,t)D(k)dk \tag{4.8}$$

As seen from the equation above, the model requires the sulfur distribution of the feed as input. Some of the sulfur distribution data obtained from the plant laboratory analysis is shown in Table 4.1 below.

Table 4.1: Plant Sulfur Distribution Data for Selected Days

	w% sulfur			
	20 vol%	**50 vol%**	**95 vol%**	**100 vol% (bulk)**
21.11.2013	0.46	0.608	1.119	1.182
28.11.2013	0.43	0.55	0.87	1.115
19.12.2013	0.43	0.635	0.931	1.170
07.01.2014	0.47	0.75	1.056	1.310
09.01.2014	0.43	0.68	1.04	1.146
14.01.2014	0.47	0.65	1.04	1.121
16.01.2014	0.5	0.66	1.05	1.282
23.01.2014	0.51	0.66	1.05	1.240
30.01.2014	0.45	0.7	1.021	1.296

Sulfur distribution data obtained from the plant is processed first as beta distribution to construct the cumulative sulfur curve (see Figure 4.5-4.10) since the shape of the cumulative sulfur distribution looks similar to cumulative beta distribution function.

The beta distribution has the general formula for the probability density function [98]:

$$P(x) = \frac{(x-a)^{p-1}(b-x)^{q-1}}{B(p,q)(b-a)^{p+q-1}} \qquad a \le x \le b;\ p,q > 0 \tag{4.9}$$

where *p* and *q* are the shape parameters, *a* is the lower bound and *b* is the upper bounds of the distribution. *B*(*p*,*q*) denotes the beta function. The formula of the beta distribution is

$$B(\alpha,\beta)=\int_0^1 t^{\alpha-1}(1-t)^{\beta-1}dt \tag{4.10}$$

The distribution is normalized since

$$\int_0^1 P(x)dx=1 \tag{4.11}$$

Figure 4.3 shows the plots of the beta probability density functions with different values of the shape parameters.

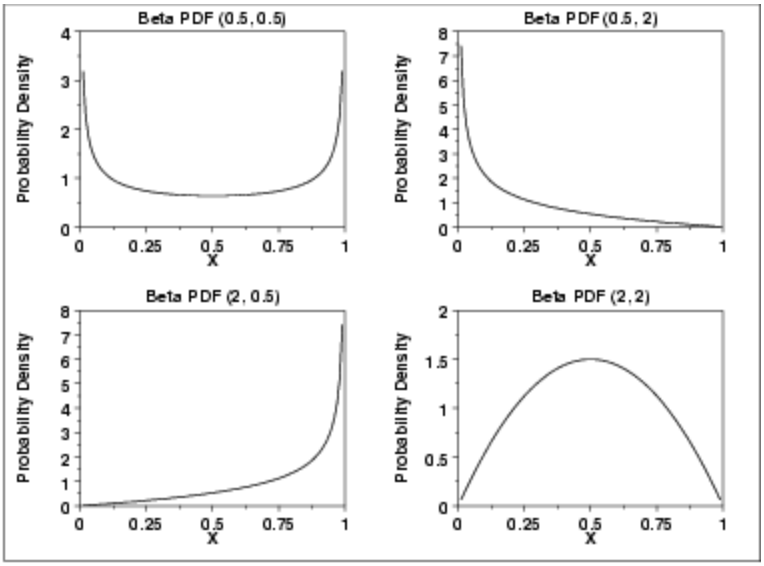

Figure 4.3: Examples of beta probability distribution functions [98]

The cumulative distribution function of the beta distribution is defined as

$$F(x) = I_x(p,q) = \frac{1}{B(p,q)} \int_0^x t^{p-1}(1-t)^{q-1} dt \qquad 0 \le x \le 1;\ p,q > 0 \tag{4.12}$$

where $B(p,q)$ denotes the beta function [98]. Figure 4.4 shows the plots of the beta cumulative distribution functions with the same shape parameters as probability plots in Figure 4.3 the shape parameters.

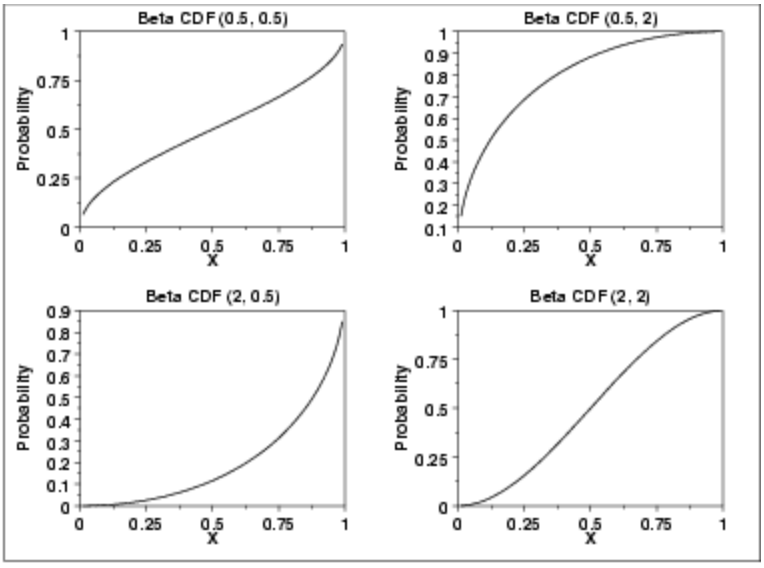

Figure 4.4: Examples of beta cumulative distribution functions [98]

The cumulative beta distribution is implemented in MATLAB as ‘‘ betacdf ’’. And the best cumulative beta distribution which passes through the plant sulfur distribution is fitted by nonlinear regression analysis. Plant sulfur distribution measurements is taken for a period of time. Feed characterization is performed for these days’ feed. Beta distributed

sulfur curves are generated for the days which have a sulfur distribution throughout the speficied liquid volumes. Examples of feed sulfur distributions for month January are given in the figures below;

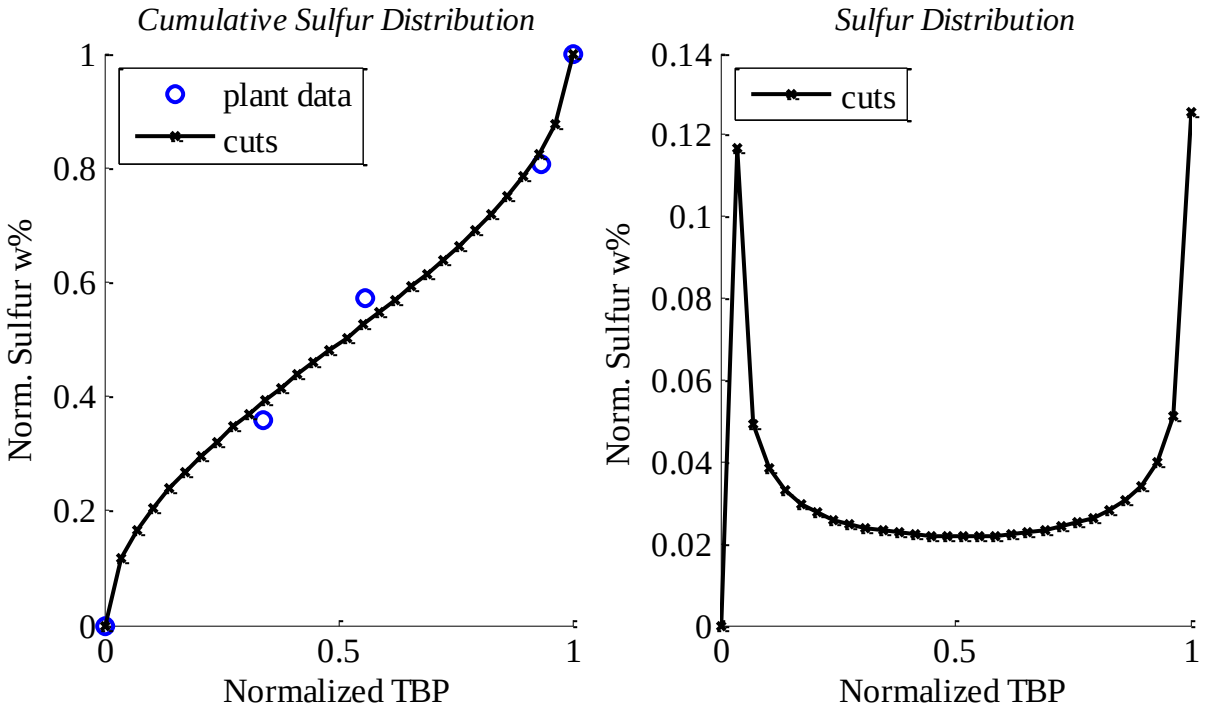

Figure 4.5: Normalized beta sulfur distribution of feed on 07.01.2014

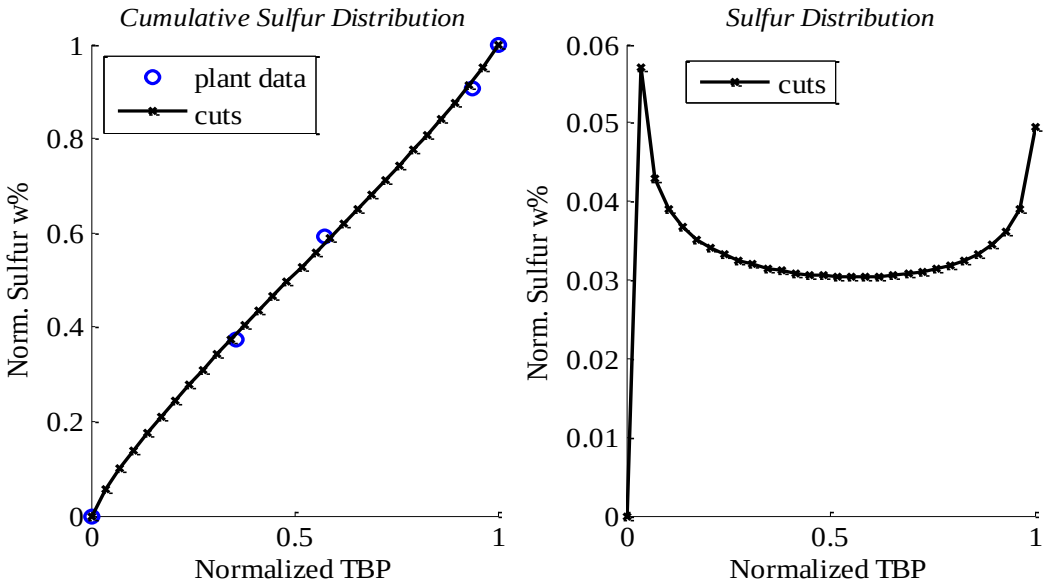

Figure 4.6: Normalized beta sulfur distribution of feed on 09.01.2014

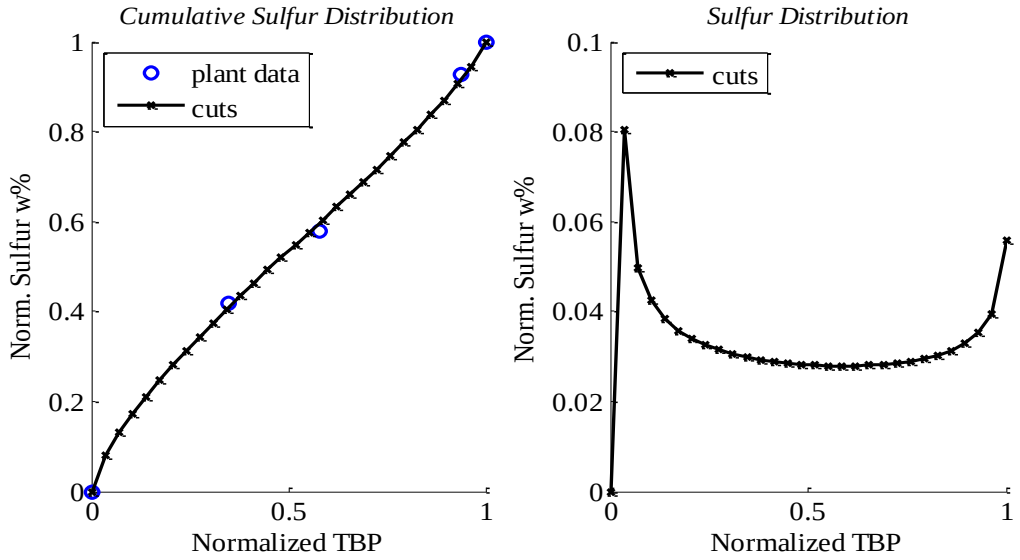

Figure 4.7: Normalized beta sulfur distribution of feed on 14.01.2014

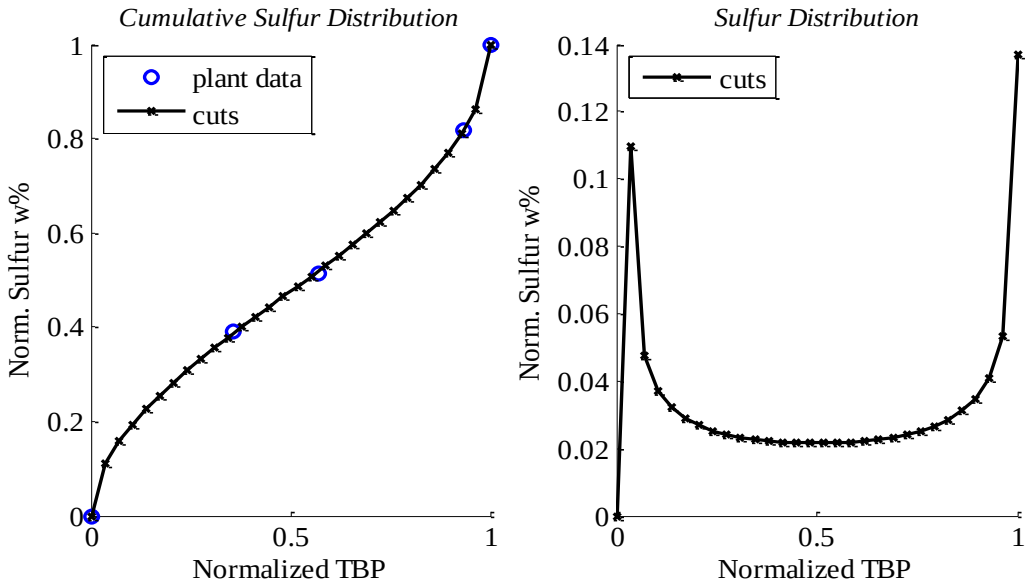

Figure 4.8: Normalized beta sulfur distribution of feed on 16.01.2014

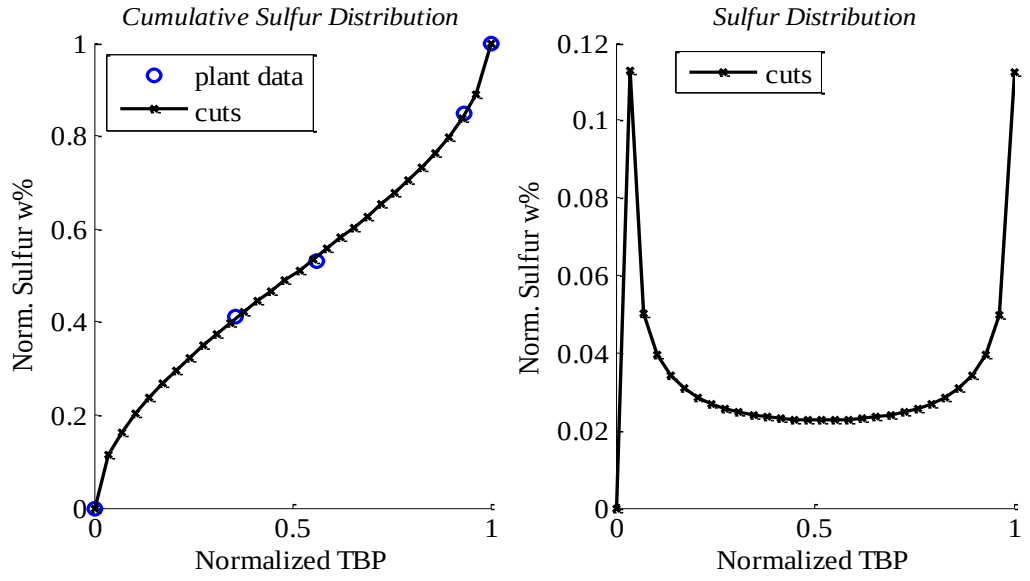

Figure 4.9: Normalized beta sulfur distribution of feed on 23.01.2014

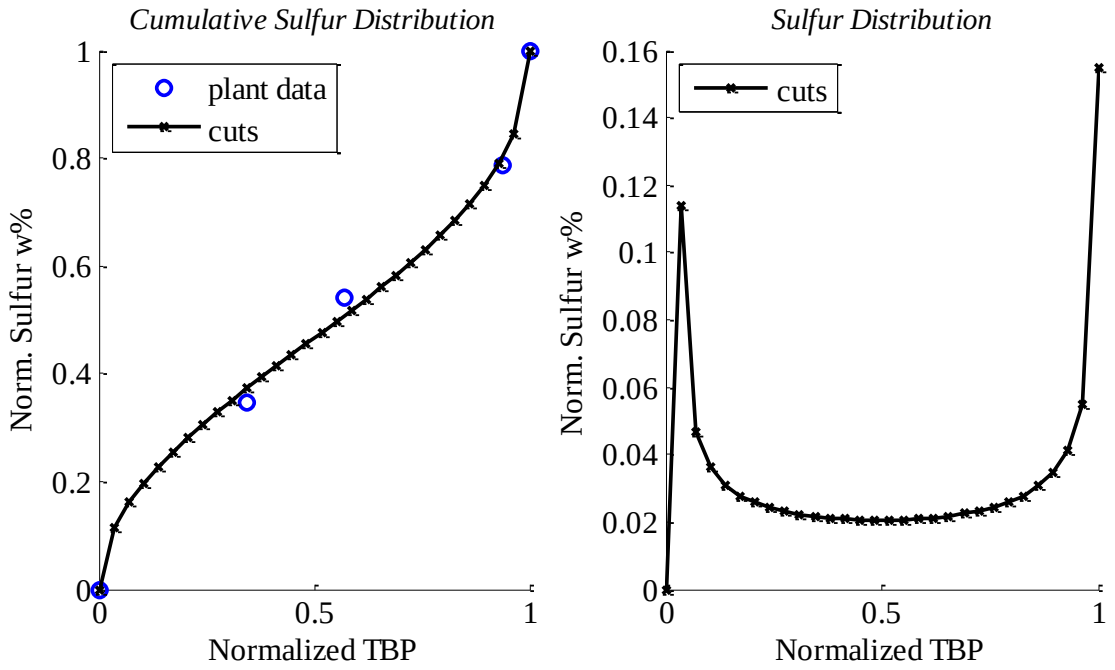

Figure 4.10: Normalized beta sulfur distribution of feed on 30.01.2014

Fitting a beta distribution to define the feed sulfur curve requires sulfur distribution measurements throughout some specified liquid volumes. These measurements must be taken on daily basis since each day can have different characteristics. This brings a problem of extra labor. So, sulfur distribution is assumed to be a uniform distribution. Uniform distribution assumes that the amount of organo-sulfur compounds are equal in each pseudocomponent and the cumulative sulfur curve is a linear curve which passes through the zero sulfur and bulk sulfur value along the boiling points. Therefore, fitting a feed sulfur curve only requires the bulk value of sulfur content. Uniform distribution is used for simulation of the model in the next chapters.

The uniform distribution has the general formula for the probability density function [98]:

$$f(x) = \frac{1}{B-A} \quad for\ A \le x \le B \tag{4.13}$$

where A is the location parameter and (B - A) is the scale parameter. Figure 4.11 is the plot of the uniform probability density function where the distribution is a standard uniform distribution with A=0 and B=1 for interval {0,1}.

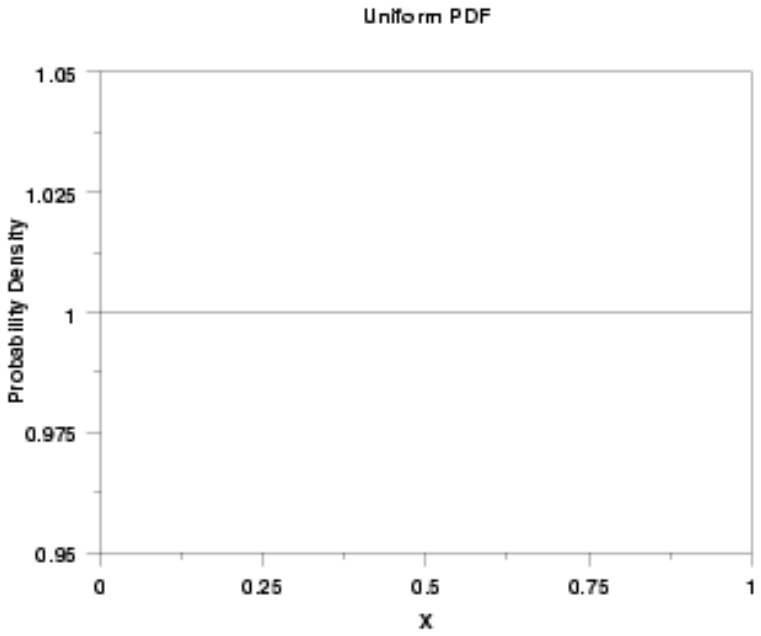

Figure 4.11: Standard uniform distribution [98]

The cumulative distribution function of the uniform distribution has the formula [98]:

$$f(x) = \frac{x}{B-A} \quad for\ A \le x \le B \tag{4.14}$$

Figure 4.12 represents the plot of the cumulative uniform distribution function where the distribution is a standard uniform distribution with A=0 and B=1 for interval {0,1}.

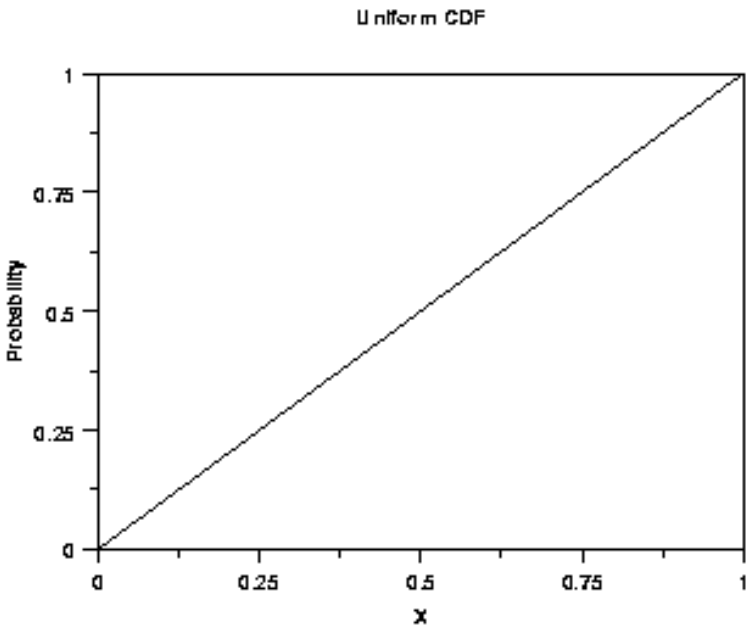

Figure 4.12: Cumulative standard uniform distribution [98]

The bulk sulfur weight percent measurements are taken daily in the plant and feed characterization is performed for each day's feed. Uniformly distributed sulfur curves are generated for the days which have a bulk sulfur weight percent measurement throughout the total liquid volume. Examples of feed sulfur distributions for month January are given in the figures below.

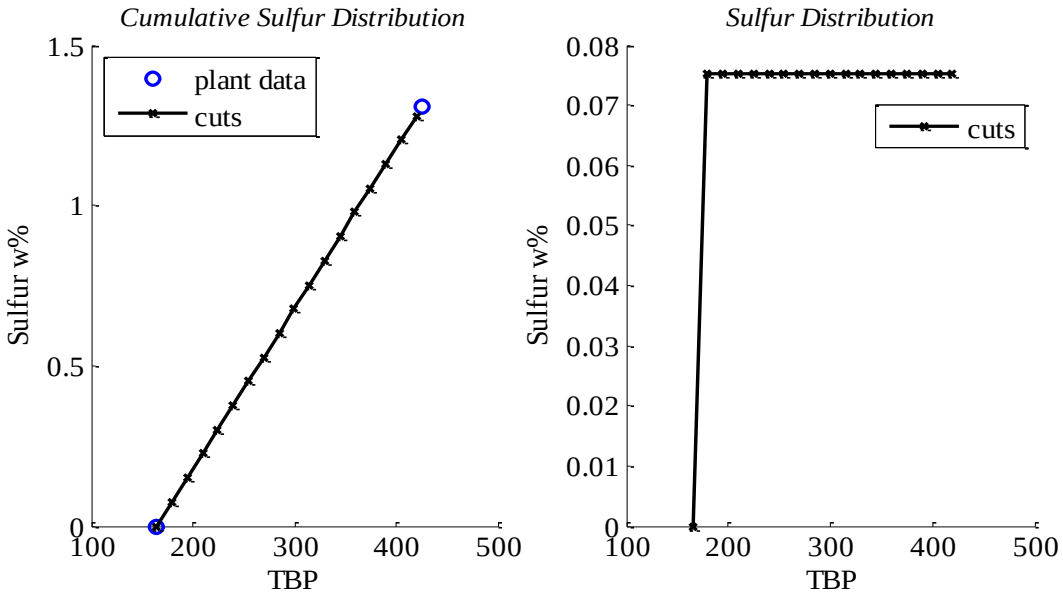

Figure 4.13: Uniform sulfur distribution of feed on 07.01.2014

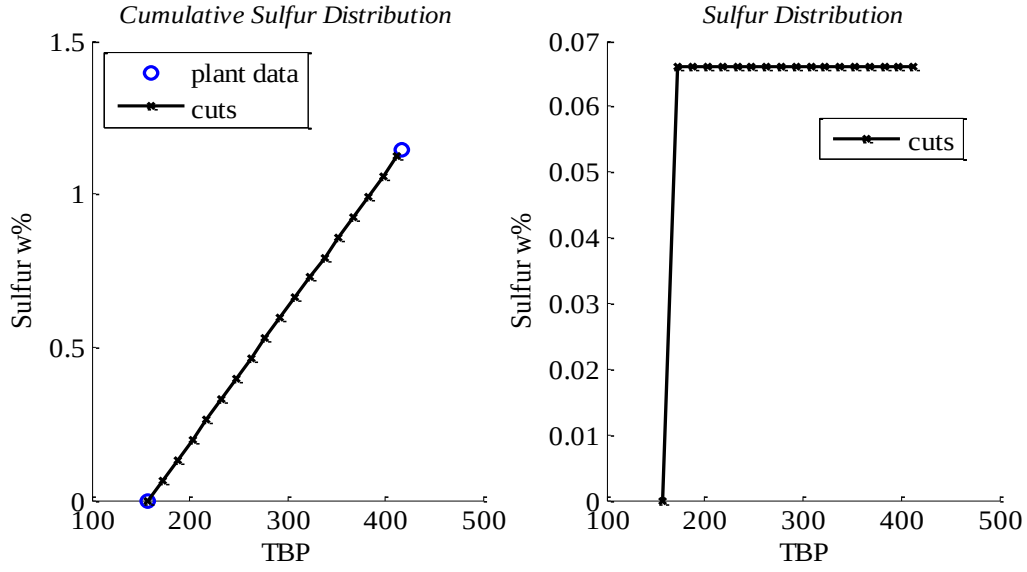

Figure 4.14: Uniform sulfur distribution of feed on 09.01.2014

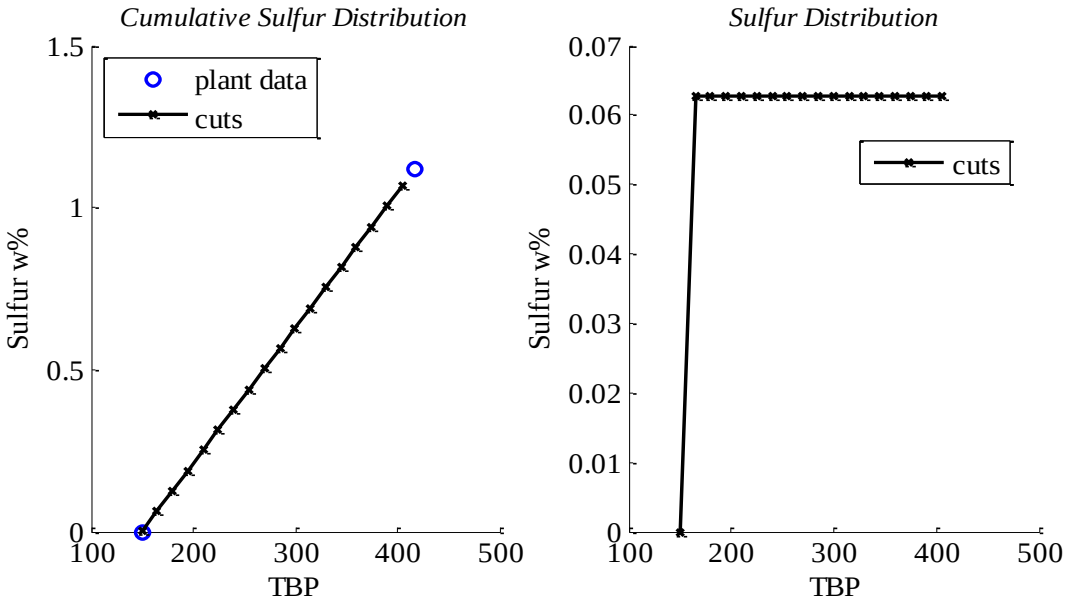

Figure 4.15: Uniform sulfur distribution of feed on 14.01.2014

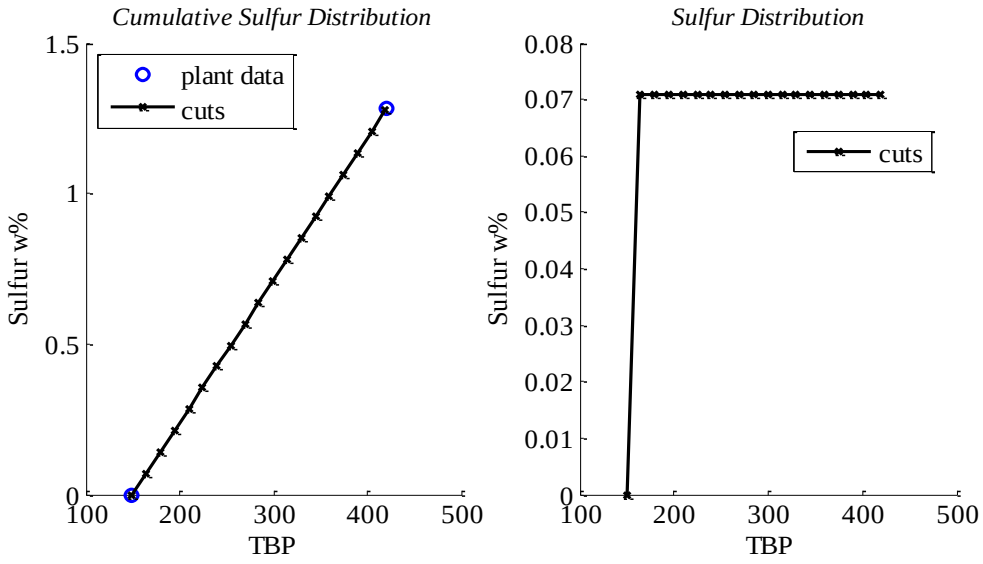

Figure 4.16: Uniform sulfur distribution of feed on 16.01.2014

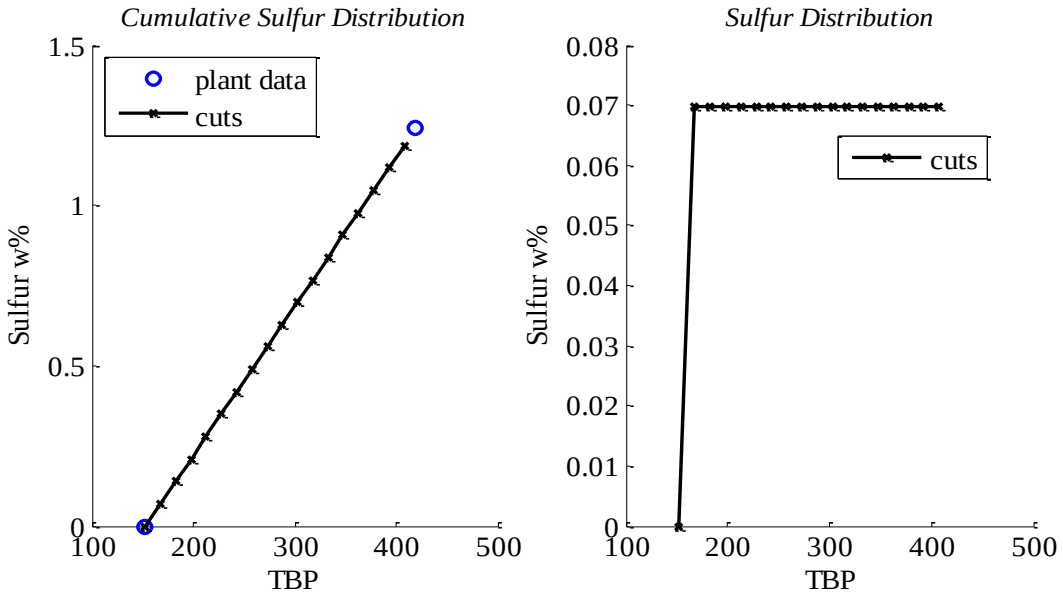

Figure 4.17: Uniform sulfur distribution of feed on 23.01.2014

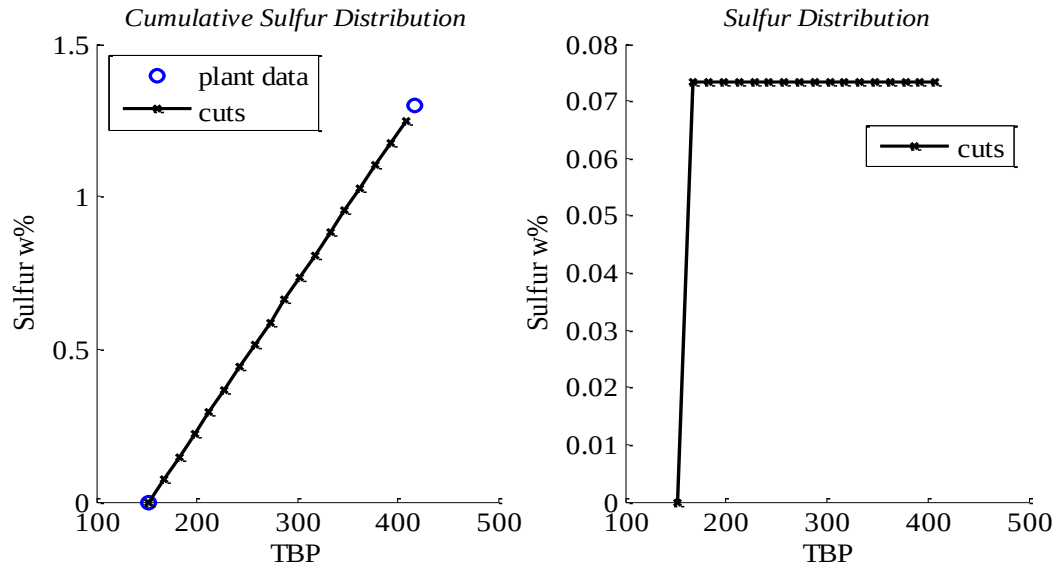

Figure 4.18: Uniform sulfur distribution of feed on 30.01.2014

4.3. Hydrodesulfurization Reactor Model (Beds 1 and 2)

Hydrodesulfurization reactor model covers the first two beds. As mentioned in Chapter 2, there are different approaches reported in the literature on modeling of hydrodesulfurization kinetics Most of the studies consider models first order or power law kinetics. There are also some studies that apply Langmuir - Hinshelwood (L-H) kinetics to account for hydrogen sulfide inhibition.

Some assumptions are made to simplify the complexity of the system;

- Organo-sulfur compounds are converted into sulfur-free hydrocarbon compunds and hydrogen sulfide in the presence of hydrogen as the following;

$$\text{Sulfur compounds} \xrightarrow{k_{HDS}} \text{Sulfur-free hydrocarbon compounds} + H_2S$$

  Power-law kinetics are applied and reaction order is considered as first-order since the previous studies reported the reaction order as 1 and at high conversion levels, desulfurization reactions follow first-order kinetics [27]. Most reactive sulfur compounds which have lower boiling points react earlier and these hydrodesulfurization reactions take place along first reactor thus more refractive sulfur compounds with higher boiling points remain to the second reactor. It is reported that the reactivities of the most reactive and the most refractive compounds are pretty different in the literature. Ma et al. [99] presented that the rate constants 0.636, 0.270, 0.118, 0.039, and 0.023 min.wt for fraction 1 (<280 ˚C), fraction 2 (280-300 ˚C), fraction 3 (300-320 ˚C), fraction 4 (320-340 ˚C) and fraction 5(>340 ˚C), respectively.

- Our model does not account for hydrogen sulfide inhibition since it requires additional parameters and it is difficult to verify from industrial data.

- The other hydrotreatment reactions such as HDN, HDO, HDA and hydrocracking of the pseudocomponents are assumed to be negligible.
- Steady-state operation is assumed.
- The reactor is assumed to operate under adiabatic conditions.
- The heat capacity value for feed and product is taken from ASPEN HYSYS Simulation Environment by simulating the crude array. Since the heat capacity values for the feed and product are approximately close, a constant heat capacity for feed and products is assumed.
- Heat of reaction is assumed to constant for each bed. An average value of heat of reaction represents the whole organo-sulfur mixture in each bed since the value of heat of reaction differs for hydrogenolysis reactions of individual organo-sulfur compounds and it is not possible to account for the reactions of all the sulfur compounds.
- Activation energy is assumed to be constant at an average value for each bed and has different values for bed 1 and bed 2 since each organo-sulfur compound has different reaction kinetics and the value of activation energy also changes for the reaction of each sulfur compound.
- Pseudo-homogeneous plug flow model is assumed. In this pseudo-homogeneous plug flow model, all pseudocomponents are assumed to exist in the liquid phase.
- Diffusional resistances are assumed to be negligible.

4.3.1. Mass Balance

Taking only HDS reactions of different sulfur compounds into consideration, material balance on species j at any instant in time, t yields the following equation in liquid phase within any system volume V:

$$\begin{bmatrix} \textit{Rate of flow} \\ \textit{of j into} \\ \textit{the system} \\ \textit{(moles/time)} \end{bmatrix} - \begin{bmatrix} \textit{Rate of flow} \\ \textit{of j out of} \\ \textit{the system} \\ \textit{(moles/time)} \end{bmatrix} + \begin{bmatrix} \textit{Rate of generation of} \\ \textit{j by chemical reaction} \\ \textit{within the system} \\ \textit{(moles/time)} \end{bmatrix} = \begin{bmatrix} \textit{Rate of accumulation} \\ \textit{of j within} \\ \textit{the system} \\ \textit{(moles/time)} \end{bmatrix}$$

$$F_{j_0} - F_j + \int_0^V r_j dV = \frac{dN_j}{dt} \tag{4.15}$$

where N_j represents the number of moles of species j in the system at time t, r_j is the rate of formation of species j and F_j represents the molar flow rate of species j. Since steady-state operation is assumed (conditions do not change with time),

$$\frac{dN_j}{dt} = 0 \tag{4.16}$$

The differential volume, ΔV, will be chosen sufficiently small such that there are no spatial variations in reaction rate within this volume. Thus,

$$F_j\Big|_V - F_j\Big|_{V+\Delta V} + r_j \Delta V = 0 \tag{4.17}$$

Dividing by ΔV and rearranging

$$\left[\frac{F_j\Big|_{V+\Delta V} - F_j\Big|_V}{\Delta V} \right] = r_j \tag{4.18}$$

Taking the limit ΔV approaches zero, the differential form of the steady state mole balance on a PFR.

$$\frac{dF_j}{dV} = r_j \tag{4.19}$$

The molar flow rate of species j, F_j can be written as below:

$$F_j = C_j.Q = C_j.A_c.v \tag{4.20}$$

where C_j is the concentration of species j given as moles per volume, Q is the volumetric flow rate, A_c is the cross-sectional area and v is the mass average velocity. And differential volume is given as:

$$dV = A_c.dz \tag{4.21}$$

where dz is the differential bed length. Assuming first-order kinetics, the mole balance becomes:

$$v\frac{dC_j}{dz} = -k.C_j \tag{4.22}$$

where C_j is the concentration of species j in unit of moles per volume. Converting the unit of concentration of sulfur species into normalized weight percent as follows:

$$c_s(k,z) = \frac{C_j(k,z)M_j}{\rho_j}\frac{m_f}{m_s} \tag{4.23}$$

where $c_s(k,z)$ is the normalized sulfur weight percent of fraction with reactivity k at axial position z, M_j is the molecular weight, ρ_j is the density, m_f is the mass flow rate of the feed and m_s is the mass flow rate of sulfur in the feed. The normalized sulfur weight percent of fraction with reactivity k is defined as:

$$c_s(k,z)dk = \frac{\dfrac{grams\ of\ S\ in\ fraction\ that\ has\ reactivity\ between\ k\ and\ k+dk}{grams\ of\ fraction}}{\dfrac{grams\ of\ fraction}{grams\ of\ total\ S\ in\ feed}} \tag{4.24}$$

The steady-state differential species mass balance becomes,

$$\frac{dc_s(k,z)}{dz} = -\frac{k}{v}c_s(k,z) = -k'c_s(k,z) \tag{4.25}$$

where $c_s(k, z)$ is the normalized sulfur weight percent of fraction with reactivity k at axial position z, dz is the differential bed length, v is the mass average velocity and k' represents the ratio of reactivity k to mass velocity, v.

Arrhenius relationship is considered to observe the effect of temperature on reactivity of sulfur compounds since the model is non-isothermal;

$$k = k_0 e^{-\frac{E_a}{R}(\frac{1}{T}-\frac{1}{T_0})} \tag{4.26}$$

where E_a is the activation energy in J/mol, k_0 is reactivity at some reference temperature T_0 which is inlet temperature in K and R is the gas constant which is 8.3144621 J/mol.K. After adding the effect of temperature, steady-state mass balance becomes,

$$\frac{dc_s(k,z)}{dz} = -k_0\, e^{-(E_a/R)((1/T)-(1/T_0))} c_s(k,z) \tag{4.27}$$

where

$$k_o = \frac{k_{\min}}{v} - \frac{k_{\max}}{v} \ln\left[e^{-1} - (e^{-1}-1)\theta^{\frac{1}{\beta}} \right] \tag{4.28}$$

with v is the average velocity, k_{min} is the minimum reactivity which shows the reactivity of the sulfur compound with highest boiling point and k_{max} is the maximum reactivity which shows the reactivity of the sulfur compound with the lowest boiling point and k_{min}, k_{max} and β are parameters to be estimated.

Because of the transformation between k and θ, pseudo-component in a particular TBP interval $d\theta$ can be thought of as a pseudo-component in a particular reactivity range dk.

4.3.2. Energy Balance

Similarly, differential steady-state energy balance in each bed is written as:

$$m_{oil}C_{p,oil}T_z - m_{oil}C_{p,oil}T_{z+\Delta z} + \int_0^{k_{max}} k_0\, e^{-(E_a/R)((1/T)-(1/T_0))} c_s(k,z)(-\Delta H_r^0) dV D(k) dk = 0 \quad (4.29)$$

Rearranging the equation gives

$$m_{oil}C_{p,oil}\frac{dT(z)}{dz} = m_s \int_0^{k_{max}} k_0\, e^{-(E_a/R)((1/T)-(1/T_0))} c_s(k,z)(-\Delta H_r^0) D(k) dk \quad (4.30)$$

with the species distribution function:

$$D(k) = N.\frac{d\theta}{dk} = N.\left(\frac{\beta}{(1-e^{-1})^{\beta}}\right).\left(e^{-\frac{(k-k_{min})}{k_{max}}} - e^{-1}\right)^{(\beta-1)}.\left(e^{-\frac{(k-k_{min})}{k_{max}}}\right).\left(-\frac{1}{k_{max}}\right) \quad (4.31)$$

where m_{oil} is the mass flow-rate of the feed in kg/h; $C_{p,oil}$ is the heat capacity of the feed in kJ/kg ; m_s is the mass flow-rate of sulfur in the feed in kg/h; $c_s(k,z)$ is the normalized sulfur weight percent of fraction and ΔH_r^0 is the heat of reaction in kJ/kg-sulfur.

From the steady-state energy balance defined in Equation 4.30, we can understand that as the sulfur compounds are removed, heat is released since reactions are exothermic.

Hydrogen consumption during the hydrodesulfurization reactions can be estimated from the equation below;

$$\frac{dm_{H_2}(z)}{dz} = -m_s \frac{MW_{H_2}}{MW_S}\gamma^{H_2} \int_0^{k_{max}} k_0\, e^{-(E_a/R)((1/T)-(1/T_0))} c_s(k,z) D(k) dk \quad (4.32)$$

where m_{H_2} is the mass flow-rate of the hydrogen consumed in kg/h; m_s is the mass flow-rate of sulfur in the feed in kg/h; MW_{H_2} and MW_S are the molecular weight of H_2 and sulfur, respectively; $c_s(k,z)$ is the normalized sulfur weight percent of fraction and γ^{H_2} is the stoichiometric coefficient of H_2 in hydrodesulfurization reactions.

Since different types of organo-sulfur compounds present in the petroleum mixture and each has different reaction chemistry, analysis of all individual sulfur compounds is required to determine the stoichiometric coefficient of hydrogen for each reaction and the study must be extended to modeling the hydrodesulfurization of each organo-sulfur compound present in the crude. However, such an analysis is not possible. So, γ^{H_2} is assumed to have an average value of 2 to have a reasonable hydrogen consumption which is close to literature values [100] with similar operating conditions.

4.4. Parameter Estimation

Extraction of information from data is one of the fundamental issues in the world of engineering and science. The branch of parameter estimation provides tools that help for the use of data efficiently and estimation of some constants in mathematical models [101].

In our HDS model, there are some constants to be estimated which appear in the model equations in section 4.2.

Since the sulfur compounds in each bed have different reactivity, k_{min1}, k_{min2}, k_{max}, β are adjustable parameters.

Since each bed has different activation energies and heat of reaction values, Ea_1, Ea_2 and ΔH_1, ΔH_2 are adjustable parameters for Bed 1 and Bed 2, respectively. Thus, unknown parameters are tabulated in Table 4.2 below;

Table 4.2: Adjustable Parameters for HDS Model

Parameter	Description
k_{min1}	Minimum reactivity of sulfur species in Bed 1
k_{max}	Maximum reactivity of sulfur species
β	B parameter in reactivity equation
k_{min2}	Minimum reactivity of sulfur species in Bed 2
Ea_1	Activation energy of the reactions in Bed 1
Ea_2	Activation energy of the reactions in Bed 2
ΔH_1	Heat of Reaction in Bed 1
ΔH_2	Heat of Reaction in Bed 2

4.4.1 Objective Function and Algorithm

The algorithm used in parameter estimation in this study is nonlinear least squares algorithm. In nonlinear least squares fitting procedure, there is generally a set of N measurements ($x_i y_i$, i=1……N) which can be simulated with a function of the independent variable,x, and a set of adjustable parameters, a_1, ……,a_M. The function which is in the form of Y(x, a_1, ……,a_M) represents the model of a nonlinear physical system and the model is simulated to explain a measurement set. The best fit of the simulation function requires minimization of the sum S of the weighted squares of the difference between the measured plant data and the simulated model data sets [102]:

$$S = \sum_{i=1}^{N} w_i [y_i - Y(x_i, a_1 ..... a_M)]^2 \tag{4.33}$$

Then, the matrix of the residuals is optimized according to least-squares criterion. Sum of the squares of all elements of the residual is minimized to find the best set of the parameters. Here, S is the objective function which is minimized.

Model predicts the total (bulk) sulfur content of the products at the end of the reactor exit, temperature difference between bed 1 inlet and bed 1 outlet and temperature difference between bed 2 inlet and bed 2 outlet. The sulfur content and temperature difference have different units, thus normalized values of these items are used in the objective function below. The objective function is formulated in the following form to estimate the best HDS model parameters by nonlinear least squares algorithm:

$$F = Min\left[w_1.\left(1-\frac{w_{s,M}}{w_{s,R}}\right)^2 + w_2.\sum_{i=1}^{2}\left(1-\frac{\Delta T_{i,M}}{\Delta T_{i,R}}\right)^2 \right] \tag{4.34}$$

where

w_1 , w_2 : weights.

w_s : total (bulk) sulfur content at the reactor exit.

ΔT : difference between inlet and outlet temperatures of each bed. Subcript *M* denotes model predictions while subscript *R* denotes real data taken from the plant.

The selection of the weights depends on the individual importance of the certain outputs. The output with highest priority has the biggest weight in most cases [103].

4.4.2. Sensitivity Analysis

Sensitivity analysis is an analysis technique to see how a certain system reacts when perturbations are applied on its input variables. In our study, the input parameters of the system are changed systematically and the effects of such changes to system outputs are

determined. This study is a helpful tool since the effect of each input tolerance in the system can be observed. It helps also determine its effect on the overall performance of the model. The models can be sensitive to input parameters in two ways: one is that the uncertainty associated with a sensitive input parameter can result in large variability of model output parameters after simulations and second way is that the outputs can be highly correlated with an input parameter thus a small change in the input variable can propagate in large changes of model results [104].

The model has the generalized form of Y=f(X) where x's are several independent variables, X= (X_1, ..., X_p), and several dependent variables Y=(Y_1, ..., Y_r).

In our sensitivity analysis X_i's denote the parameters to be perturbed and Y_i's are model outputs to be observed for the effect of perturbations on the parameters. The perturbation of a parameter X_j may cause a change in state Y_i and this change can be captured by the sensitivity coefficient as:

$$S_{ij} = \frac{\delta Y_i}{\delta X_j}\left(\frac{X_j}{Y_i}\right) \tag{4.35}$$

where X_i represents the value of the input variable in the system while Y_i is the value of output parameter of the system. The sensitivity is defined as ratio of change in output to change in input while other variables remain same. Since the units of outputs and inputs may differ, the quotient, X_i/Y_i , is introduced to normalize the coefficient by removing the affects of units [104]. Equation 4.27 can be simplified further for small changes as follow:

$$S = S_{ij} = \frac{\Delta Y_i / Y_i}{\Delta X_j / X_j} \tag{4.36}$$

Sensitivity analysis allows ranking the most important parameters that affect the outputs due to perturbations in the parameters. To characterize a system, it is important to discover the minimal set of model parameters which are independent parameters since some model parameters are correlated with each other. Fisher information matrix is a measure of the quality of the estimated parameters since it carries the maximum amount of information about the parameters. The FIM determines the variation of output variables caused by a variation of model parameters and summarizes the importance of each model parameter over the outputs. Taking the matrix of the sensitivity coefficients and assuming there are estimations of measurement errors which have Gaussian distributions, FIM can be calculated as follows to extract information from these measurements for discrete time steps [105]:

$$F = \sum_{k=1}^{N_t} S^T(t_k) V^{-1}(t_k) S(t_k) \tag{4.37}$$

where k represents each sampling data point , N_t is the total number of time steps and V which is the estimate of measurement covariance. F is a pxp matrix since it is calculated for r output variables and p parameters and V is rxr covariance matrix of measurement noise. S is the sensitivity function matrix which is pxr [105].

In our study, it is assumed that any measurement errors exist, thus the FIM is calculated using the Equation 4.30:

$$F = S^T S \tag{4.38}$$

The rank of the Fisher information matrix denotes if the matrix is degenerate and the condition number which is the ratio of maximal to the minimal eigenvalue denotes if it is ill

conditioned. It is also possible to determine if the parameters are correlated from both of these concepts.

Ioslovich et al. [103] proposed a method to identify the correlated parameters by forming a normalized Fisher matrix. First, the normalized sensitivity matrix S_n^{ij} is formed by dividing the sensitivity matrix S^{ij} to the Euclidean norm:

$$S = S_n^{ij} = \frac{S^{ij}}{\sqrt{(S^{ij})'(S^{ij})}} \tag{4.39}$$

Then, the normalized Fisher matrix is defined as

$$F_n = S_n' S_n \tag{4.40}$$

As follows, all the diagonal elements of the normalized Fisher matrix are equal to one and each off-diagonal element F_n^{ij} is just the scalar product of the corresponding normalized sensitivity vectors, $S_n^{ij\prime} S_n^{ij}$ i.e. the cosine of the angle between them. For non-correlated parameters the scalar product is small [103].

The sensitivity matrix which includes all model parameters was built to see which parameters are correlated with each other and reduce the number of parameters. When the model consists of many parameters, estimation of all the parameters is a difficult task. Because of this, minimization of the number model parameters is necessary by fixing some parameters. An example is shown below. First, the parameters are perturbed by 10% changes both positively and negatively. The effects of these changes on the outputs are plotted in the figures below:

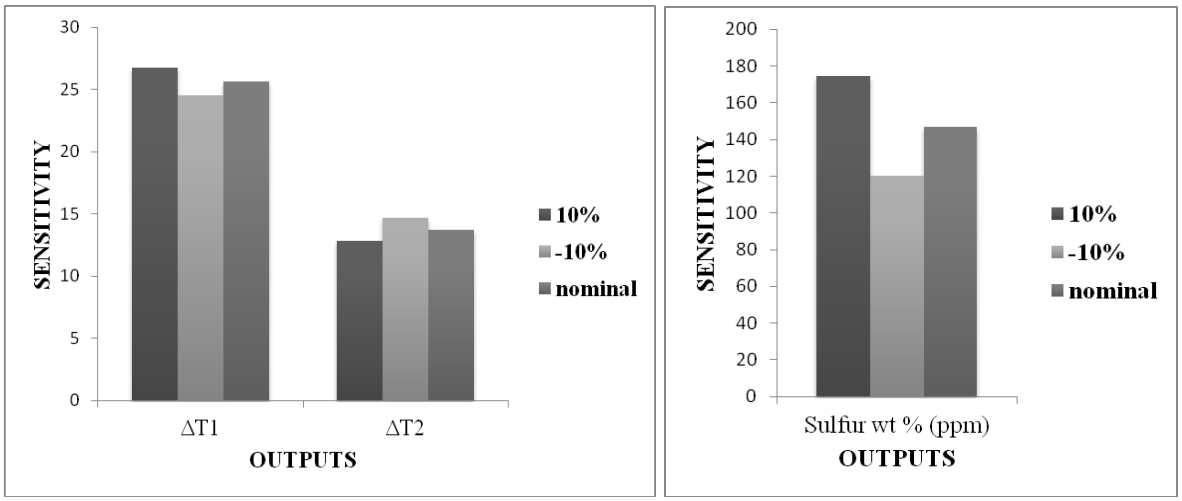

Figure 4.19: Effect of k_{min1} on model outputs for a perturbation of ±10 %

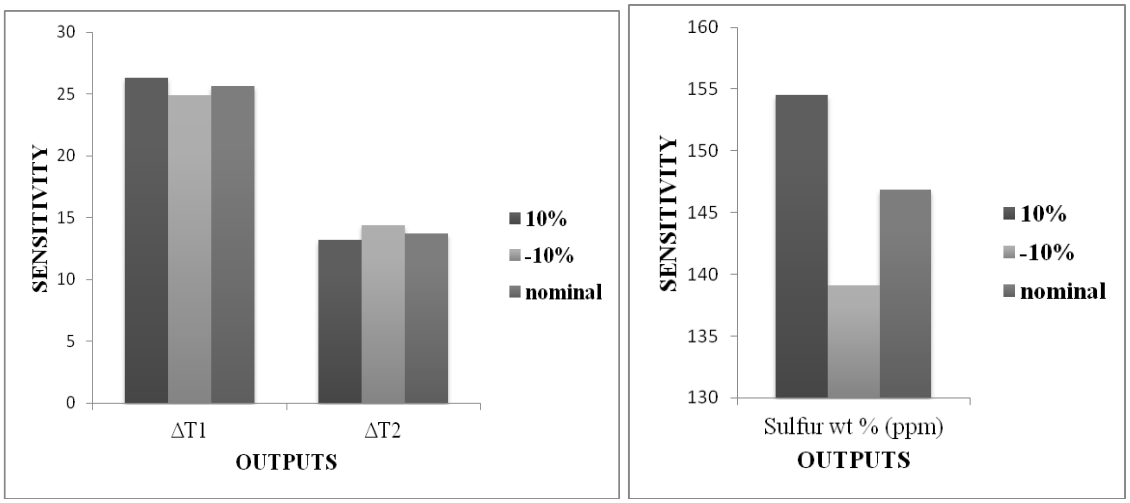

Figure 4.20: Effect of k_{max} on model outputs for a perturbation of ±10 %

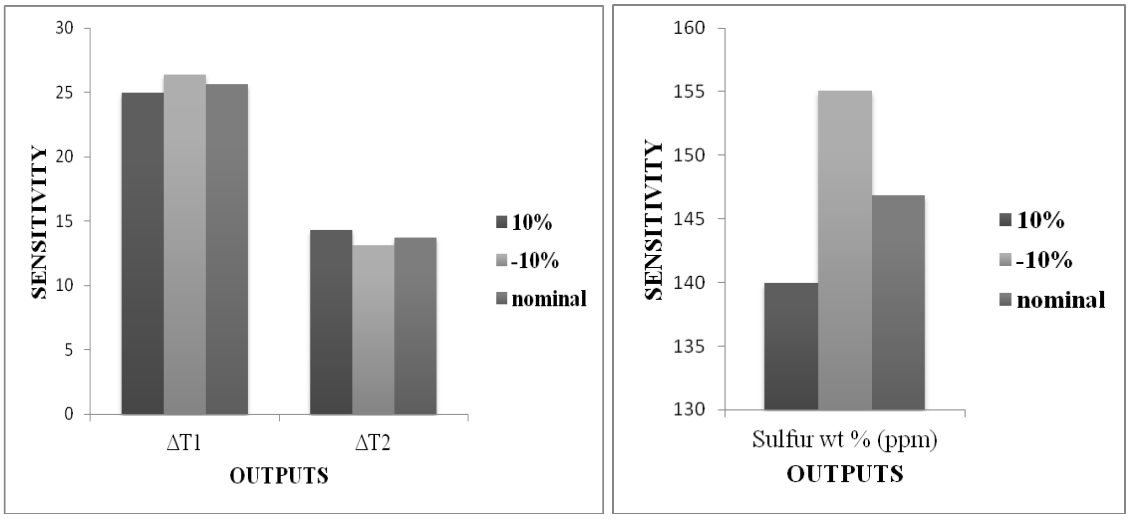

Figure 4.21: Effect of β on model outputs for a perturbation of ±10 %

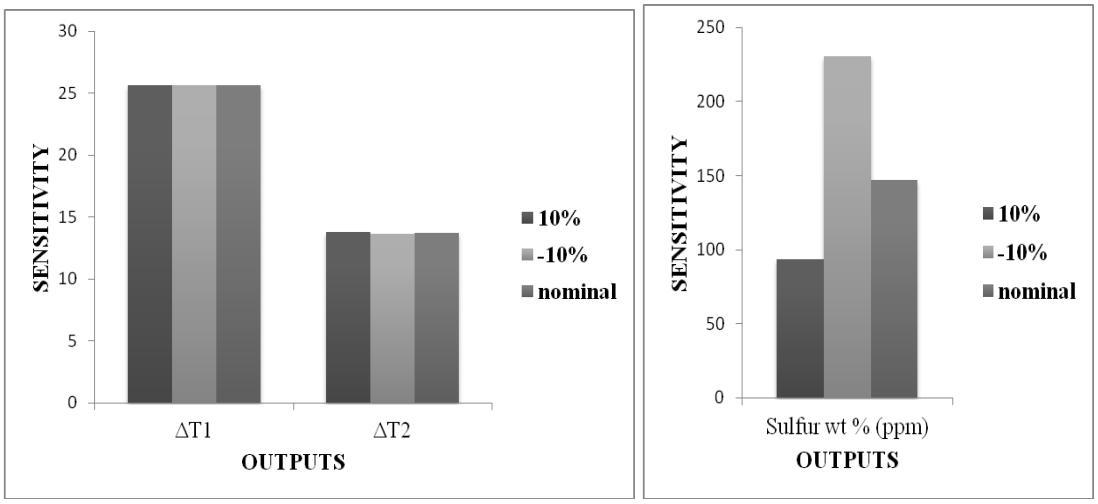

Figure 4.22: Effect of k_{min2} on model outputs for a perturbation of ±10 %

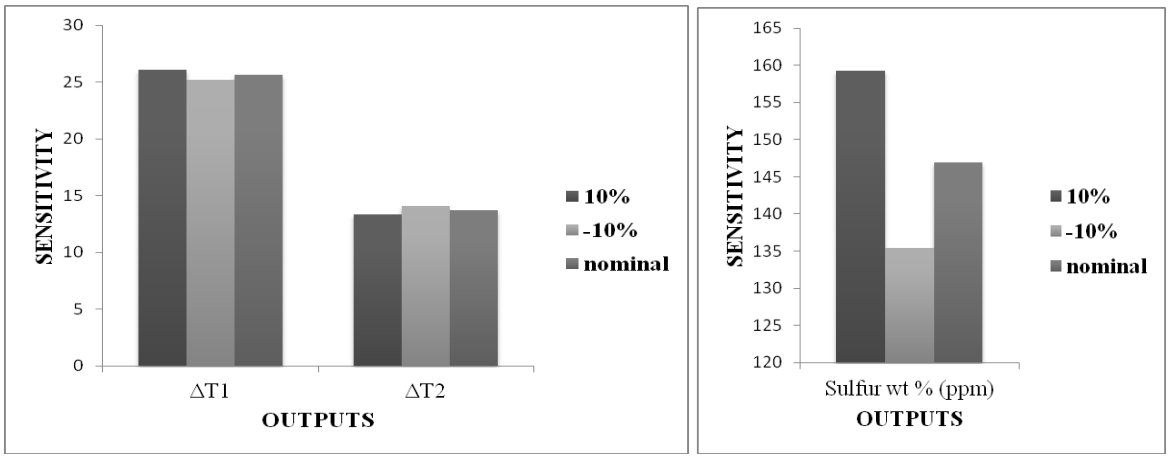

Figure 4.23: Effect of E_{a1} on model outputs for a perturbation of ±10 %

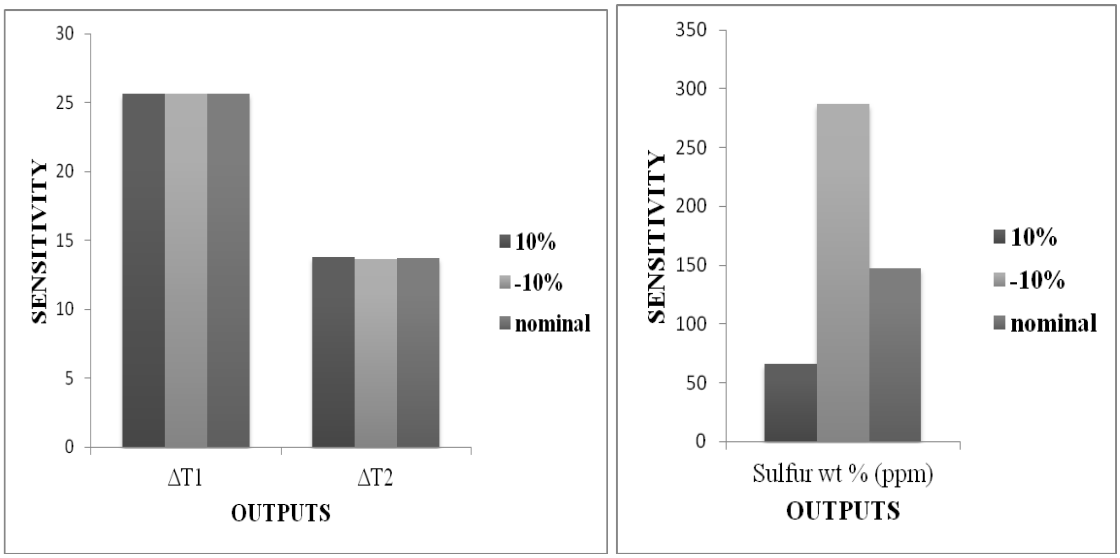

Figure 4.24: Effect of E_{a2} on model outputs for a perturbation of ±10 %

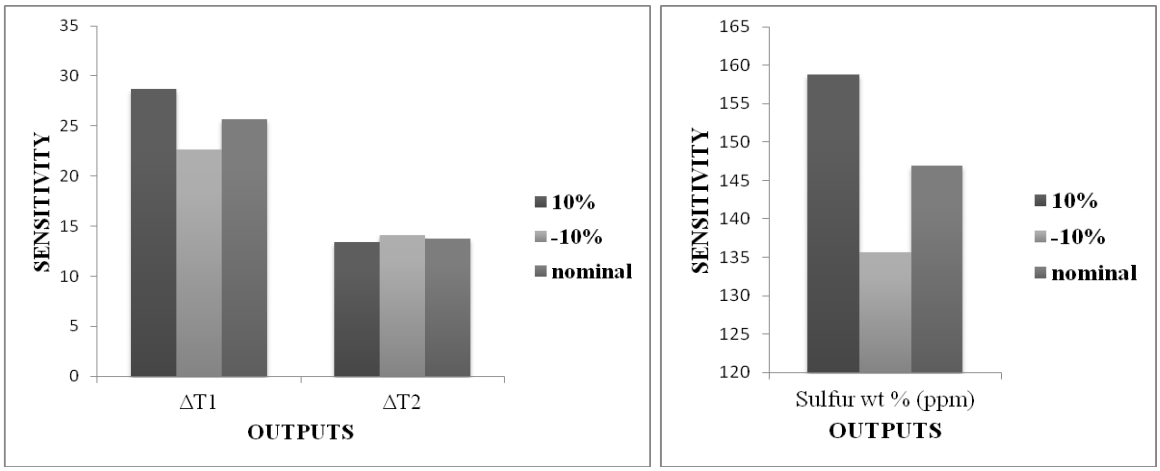

Figure 4.25: Effect of ΔH_1 on model outputs for a perturbation of ±10 %

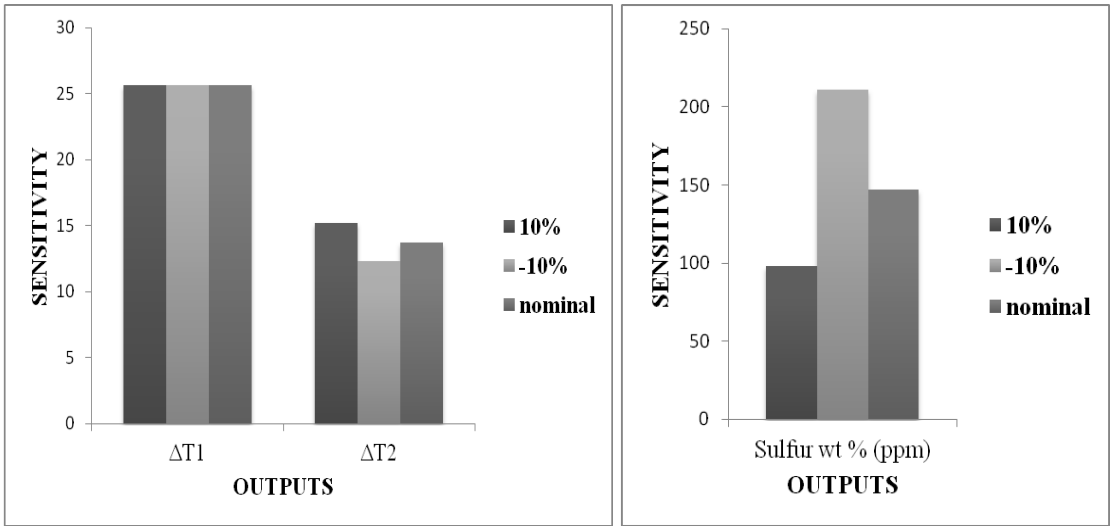

Figure 4.26: Effect of ΔH_2 on model outputs for a perturbation of ±10 %

The plotted changes of the outputs due to perturbations on parameters are recorded in Tables 4.3 and 4.4 to construct the normalized sensitivity matrix.

Table 4.3: Effects of 10% Perturbation in Parameters of 07.01.2014

		Effects of 10% Change in Parameters on Outputs (ΔY_i)							
		k_{min1}	**k_{max}**	**Beta**	**k_{min2}**	**E_{a1}**	**E_{a2}**	**ΔH_1**	**ΔH_2**
	nominal	*0.08641*	*1.45901*	*5.3705*	*0.1535*	*59649.41*	*243893*	*-9797.63*	*-7937.31*
sulfur wt%	*146.88*	174.28	154.56	140	93.398	159.22	66.257	158.83	98.376
ΔT_1	*25.641*	26.729	26.342	24.985	25.641	26.103	25.641	28.698	25.641
ΔT_2	*13.748*	12.841	13.173	14.286	13.799	13.362	13.824	13.374	15.173

Table 4.4: Effects of -10% Perturbation in Parameters of 07.01.2014

		Effects of -10% Change in Parameters on Outputs (ΔY_i)							
		k_{min1}	**k_{max}**	**Beta**	**k_{min2}**	**E_{a1}**	**E_{a2}**	**ΔH_1**	**ΔH_2**
	nominal	*0.08641*	*1.45901*	*5.3705*	*0.1535*	*59649.41*	*243893*	*-9797.63*	*-7937.31*
sulfur wt%	*146.88*	120.2	139.09	155.11	230.36	135.42	287.01	135.69	210.93
ΔT_1	*25.641*	24.503	24.905	26.402	25.641	25.196	25.641	22.686	25.641
ΔT_2	*13.748*	14.696	14.352	13.124	13.669	14.119	13.616	14.11	12.319

Then the average of the values of effects caused by perturbations is calculated and sensitivity matrix is built. An example of sensitivity matrix is given in Table 4.5:

Table 4.5: Sensitivity Matrix S_{ij} for 07.01.2014

Sensitivity Matrix for 10% Change in Parameters								
	k_{min1}	**k_{max}**	**beta**	**k_{min2}**	**E_{a1}**	**E_{a2}**	**ΔH_1**	**ΔH_2**
sulfur wt%	124.860	0.122	-0.0079	-77.218	1.32E-10	-5.6E-11	4.73E-09	-3E-08
ΔT_1	28.400	0.0636	-0.0043	0	2.83E-11	0	6.95E-09	0
ΔT_2	-44.156	-0.098	0.00657	0.78670	-4.4E-11	5.64E-13	-1.6E-09	9.24E-09

After normalizing the sensitivity matrix and building normalized Fisher information matrices for some sets of parameters, the best set of parameters are determined by examining the related Fisher matrix as in Table 4.6 below:

Table 4.6: Fisher Information Matrix for 07.01.2014

k_{min1}	**k_{min2}**	**ΔH_2**
1	2.39E-15	2.39E-15
2.39E-15	1	6.05E-15
2.39E-15	6.05E-15	1

The diagonal elements of the Fisher matrix are equal to one and the scalar products are small like defined above for non-correlated parameters. The parameters k_{min1}, k_{min2} and ΔH_2 are independent from each other and their variability can define the system best. The other adjustable parameters are fixed to average values which are determined after many simulations. Table 4.7 gives the nominal values of the fixed parameters:

Table 4.7: Nominal Values of the Fixed Parameters

Parameter	Nominal Value
k_{max1}	1.495646
β_1	5.179445
Ea_1	61672.59
Ea_2	230760.6
ΔH_1	-10331.3

Since the model parameters are some kinetic parameters, it is important to determine if they are reliable or not. To do this, the related parameters are investigated in the literature and literature ranges of these parameters are constructed. The values are tabulated as follows:

Table 4.8: Literature Ranges for Parameters of HDS Model

Parameter	Value	Unit	Reference
$\mathbf{k_{min}}$	0.08	h^{-1}	[27]
$\mathbf{k_{max}}$	7.5	h^{-1}	[27]
β	2	-	[27]
	5.27	-	[49]
Ea	79800 to 244740	J/mol	[106]
	131993	J/mol	[65]
	30 to 52	kcal/mol	[107]
$\mathbf{\Delta H_{rxn}}$	-251000	J/mol	[65]
	-7128	kJ/kg sulfur	[108]
	-13 to -68	kcal/mol organosulfur reactant	[24]
	-57 to -262	kJ/mol organosulfur reactant	[109]
	-11 to -62	kcal/mol	[110]

The simulations are done with estimating these three parameters for hydrodesulfurization model and the results are discussed in Chapter 6.

Chapter 5

MODELING OF HYDROCRACKING REACTOR

5.1. Introduction

In this chapter, modeling studies for hydrocracker are presented. Hydrocracker model is adopted from the study presented by Sildir H. and Arkun Y. et al. [91] and modified according to DHP unit which is under investigation.

As mentioned in Chapter 4, hydrocracking reactions are assumed to occur only in the third bed. Some assumptions are made to simplify the complexity of the system;

- We assume that the TBP curve for the feed does not change during hydrodesulfurization in Beds 1 and 2. The blended diesel feedstock enters the first reactor in which only the hydrodesulfurization reactions are assumed to occur and after the first reactor, the desulfurized feedstock enters to second reactor in which hydrocracking reactions take place. After the hydrodesulfurization reactions, boiling points of the desulfurized compounds decrease but this change in the boiling point curve is negligible since the sulfur amount is very little when compared to other species such as the amount of hydrocarbons. Therefore it is not possible to collect samples at the exit of the hydrotreater to characterize the feed entering the first bed of the hydrocracker. Since cracking in the hydrotreater is negligible compared to the first bed, we have assumed that the properties of the feed entering the first bed remains the same as the fresh feed entering the hydrotreater.

- Steady-state operation is assumed.
- The reactor is assumed to operate under adiabatic conditions.
- The value of heat capacity is assumed to be same with hydrodesulfurization reactor model.
- Pseudo-homogeneous plug flow model is assumed. In this pseudo-homogeneous plug flow model, all pseudocomponents are assumed to exist in the liquid phase and no gas-liquid equilibrium calculations are performed.
- Diffusional resistances are assumed to be negligible.

To treat the complex mixture of petroleum as continuum, the method of continuous lumping is employed. The concentrations of the pseudocomponents are characterized in terms of reactivity which is a monotonic function of true boiling point of the mixture [91].

Considering a mixture consists of N reactant species in discrete time, the total concentration at any time can be defined by

$$C(t) = \sum_{i=1}^{N} c_i(t) \tag{5.1}$$

One can express the discrete mixture by a continuous concentration function, $c(k,t)$ to represent the concentration of species with reactivity k at time t.

$$C(t) = \int_0^{\infty} c(k,t)D(k)dk \tag{5.2}$$

The equation approximates the sum over i-type species, by an integral over reactivity k. To do this, a transformation is necessary from “i coordinate” to “k coordinate” by introducing the species-type distribution function $D(k)$

$$D(k_i) = \frac{\Delta i}{\Delta k} = \frac{di}{dk} \tag{5.3}$$

where $D(k_i)$ is defined at the discrete points of k_i and as the number of pseudocomponents, N approaches infinity. $D(k_i)$ can be treated as a continuous function of k. D(k)dk describes the number of species between k and k+dk. Species-type distribution function provides the consistency between discrete and continuous lumping [91].

For large number of species, Equation 5.3 becomes

$$\frac{1}{N}\int_0^{\infty} D(k)dk = 1 \tag{5.4}$$

5.2. Hydrocracker Reactor Model

As the hydrocracking reactions take place in the reactor in other words as the residence time of hydrocracking reactions increases , more the heavier hydrocarbons in the reaction mixture are converted into lighter components. In the meantime, the TBP distribution curve of the mixture changes continuously. Thus, the TBP curve is converted into a distribution function which describes the weight fraction of any component as a function of normalized TBP, which is defined as

$$\theta = \frac{TBP - \min(TBP)}{\max(TBP) - \min(TBP)} \tag{5.5}$$

where *min(TBP)* is the lowest TBP (Initial Boiling Point) and *max(TBP)* is the highest TBP (Final Boiling Point) in the fraction.

Now a transformation is required between normalized TBP, θ and reactivity of components, k. This transformation is based on experimental evidence that suggest a power law type relationship

$$\frac{k}{k_{\max}} = \theta^{1/\alpha} \tag{5.6}$$

where k_{max} is the reactivity of the species with highest boiling point which corresponds to $\theta = 1$ and both k_{max} and α are adjustable parameters. This relationship is a monotonic function which explains that molecules with a higher boiling point (heavier molecules) crack faster than molecules with a lower boiling point [91, 111].

Rewriting the species type distribution function in the form of

$$D(k) = \frac{di}{dk} = \frac{di}{d\theta}\frac{d\theta}{dk} \tag{5.7}$$

where the term $di/d\theta$ can be approximated to N, total number of species by assuming the species index, i values are equally spaced. Then, D(k) becomes

$$D(k) = \frac{di}{dk} = \frac{di}{d\theta}\frac{d\theta}{dk} = N\frac{\alpha}{k_{\max}^{\alpha}}k^{\alpha-1} \tag{5.8}$$

5.2.1. Generation of Feed and Product Mass Fraction Curve

Application of continuum lumping requires the information of the weight fractions of pseudocomponents as a function of normalized TBP. For this purpose, TBP curve is

converted into a distribution function which describes the weight fraction of any component as a function of normalized TBP.

The plant data consists of the collection of ASTM D86 distillation data of the blended diesel feedstock, the diesel product and naphta product which corresponds to particular liquid volumes distilled. It is not possible to collect distillation data after hydrocracker due to safety and physical operation considerations. After hydrocracking reactor, product enters a fractionator in which the product is separated into naphta and diesel. Thus, the hydrocracking reactor is a blend of naphta and diesel before fractionation. The distillation data is obtained for each separated products after fractionation column.

A blending procedure is conducted in ASPEN HYSYS Oil Manager to obtain the reactor product by using the plant ASTM information of naphta and diesel. First, crude assays for naphtha and diesel are constructed by entering ASTM data. The program converts ASTM distillation data into TBP data automatically. Then, a blend is created by mixing these two assays in proportion of mass fractions in the products since the mass flow rates of each stream is given as plant data.

Table 5.1: Plant Data of Naphta Product

NAPHTA													
				D86									
DATE	**ton/d**	**API**	**S (ppmwt)**	**IBP**	**5**	**10**	**20**	**30**	**50**	**70**	**90**	**95**	**SKN**
07.01.14	329.853	65.7	390	31	39	49	-	76	97	118	154	167	202
09.01.14	370.992	66.8	180	31	36	47	61	73	95	118	156	172	207
14.01.14	364.051	67.1	286	30	43	51	-	75	96	118	155	171	208

Table 5.2: Plant Data of Diesel Product

DIESEL												
				D86								
DATE	**ton/d**	**API**	**S (wt %)**	**IBP**	**5**	**10**	**30**	**50**	**70**	**90**	**95**	**SKN**
07.01.14	2468.972	40.5	7.34	157	187	206	247	273	300	339	360	376
09.01.14	2405.571	41	7.19	159	187	204	244	270	296	333	352	370
14.01.14	2455.192	41	6.37	155	183	198	239	267	295	335	354	371

After the blending procedure is completed in ASPEN HYSYS Oil Manager and the TBP curve of the reactor product is found, the mass fraction of the lumps of product and the mass fractions of the lumps of naphta and diesel are calculated by the correlations declared in Chapter 3 in the MATLAB. The TBP curve of the product that is generated from naphta and diesel TBP curves in ASPEN HYSYS Oil Manager is given in Figure 5.1. It is clear to see that product stream has a TBP curve between TBP curves of naphta and diesel products since it is a mixture of these product streams.

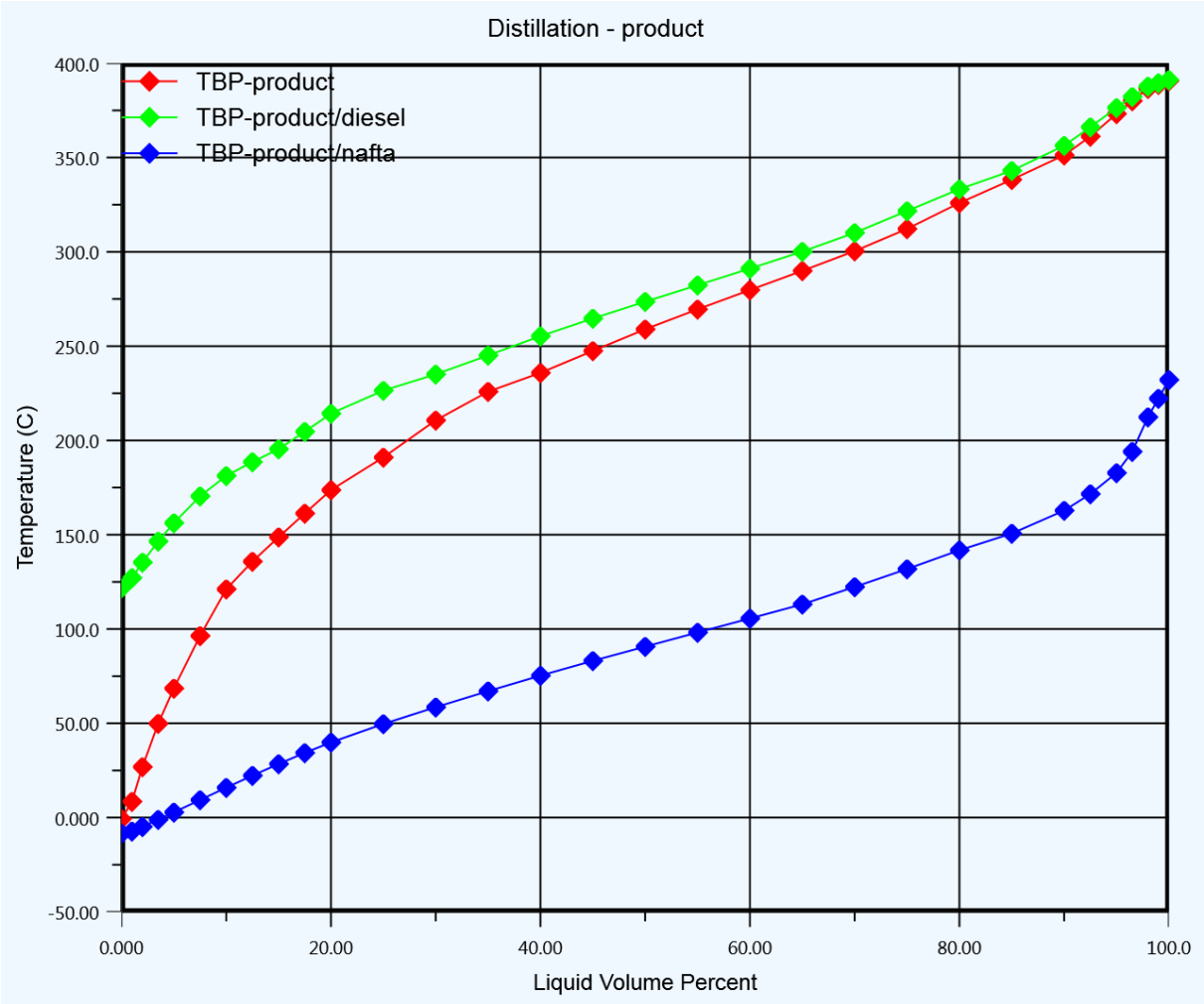

Figure 5.1: Product TBP curve for 07.01.2014 in ASPEN HYSYS

The product TBP curves are generated for the days which are simulated for hydrocracking model. Some examples are tabulated for selected days in Table 5.3.

Table 5.3: TBP versus Liquid Volume Data for Selected Days

Liquid Volume %	07.01.2014	09.01.2014	14.01.2014	16.01.2014	23.01.2014	30.01.2014
0	-0.80118	-4.4146	1.894725	-0.71792	8.031657	3.6701
1	11.86776	4.96718	14.47106	8.527042	23.26719	19.98552
2	33.93173	27.2576	31.19779	26.88219	41.70938	41.56074
3.5	55.89759	46.74477	50.92394	49.88054	64.22294	66.56176
5	74.38116	64.02292	67.74885	68.52534	83.886	88.23701
7.5	101.9993	90.48978	94.02093	96.39398	112.5827	120.3386
10	123.3784	115.3094	117.0521	121.1386	133.9854	137.2061
12.5	138.9072	131.3703	133.0441	135.8274	147.543	153.2007
15	153.9503	145.9846	147.368	148.741	158.5228	167.1132
17.5	167.6687	160.0479	159.3855	161.3051	170.1741	178.7225
20	179.762	172.2749	169.8969	173.7061	184.4555	188.7004
25	196.7949	192.6923	187.8059	191.0284	201.2207	207.4655
30	217.1914	210.4452	204.62	210.6739	222.2312	222.2622
35	232.2342	224.2409	218.7782	225.8819	234.4181	233.7266
40	241.8659	235.8037	231.2047	235.8701	244.0395	244.4898
45	253.2966	247.5359	243.5121	247.4848	255.0916	255.4096
50	263.9145	258.6154	255.0375	258.9538	265.4364	265.468
55	273.6662	268.6945	265.701	269.5458	275.0529	274.9621
60	283.3312	278.4312	276.0025	279.7537	284.6445	284.4224
65	293.1868	288.2051	286.2957	289.9313	294.3953	294.0418
70	303.3646	298.2013	296.8375	300.4209	304.4691	304.0662
75	314.7504	309.1776	308.501	312.1877	315.6808	315.384

80	327.8689	321.9762	322.0347	325.9438	328.3365	328.3686
85	339.8564	333.2828	334.1996	338.2834	339.6571	339.2271
90	351.6468	345.1778	346.9214	351.2639	351.3604	351.7895
92.5	362.3629	354.8354	356.7752	361.2119	361.7972	361.6056
95	375.623	367.1075	368.881	373.1796	374.2057	373.2808
96.5	382.9295	374.4196	375.9762	380.0572	380.9682	380.0586
98	389.6063	381.53	382.8585	386.5918	387.1064	386.3961
99	391.5853	383.9328	385.0562	388.7198	388.9996	388.5937
100	393.5643	386.3356	387.2304	390.6427	390.7053	390.7913

Then, the necessary transformations are done to calculate the weight fractions of the product streams (see Chapter 3) and plot the graphs of weight fraction versus normalized boiling point like in Figure 5.2 below.

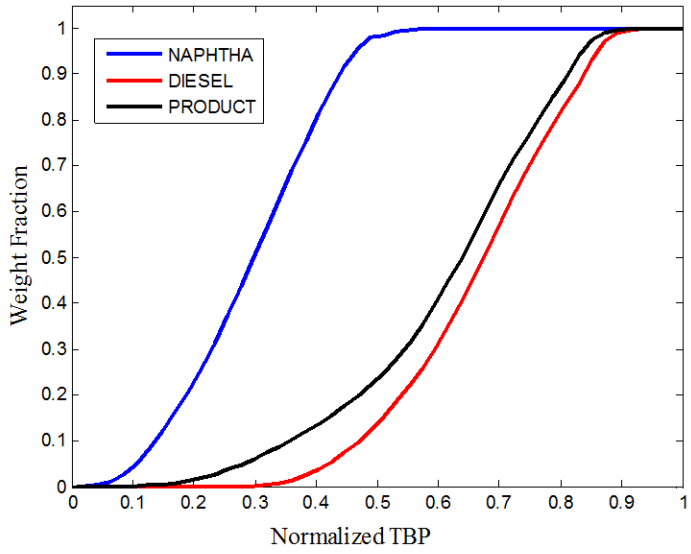

Figure 5.2: Cumulative mass fraction curves for product, naphta and diesel

Since the product is separated into specified products after fractionation, a concept is defined to estimate the individual weight fractions of the products from the TBP curve of the product. This concept is cut-point temperature which corresponds to the boiling point on the cumulative TBP curve that defines the amounts of petroleum fractions to be produced. As seen from Figure 5.2 TBP curves of naphta and diesel overlap which means that the separation of these adjacent cuts is not 100%. Cut-point temperature is defined as mid-boiling point of the TBP overlapping temperatures:

$$TBP_{cut\text{-}point} = \frac{(FBP_L + IBP_H)}{2} \tag{5.9}$$

where FBP_L is the final boiling point of the light fraction and IBP_H is the initial boiling point of adjacent the heavy fraction [91, 112]. Thus, the weight fractions of the naphta and diesel in the product can be calculated from the cut-point temperature which corresponds to separation of these two fractions.

Generation of feed mass fraction curve is a must for continuous lumping. To convert the TBP curve of feed into a feed weight fraction versus normalized TBP curve, first this ASTM distillation data is converted into TBP by the correlation proposed in Chapter 3 and a large number of lumps are generated. Then, the weight fractions of the pseudocomponents generated are calculated. Examples of cumulative feed and product weight fraction curves of selected days are presented in Figure 5.3 and Figure 5.4 below;

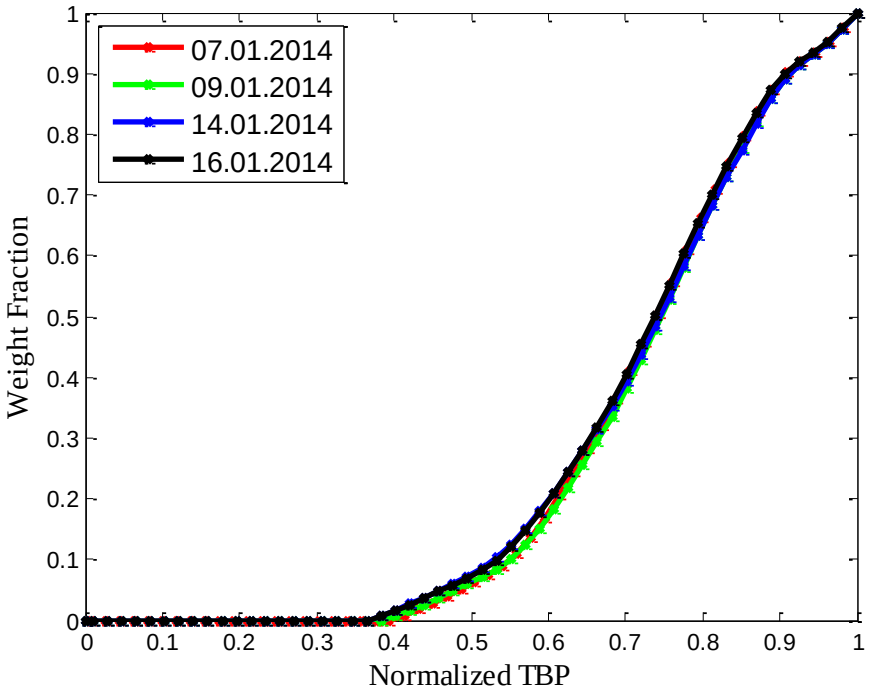

Figure 5.3: Cumulative feed mass fractions of pseudocomponents versus normalized TBP for four days

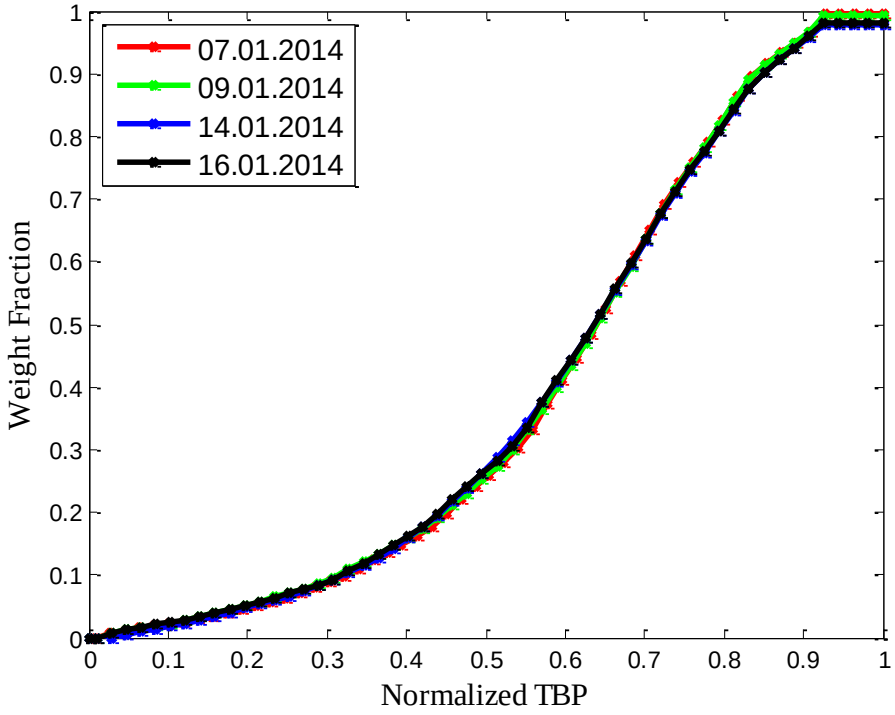

Figure 5.4: Cumulative product mass fractions of pseudocomponents versus normalized TBP for four days

The distributions of feed and product mass fractions can be seen more clearly from the distribution plots which are mass fractions in each pseudocomponent with respect to normalized TBP in Figure 5.5 and 5.6.

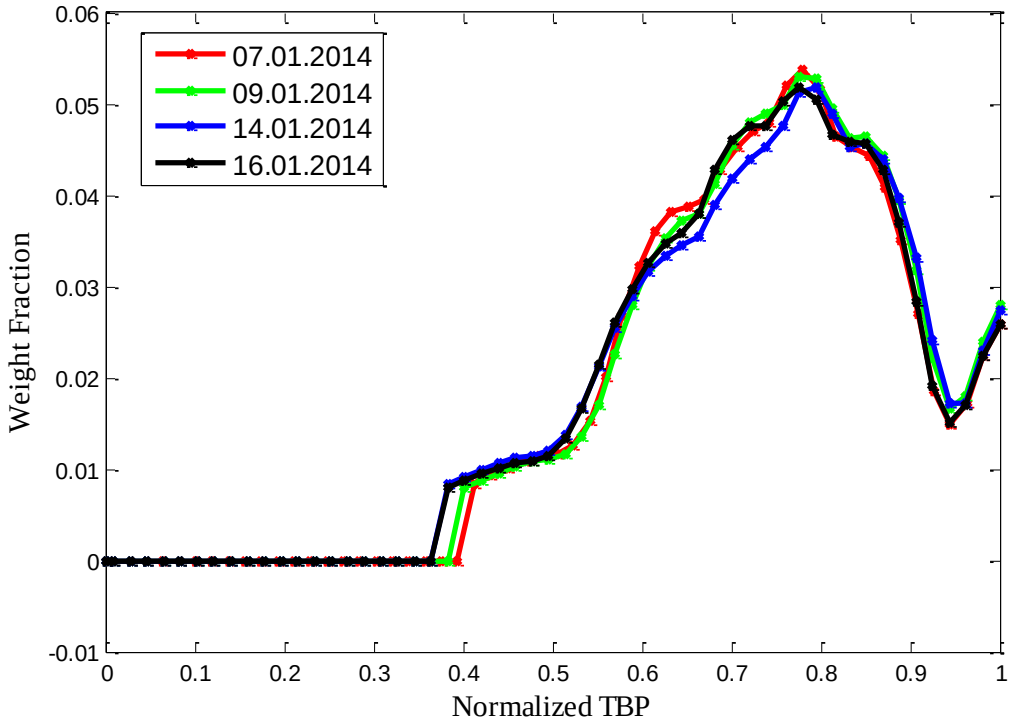

Figure 5.5: Feed mass fraction distributions of pseudocomponents versus normalized TBP for four days

From the Figure 5.5, it is possible to see that the feedstock of the hydrocracker contains mostly heavier compounds which have higher boiling points and higher reactivity.

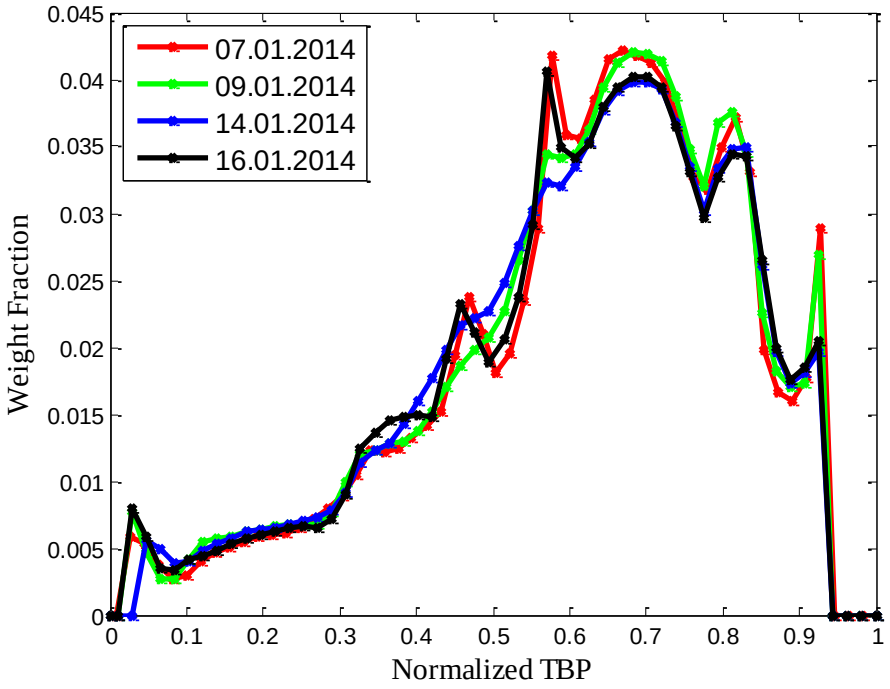

Figure 5.6: Product mass fraction distributions of pseudocomponents versus normalized TBP for four days

As seen from Figure 5.6, the product mass fraction curves of these four days are similar since the operating conditions are adjusted to have similar amounts of products in the plant. After the cracking of the heavier compounds into lighter species exist in the feedstock, the mass fractions of the lighter pseudocompounds increase and the boiling point range of the products shifts to lower values as seen in Figure 5.7.

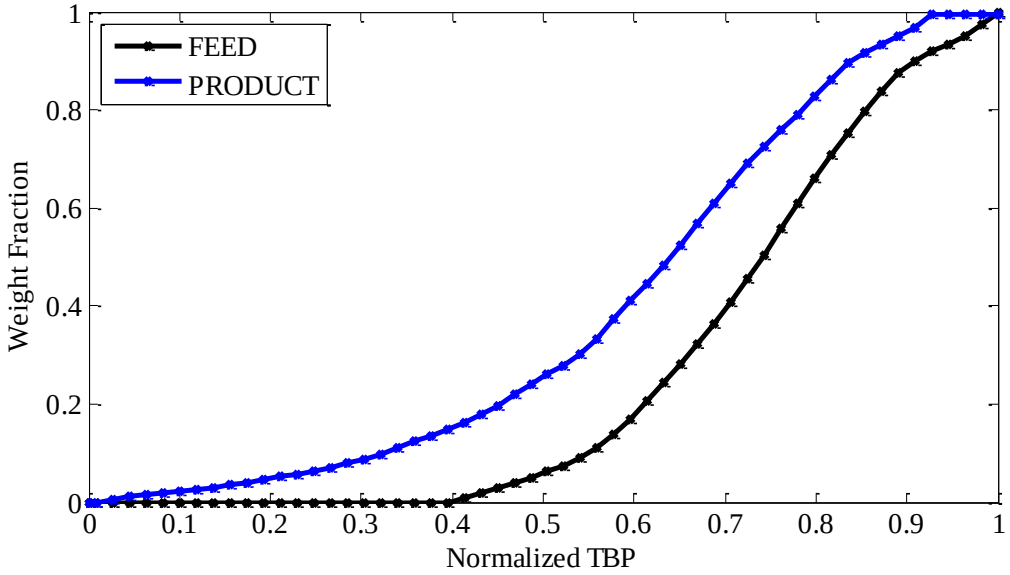

Figure 5.7: Superimposed plots of feed and product cumulative mass fraction curves for 07.01.2014

5.2.2. Mass Balance

Similar to hydrodesulfurization model, Arrhenius relationship is considered to observe the effect of temperature on reactivity of sulfur compounds since the model is non-isothermal;

$$k = k_0 e^{-\frac{E_a}{R}(\frac{1}{T}-\frac{1}{T_0})} \tag{5.10}$$

where E_a is the activation energy in J/mol, k_0 is reactivity at some reference temperature T_0 which is inlet temperature in K and R is the gas constant which is 8.3144621 J/mol.K.

Component mass balance along the bed given by:

$$v\frac{dc(k,z)}{dz} = -k_0\, e^{-(E_a/R)((1/T)-(1/T_0))}c(k,z) + \int p(k,K)K_0 e^{-(E_a/R)((1/T)-(1/T_0))}c(K,z)D(K)dK \qquad (5.11)$$

where c(k, z) is the mass fraction of species with reactivity k at axial position z; v is the mass average velocity; E_a is the activation energy; k_0 and K_0 are reactivities at some reference temperature T_0. The term on the left hand side of Eq. (5.11) denotes the net rate of addition of mass by convection; the first term on the right hand side is the consumption of the species with reactivity k due to its cracking to lighter species; and the second term is the generation of the species with reactivity k by cracking heavier species under steady state and isothermal conditions. The yield function p(k,K) represents the formation of the species with reactivity k from hydrocracking of heavier species that has reactivity K [91].

There are some criteria to choose a proper yield function [42];

(1) p(k, K) is equal to zero for k = K since the species with reactivity k cannot yield to itself by cracking.

(2) The function of p(k,K) is positive between the ranges of validity of model parameters.

(3) p(k,K) has a small non-zero value when k=0 since the species with reactivity K cracks into smaller species even in traces.

The yield function is given by [42]:

$$p(k,K) = \frac{1}{S_0\sqrt{2\pi}}\left[exp - [\{(k/K)^{q_0} - 0.5\}/a_1]^2 - exp(-(0.5/a_1)^2 + \delta(1 - k/K)\right] \qquad (5.12)$$

There is also a mass balance criterion [42]:

$$\int_o^K p(k,K)D(k)dk = 1 \qquad (5.13)$$

According to the criterion, S_o which is a normalization function can be defined as;

$$S_0 = \int_0^K \frac{1}{\sqrt{2\pi}} \left[\exp - \left[\frac{\left\{ (k/K)^{a_0} - 0.5 \right\}}{a_1} \right]^2 - \exp\left(- \left(\frac{0.5}{a_1} \right)^2 + \delta \left(\frac{1-k}{K} \right) \right) \right] D(k)dk \tag{5.14}$$

The following parameters are estimated: k_{max}, α, a_0, a_1 and E_a.

5.2.3. Energy Balance

Energy balance in hydrocracking bed is described by:

$$\frac{dT(z)}{dz} = \frac{\int_0^{k_{max}} k_0 \, e^{-(E_a/R)((1/T)-(1/T_0))} c(k,z)(-\Delta H_r^0(k)) D(k)dk}{\int_0^{k_{max}} c(k,z) C_{p,oil} D(k)dk} \tag{5.15}$$

where $C_{p,oil}$ is the heat capacity of the oil in kJ/kg; and $\Delta H_r^0(k)$ is the heat of cracking reaction for the species with reactivity k in kJ/mol. There is not any term related to hydrogen since hydrogen is excess [91]. From the steady-state energy balance defined in Equation (5.15), we can understand that as the hydrocracking reactions take place, heat is released since the reactions are exothermic in overall and the mixture of all species is heated with this energy.

For most of the operating range of interest to us, the behavior of standard heat of reaction versus TBP is almost linear [91]. Therefore, the following linear expression can be used:

$$\Delta H_r^0(k) = m.\theta(k) + c \tag{5.16}$$

where m and c are adjustable parameters that will be estimated to match the plant data.

After constructing the integro-differential mass and energy balances, the starting point to construct a continuous concentration function to apply the continuous lumping method is the TBP data of reactor feedstock. Building of the initial concentration distribution of the feed, $c(k,0)$ is required to solve the equations. The feed is first divided into N lumps and each lump boils in a particular temperature range and has a particular weight fraction in the feed. With this information, one can write the weight fraction w_i of the pseudocomponent *i* by reactivities k_{i-1} and k_i as

$$w_i = \int_{k_{i-1}}^{k_i} c(k,0)D(k)dk \tag{5.17}$$

where the total number of the pseudocomponents (lumps) is N derived from feed TBP curve. The aim is to find the function of $c(k,0)$, then the normalization criteria of the mass balance is satisfied:

$$\sum_{i=1}^{N} w_i = 1 = \int_0^{k_{\max}} c(k,0)D(k)dk \tag{5.18}$$

$c(k,0)$ can be obtained when the weight fractions of the feed are available by a method developed by Riggs and Govindhakannan [89]. Then, one can solve the integro-differential mass and energy balance equations by using inlet reactor temperature and the information gathered from obtaining the initial concentration distribution $c(k,0)$.

5.3. Parameter Estimation

5.3.1. Objective Function and Algorithm

In our HC model, there are some constants to be estimated which appear in the model equations in section 5.2.

Table 5.4: Adjustable Parameters for HDS Model

Parameter	Description
k_{max}	Maximum reactivity of hydrocarbon species
α	parameter in reactivity equation
a_0	parameter in yield function
a_1	parameter in yield function
Ea	Activation energy for the hydrocracking reactions
c	intersection for heat of reaction
m	slope for heat of reaction

Model predicts the weight fraction of each pseudocomponent at the end of the hydrocracking reactor and temperature difference between bed 3 inlet and bed 3 outlet. The mass fractions and temperature difference have different units, thus normalized values of these items are used in the objective function below.

The objective function which is to be minimized is formulated in the following form to estimate the best HC model parameters by nonlinear least squares algorithm:

$$F = Min\left[w_1 \cdot \sum_i \left(1 - \frac{C_{i,M}}{C_{i,R}}\right)^2 + w_2 \cdot \left(1 - \frac{\Delta T_{i,M}}{\Delta T_{i,R}}\right)^2 + w_3 \cdot \left(1 - \frac{x_{naphta,M}}{x_{naphta,R}}\right)^2 \right] \quad (5.19)$$

where

w_1 , w_2 , w_3 : weights.

C_i : weight fraction of i^{th} pseudocomponent at the reactor exit.

ΔT : difference between inlet and outlet temperatures of the bed.

x_{naphta} : weight fraction of naphta in the product

Subcript *M* denotes model predictions while subscript *R* denotes real data taken from the plant. The selection of the weights depends on the individual importance of the certain outputs. The output with highest priority has the biggest weight in most cases [103].

5.3.2. Sensitivity Analysis

Similar to the sensitivity analysis of hydrodesulfurization reactor model (see Chapter 4), the sensitivity matrix which includes all model parameters is built to see which parameters are correlated with each other and reduce the number of parameters. Same procedure is applied: the parameters are perturbed by 10% changes both positively and negatively. The effects of these changes on the outputs are plotted in the figures below:

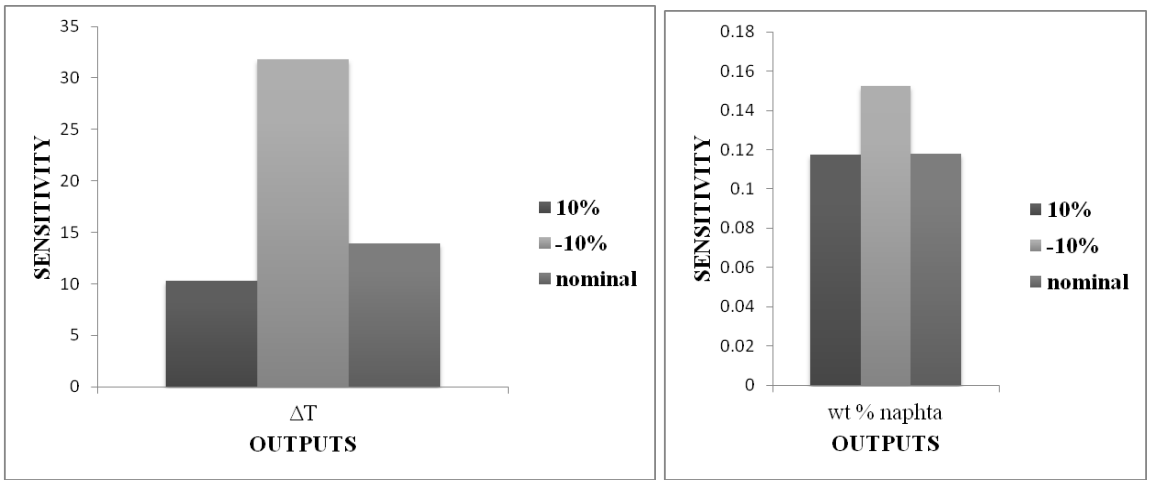

Figure 5.8: Effect of k_{max} on model outputs for a perturbation of ±10 %

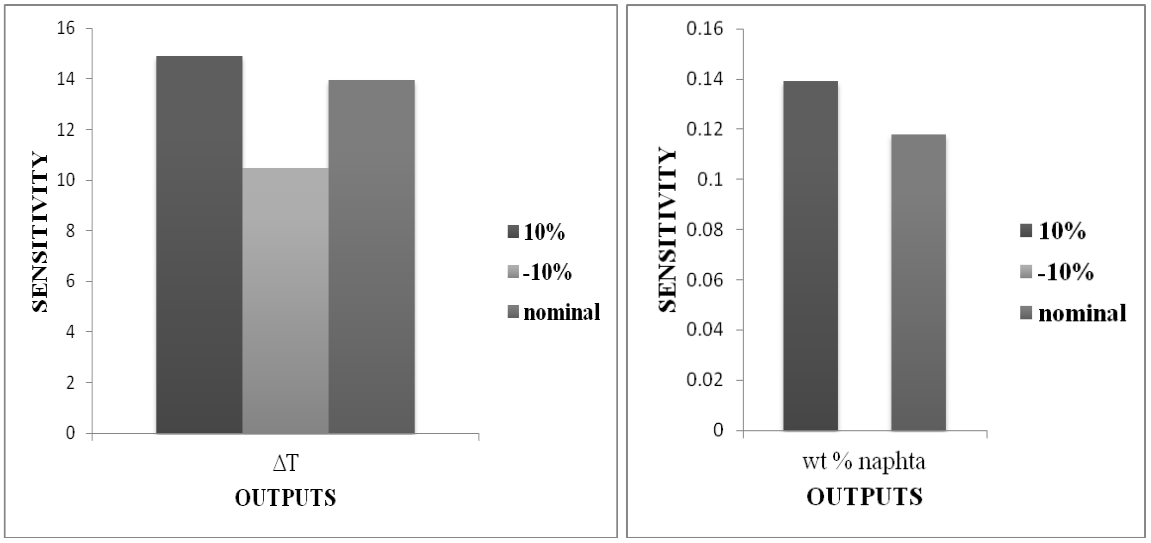

Figure 5.9: Effect of α on model outputs for a perturbation of ±10 %

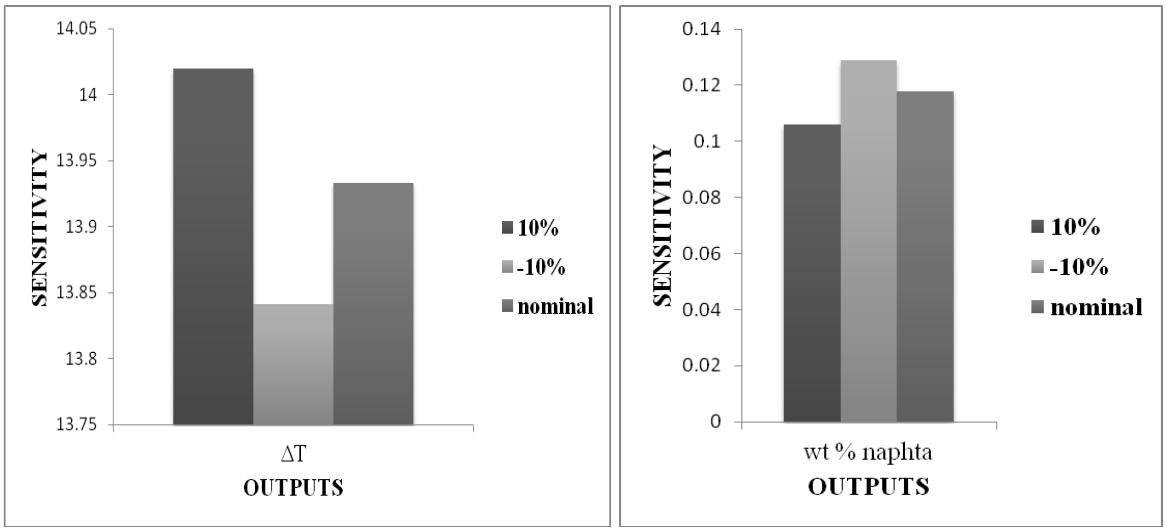

Figure 5.10: Effect of a_0 on model outputs for a perturbation of ±10 %

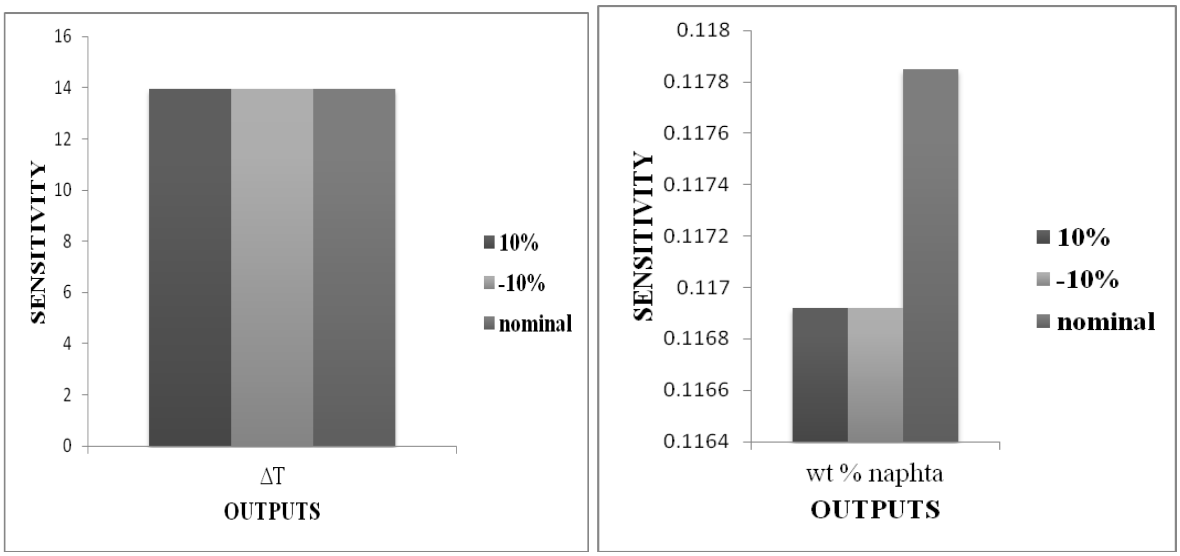

Figure 5.11: Effect of a_1 on model outputs for a perturbation of ±10 %

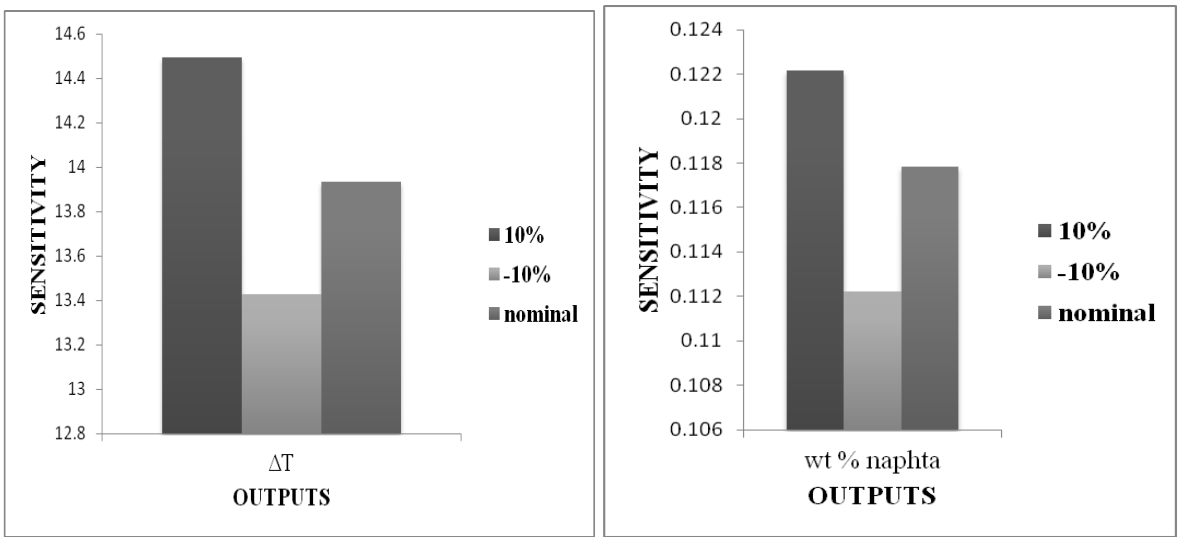

Figure 5.12: Effect of E_a on model outputs for a perturbation of ±10 %

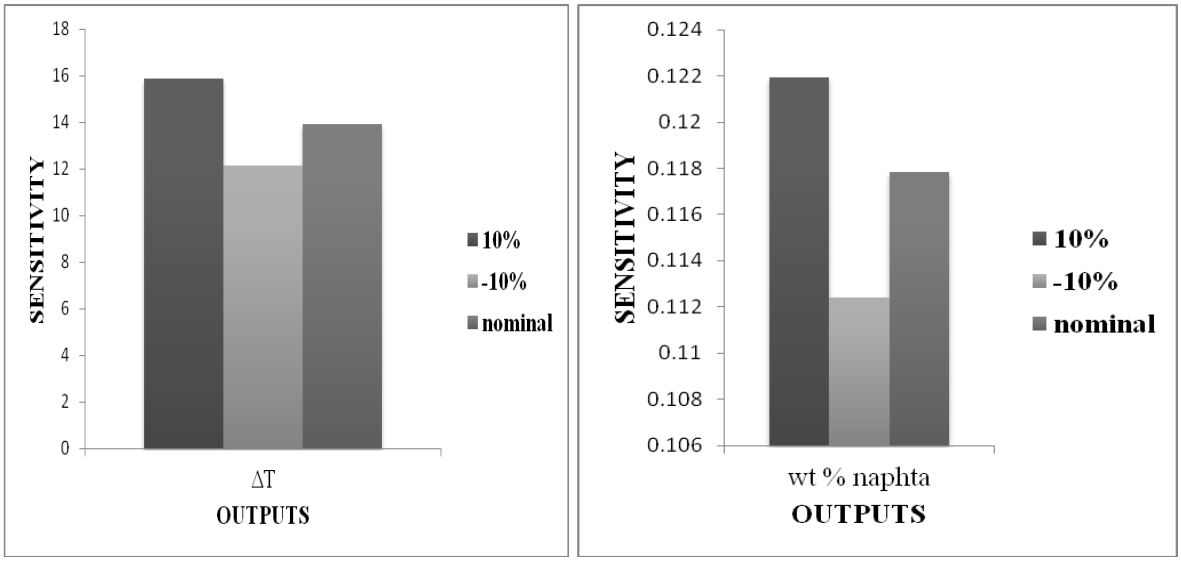

Figure 5.13: Effect of *c* on model outputs for a perturbation of ±10 %

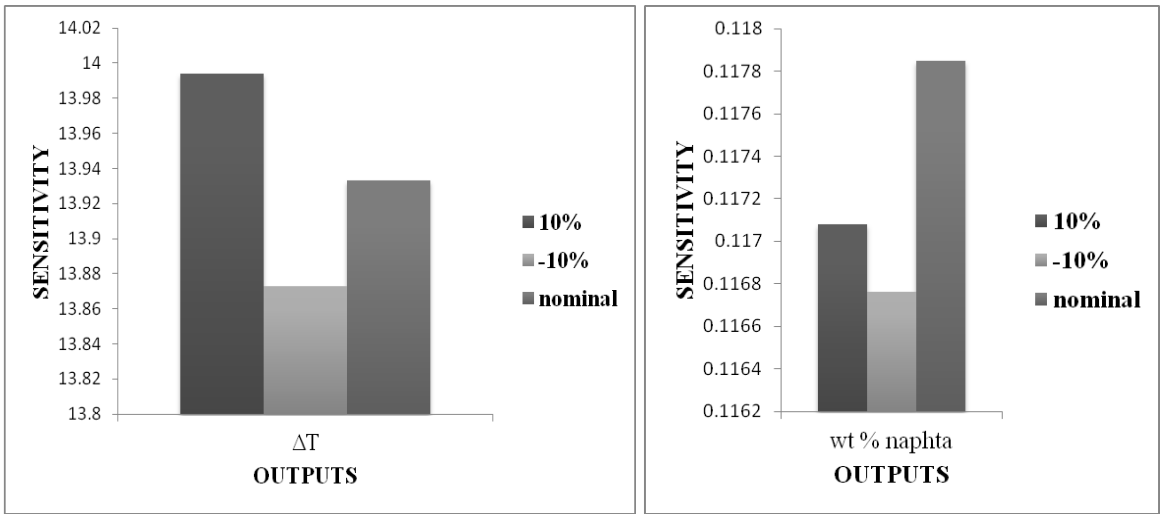

Figure 5.14: Effect of *m* on model outputs for a perturbation of ±10 %

The plotted changes of the outputs due to perturbations on parameters are recorded in Tables 5.5 and 5.6 to construct the normalized sensitivity matrix.

Table 5.5: Effects of 10% Perturbation in Parameters of 07.01.2014

Effects of 10% Change in Parameters on Outputs (ΔY_i)								
		k_{max}	***α***	***a_0***	***a_1***	***Ea***	***c***	***m***
	nominal	*0.1164*	*0.5569*	*1.0803*	*23.175*	*167856.3*	*-113.319*	*-0.01163*
naphta wt% (x_{naphta})	*0.1179*	0.1176	0.1393	0.1061	0.1169	0.12218	0.12192	0.11708
ΔT	*13.933*	10.299	14.882	14.02	13.933	14.496	15.869	13.994

Table 5.6: Effects of -10% Perturbation in Parameters of 07.01.2014

Effects of -10% Change in Parameters on Outputs (ΔY_i)								
		k_{max}	***α***	***a_0***	***a_1***	***Ea***	***c***	***m***
	nominal	*0.1164*	*0.5569*	*1.0803*	*23.175*	*167856.3*	*-113.319*	*-0.01163*
naphta wt% (x_{naphta})	*0.1179*	0.15262	0	0.12899	0.11692	0.11221	0.11241	0.11676
ΔT	*13.933*	31.837	10.479	13.841	13.933	13.426	12.145	13.873

Then the average of the values of effects caused by perturbations is calculated and sensitivity matrix is built. An example of sensitivity matrix is given in Table 5.7:

Table 5.7: Sensitivity Matrix S_{ij} for 07.01.2014

Sensitivity Matrix for 10% Change in Parameters							
	k_{max}	***α***	***a_0***	***a_1***	***Ea***	***c***	***m***
naphta wt% (x_{naphta})	-132.734	23.05617	-1.00999	0	1.81654E-11	3.8E-05	121.3862
ΔT	-690.688	6.163657	0.066601	0	1.64899E-11	0.000126	388.2304

After normalizing the sensitivity matrix and building normalized Fisher information matrices for some sets of parameters, the best set of parameters are determined by examining the related Fisher matrix as in Table 5.8 below:

Table 5.8: Fisher Information Matrix for 07.01.2014

k_{max}	c
1	7.82707e-15
7.82707e-15	1

The diagonal elements of the Fisher matrix are equal to one and the scalar products are small like defined above for non-correlated parameters. The parameters k_{max} and c are independent from each other and their variability can define the system best. Since these parameters are non-correlated, it is observed that adjusting only one parameter is enough to fit the plant data after many simulations since the yield of the product is adjusted to be similar in the plant and only temperature difference in the bed 3 is changing about 1-2.5 ˚C for different days. Then, only k_{max} is estimated in the simulations.

The other adjustable parameters are fixed to average values which are determined after many simulations. Table 5.9 gives the nominal values of the fixed parameters:

Table 5.9: Nominal Values of the Fixed Parameters

Parameter	Nominal Value
α	0.506552
a_0	0.962964
a_1	20.39343
Ea	149562.7
c	-105.349261
m	-0.01111

Since the model parameters are some kinetic parameters, it is important to determine if they are reliable or not. To do this, the related parameters are investigated in the literature and literature ranges of these parameters are constructed. The values are tabulated as follows:

Table 5.10: Literature Ranges for Parameters of HDS Model

Parameter	Value	Unit	Reference
k_{max}	0.74	h^{-1}	[113]
	1.35	h^{-1}	[42]
	0.18	h^{-1}	[27]
	0.0747		[91]
α	1.35	-	[42]
	0.72	-	[113]
	0.35	-	[27]
a_0	6.41	-	[42]
	3.08	-	[113]
	1.5	-	[27]
a_1	28.15	-	[42]
	26.13	-	[113]
	22	-	[27]
Ea	207-235	kJ/mol	[91]
	32.57 to 70.43	kcal/mol	[114]
c	-136.7	kJ/mol	[91]

The simulations are done with estimating only k_{max} parameter for hydrocracker model and the results are discussed in Chapter 6.

Chapter 6

RESULTS AND DISCUSSION

Results obtained in this study are going to be presented in this chapter. A user-friendly interface is introduced and simulations are carried out via this interface.

6.1. Interface for Simulation and Parameter Update Purposes

Development of a robust model is very important since it is not affected by the disturbances in the operating conditions and physical properties of the feedstock too much. But if the system is too sensitive to the disturbances and feed properties (e.g. reactor inlet temperature, total sulfur content, sulfur compounds) or if the operation conditions are different for every day, it is difficult to simulate all the days with one set of parameters. In these cases, the model can be modified by a disturbance model and/or parameters are updated online.

After construction of the first principle model for the hydrodesulfurization and hydrocracking reactors and deciding the number of parameters, simulations are done to observe the relationship between the operating conditions and the model parameters. In the plant, each day has different characteristics and this makes difficult to define a constant parameters set. Furthermore, the characteristics of the shifts in same day may differ since the system is continuous. The effects of these small changes on hydrodesulfurization and hydrocracking reactors cannot be ignored. Thus, parameters may be updated for each shift if needed. The plant operates within three shifts; shift one is between 00:00-08:00, shift two

is between 08:00-16:00 and shift three operates between 16:00-24:00. Sulfur content of naphta product and distillation data for naphta product are only measured in shift two by analysis in the laboratory over a period of time (e.g. once a week) and distillation data for feed, distillation data for diesel product and sulfur content of the diesel product are measured in every shift. To simulate the HDS and HC reactors together, a data set is generated from the plant data that includes necessary information needed in the model. The trend in the temperature difference in the first and second beds of the HDS reactor, temperature difference in the hydrocracker bed, mass flow rate of sulfur in the HDS reactor feed, product sulfur content at the reactor exit and mass fraction of naphta in the product is monitored for 18 shifts selected from the data set in figures below to observe the trend of change.

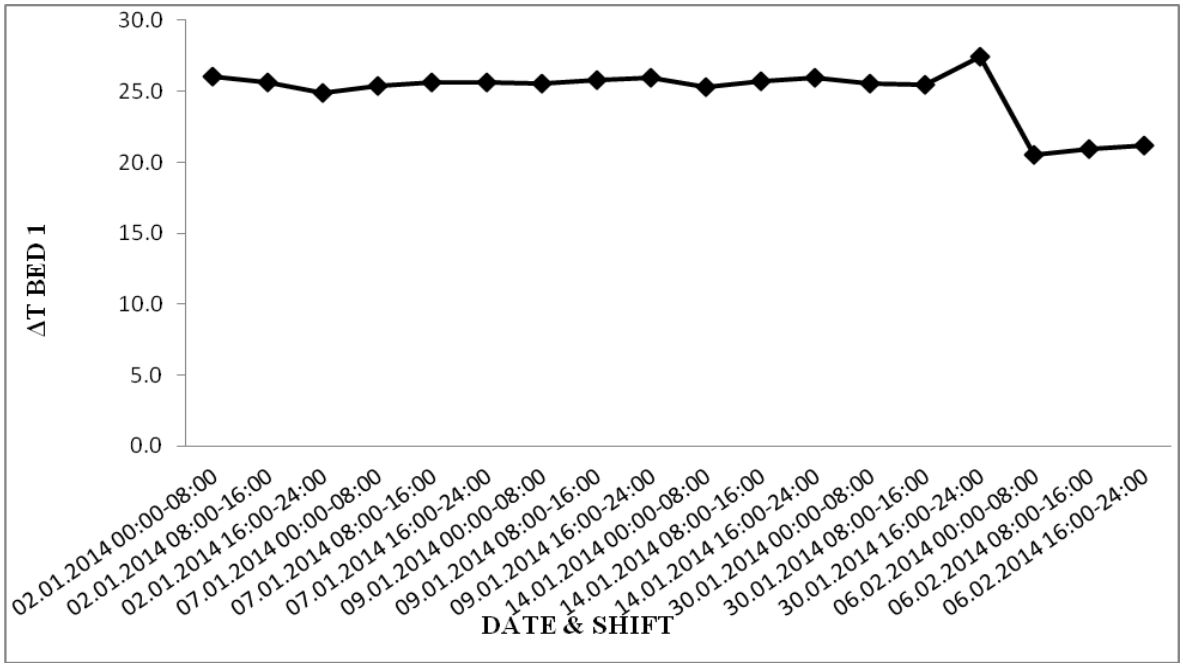

Figure 6.1: Plant data for temperature difference in bed 1

The temperature difference in the first bed of the hydrodesulfurization reactor varies 0.5-3˚C and these changes are related to amount of sulfur entering the bed and the compound types of the sulfur removed in this bed since each compound has different heat of reaction values [109].

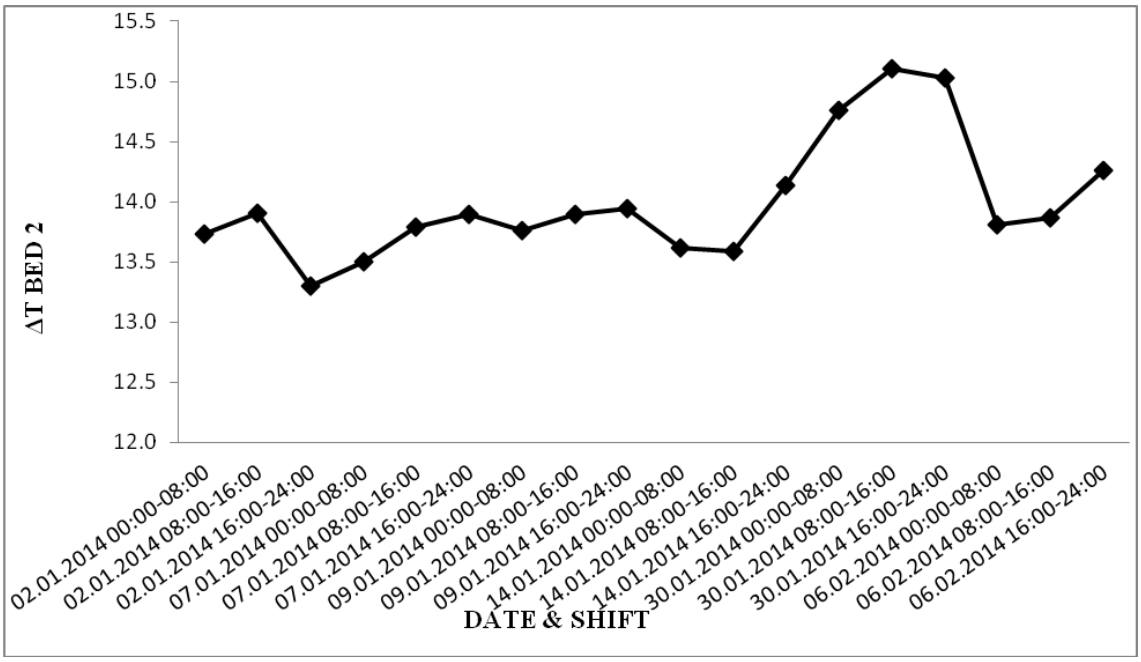

Figure 6.2: Plant data for temperature difference in bed 2

The temperature difference in the second bed of the hydrodesulfurization reactor varies 1-4 ˚C.

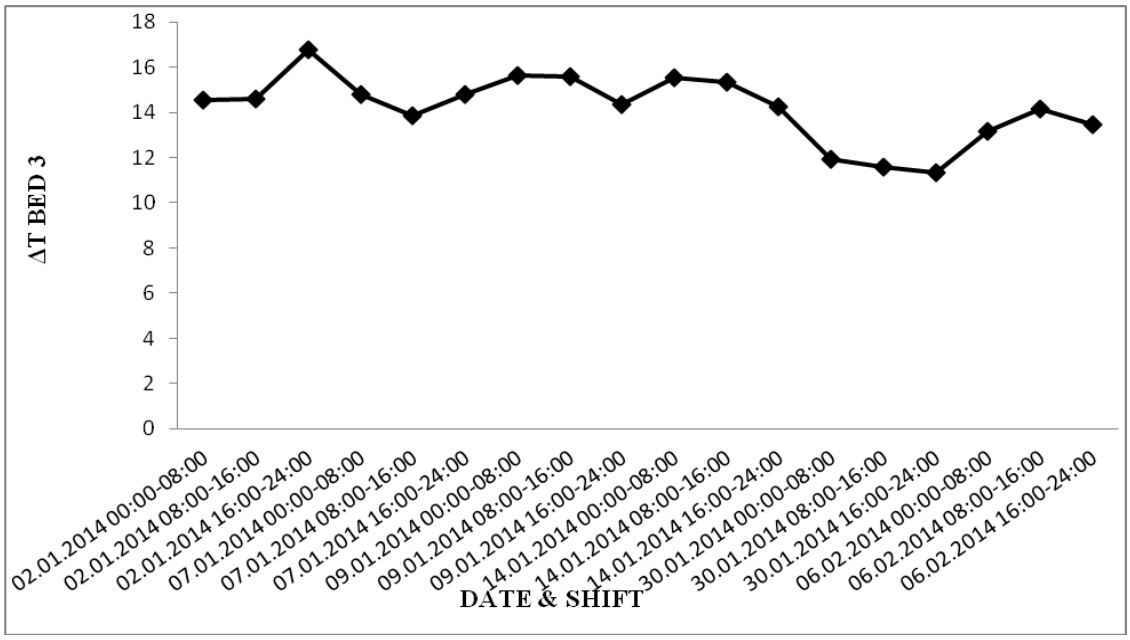

Figure 6.3: Plant data for temperature difference in bed 3

As seen from Figure 6.3, the temperature varies in the hydrocracker bed. Thus, it is difficult to simulate the hydrocracker with a constant parameter set, updating only one parameter (see Chapter 5) is necessary to catch the trend in the plant.

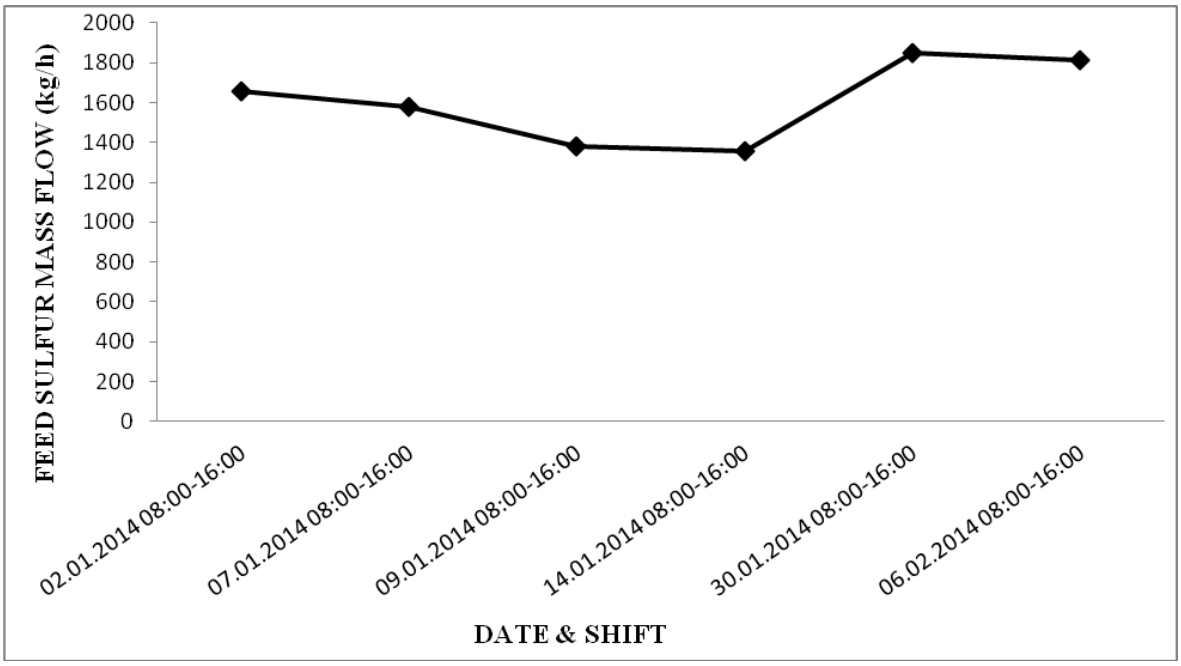

Figure 6.4: Plant data for sulfur mass flow rate measurements of feed

The sulfur content of the HDS reactor feed is measured only in shift two which operates between 08:00 and 16:00. The feedstock of the hydrodesulfurization reactor is a blended diesel stream and it has different sulfur contents for each day since the blended streams have also different sulfur contents and the more heavier fractions contain more sulfur and heavier sulfur compounds.

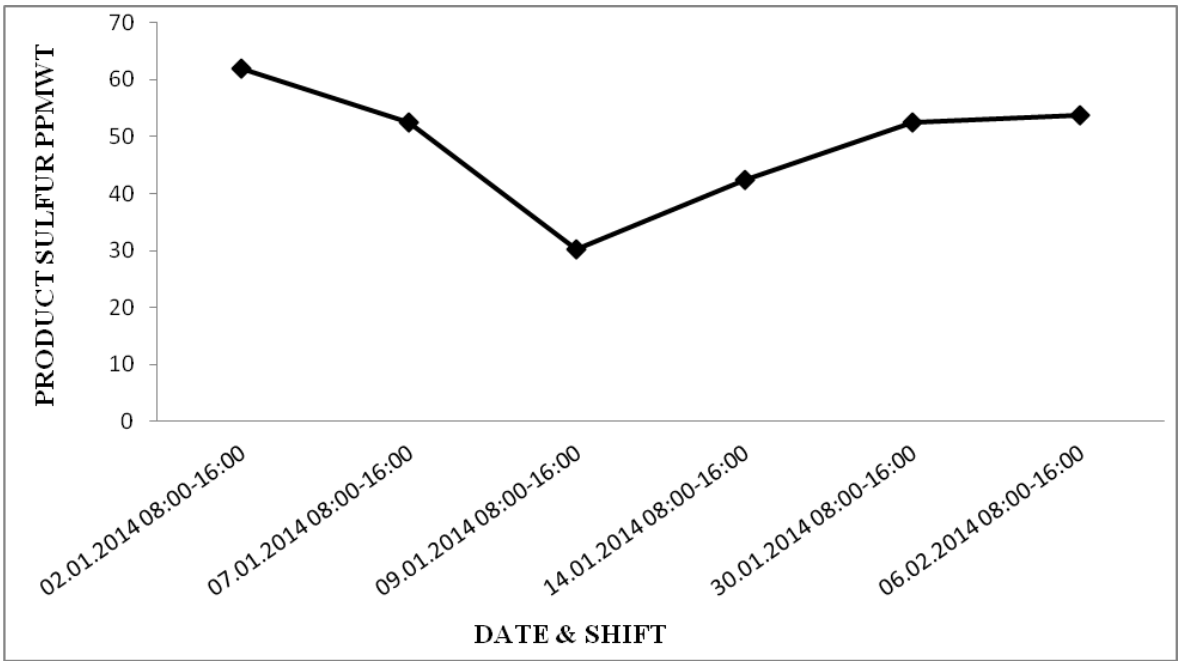

Figure 6.5: Plant data for sulfur ppmwt in product

The sulfur content of the naphta is measured only in shift two which operates between 08:00 and 16:00 once a week or occasionally. Thus, the total sulfur content of the product is calculated for these data points. In the hydrodesulfurization reactor, conversion of the HDS reaction is always about 99% in the plant and very small amount of sulfur remains in the mixture. Since this amount is really small at ppmwt level, the model has to be very sensitive to estimate such an amount with true parameters. So, generating a constant parameter set is difficult and real-time update of the parameters is required in the plant.

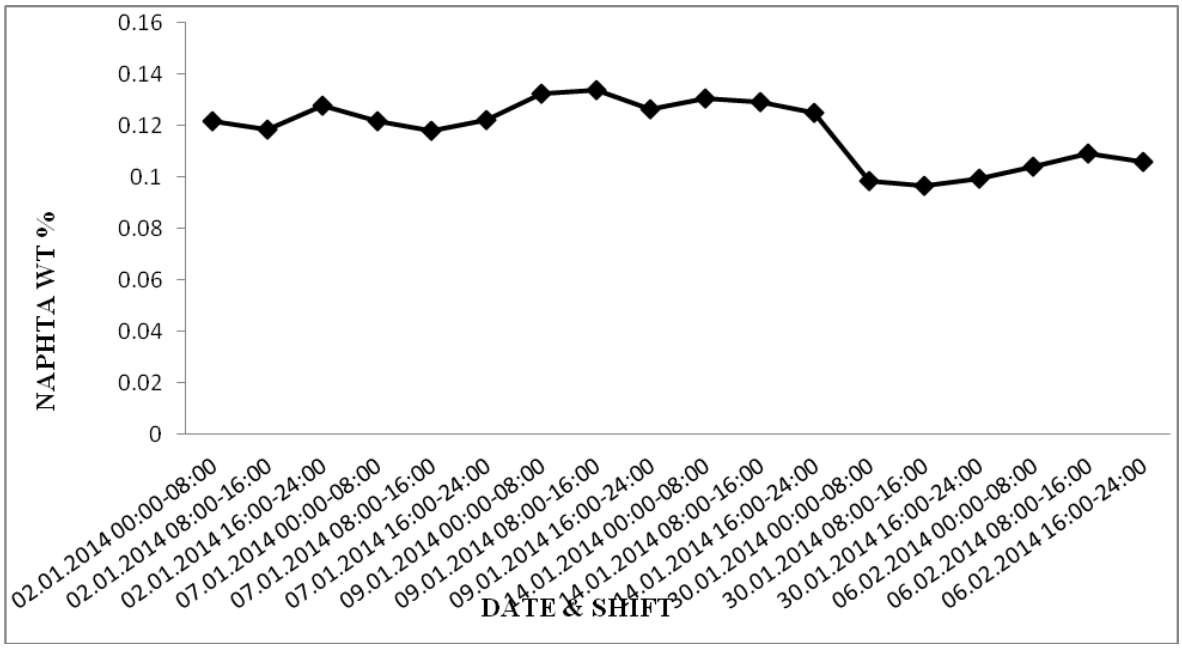

Figure 6.6: Plant data naphta wt% in product

As seen from Figure 6.6, the amount of naphta in the product differs for different days and shifts. This requires updating the parameter in the hydrocracking model.

As seen from the figures above, the days and shifts have different characteristics from each other. Besides, the limits on the operating conditions of the plant have to be considered for the safety of the reactor, catalyst deactivation, product specifications and some other physical constraints. Even 1 ˚C change is very important if we take the catalyst deactivation into account. This brings a necessity of development of an interface to simulate every day and every shift in the plant and update the model parameters due to changes in the real-time.

The user-friendly interface requires some plant data as input to simulate the plant and if there is a need, the model parameters can be updated. As mentioned in Chapter 3, D86

distillation data of the feed, naphta and diesel is required to build weight fraction versus normalized TBP curves after some conversions. Product TBP data is taken from ASPEN HYSYS Oil Manager and used to build product weight fraction curve. The cuts are constructed on a width basis 8˚C. Total sulfur content is necessary to construct a sulfur curve for hydrodesulfurization model and the other data such as inlet and outlet temperatures are used to compare the results of the model with the plant. Some default values are entered to give the user an idea about the inputs. In the first step, the interface requires these inputs, then the necessary model parameters for both hydrodesulfurization and hydrocracking models are entered to simulate the reactors. In this study, the adjustable model parameters are determined as k_{min1}, k_{min2} and ΔH_2 for the hydrodesulfurization model and k_{max} for the hydrocracking model. The snapshots of the interface are given in the Figure 6.7 and 6.8 below;

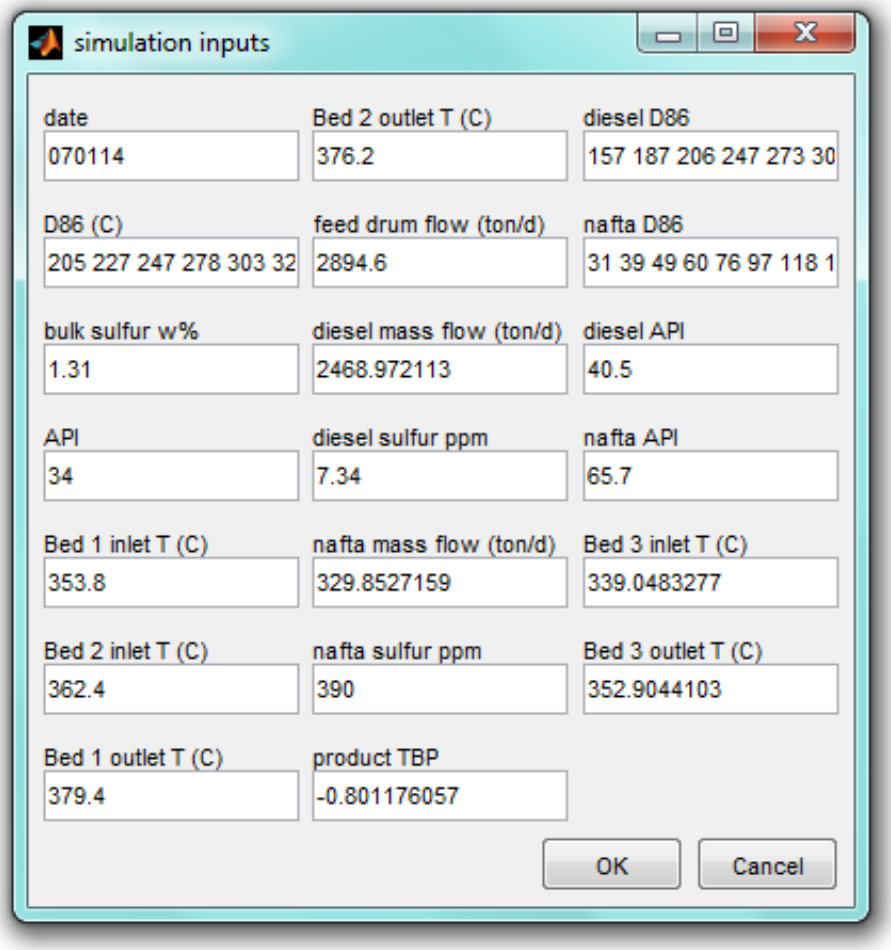

Figure 6.7: Interface window for inputs of simulation

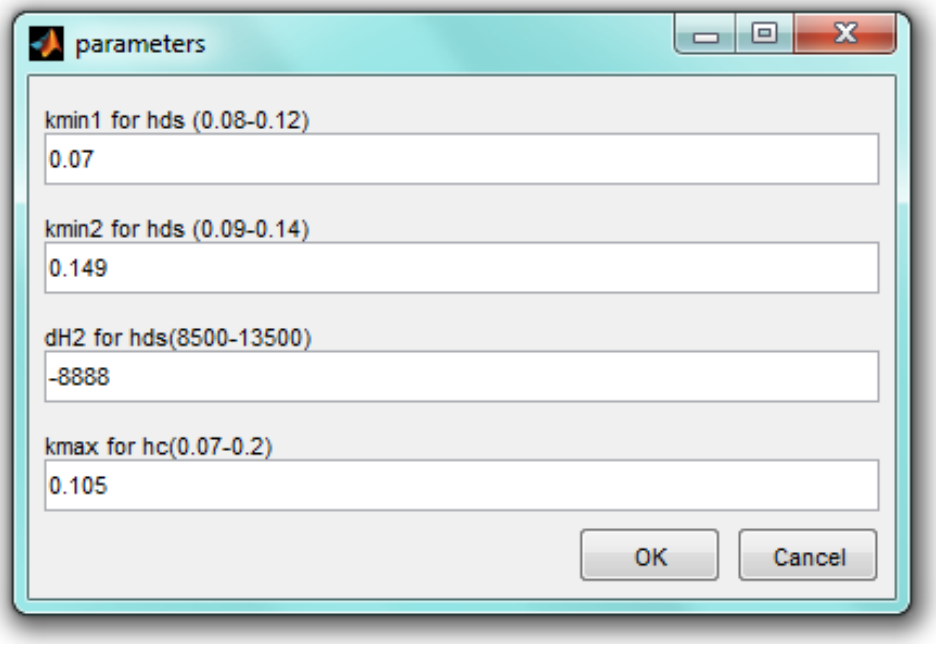

Figure 6.8: Interface window for input parameters of simulation

6.2. Simulations of Days

The interface simulates the model like a real plant after entering the necessary data and the simulation gives some plots to observe the results. Examples of the plots are shown for a selected day (30.01.2014 shift: 08:00-16:00) in figures below. For the day under interest, parameters are estimated and the model results agree well with the plant data.

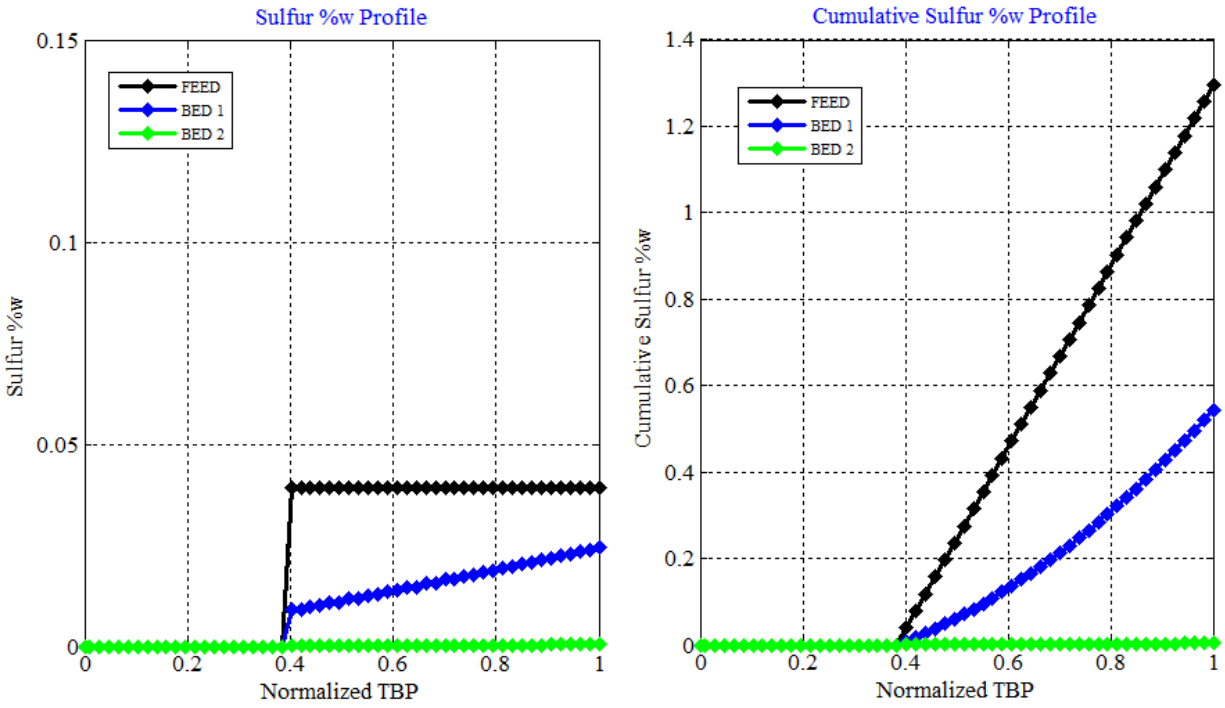

Figure 6.9: Simulation results of HDS reactor

As mentioned in Chapter 4, the feed sulfur distribution is assumed to be uniform and the cumulative sulfur wt % curve is a linear curve which is marked as black in Figure 6.9 above. Before entering the hydrodesulfurization reactor, the feed contains 1.296 wt % sulfur which corresponds to the end point of the black cumulative sulfur curve. As the hydrodesulfurization reaction takes place, sulfur is removed from the pseudocomponents and some sulfur species remains at the exit of the bed 1 which is represented as blue line. Higher boiling point compounds which corresponds higher value of θ contain more refractive sulfur compounds and since their reactivity is lower, they remain in the higher boiling point cuts as can be seen. The green line represents the amount of sulfur remained after bed 2. In the second bed of the hydrodesulfurization reactor, more sulfur species is

removed but there are still remaining sulfur species which are the most refractory compounds which can be seen in Figure 6.10 by zooming into the green line.

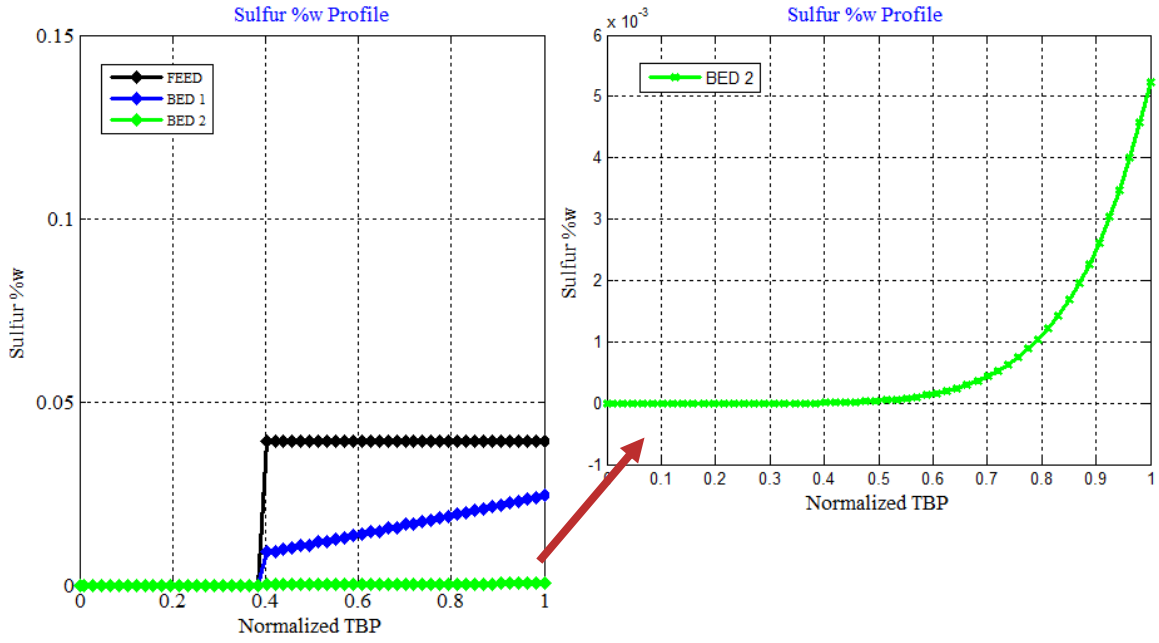

Figure 6.10: Remaining sulfur at the HDS reactor exit

The amount of the remaining sulfur at the hydrodesulfurization bed is very small and most of the sulfur which presents in the feedstock is removed. The consumption of sulfur along the HDS reactor is plotted in Figure 6.11 below. For the day under interest, the plant data is given in red with subscript p and the blue represents the model results with subscript m. As seen from Figure 6.11, sulfur is consumed along the reactor length for both hydrodesulfurization beds due to HDS reactions. The consumed sulfur amounts and remaining sulfur in the product are quite close with the estimated parameters for this particular day.

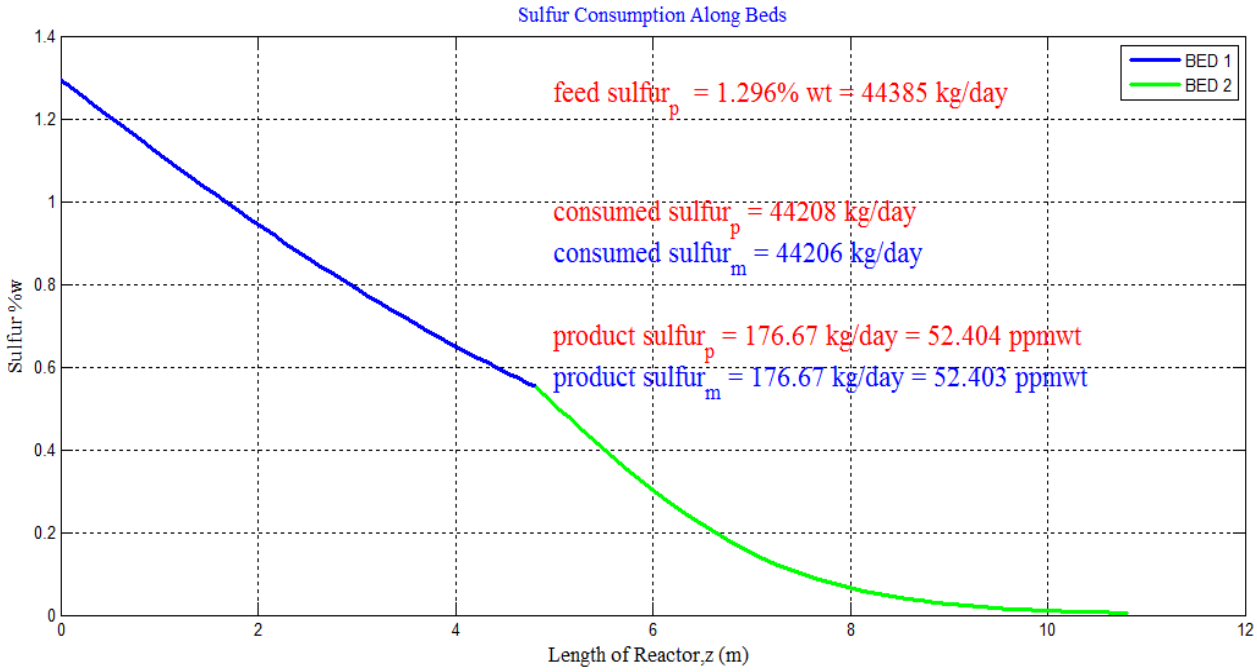

Figure 6.11: Remaining sulfur at the HDS reactor exit

Since the models are non-isothermal and the effect of the temperature is considered, the temperature profiles are other outputs of the both hydrodesulfurization and hydrocracking models. The temperature profile for the hydrodesulfurization reactor is given in Figure 6.12. Hydrodesulfurization reactions are exothermic due to hydrogenation and the temperature increases as the reaction proceeds along the bed 1. Products of the bed 1 are cooled by hydrogen quench between beds and the cooled products enter to bed 2 with a lower temperature and again temperature of the bed 2 increases due to reactions. With same coding, the red data show the plant temperature differences in the bed 1 and bed 2 and the blue ones indicates the model results. It can be seen that model results fit the plant data if the model is simulated with the estimated parameters of a particular day. Hydrogen

consumption is estimated for bed 1 and bed 2 and total hydrogen consumption is calculated after the assumptions made in Chapter 4. Since, the hydrogen consumption data is not available for only the hydrodesulfurization reactor, comparison with the plant data is not possible.

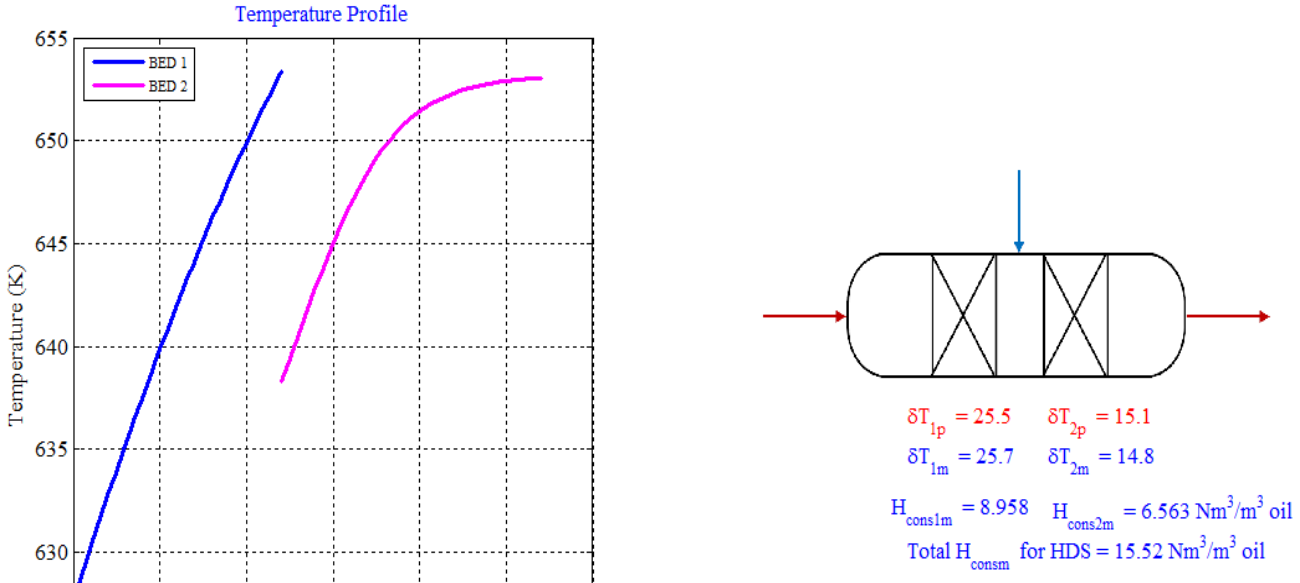

Figure 6.12: HDS reactor temperature profile

The sulfur-free hydrocarbon mixture enters the hydrocracker after the hydrodesulfurization reactor. The results of the simulation of the hydrocracker is plotted in Figure 6.13. In hydrocracker, higher boiling point species crack into lower boiling point species via hydrocracking reactions to yield products (black) that have boiling point range less than of the feed (green). To obtain the plant product mass fraction curve, naphta and

diesel is blended as mentioned in Chapter 5. Black line represents the plant data while black circles indicate the cumulative mass fractions versus normalized TBP which are model outputs. It can be seen that black circles which represents the model outputs overlap with black curve that indicates the plant data. The mass fraction of the naphta (N_w) and the mass fraction of diesel (D_w) in the product are calculated by the cut-point concept defined in Chapter 5 and the model and plant yields are compared. The model results agreed well with the plant data after the simulation with estimated hydrocracker model parameter, k_{max}.

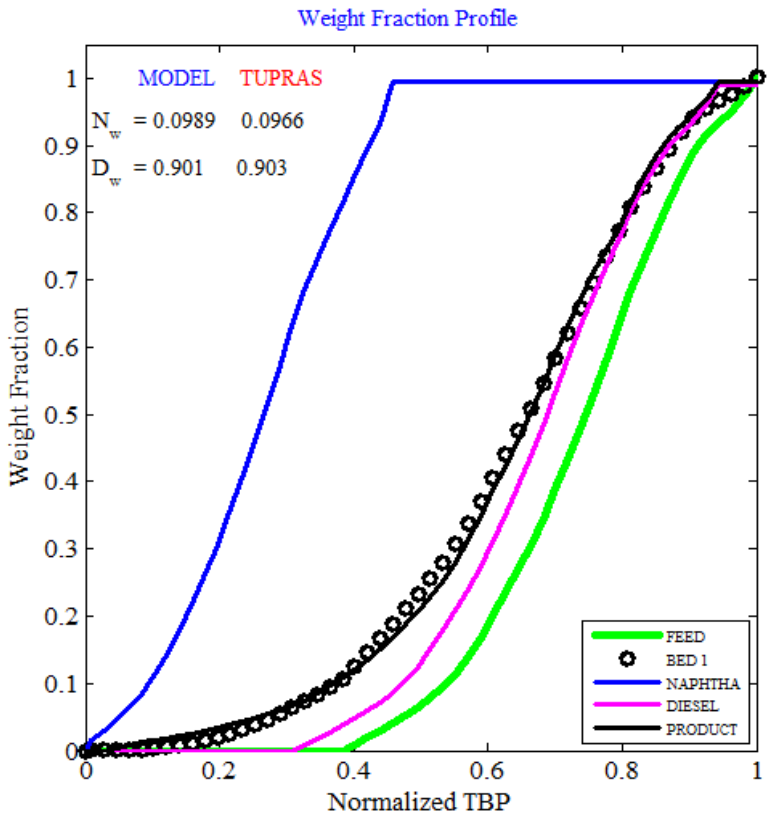

Figure 6.13: Results of HC simulations

The temperature profile for the hydrocracking reactor is given in Figure 6.14. Hydrocracking reactions are exothermic in nature and the temperature increases as the reaction proceeds along the bed 3. Red data show the plant temperature difference in the hydrocracker bed 3 and the blue one indicates the model result. It can be seen that model result fits the plant data if the model is simulated with the estimated parameters of a particular day.

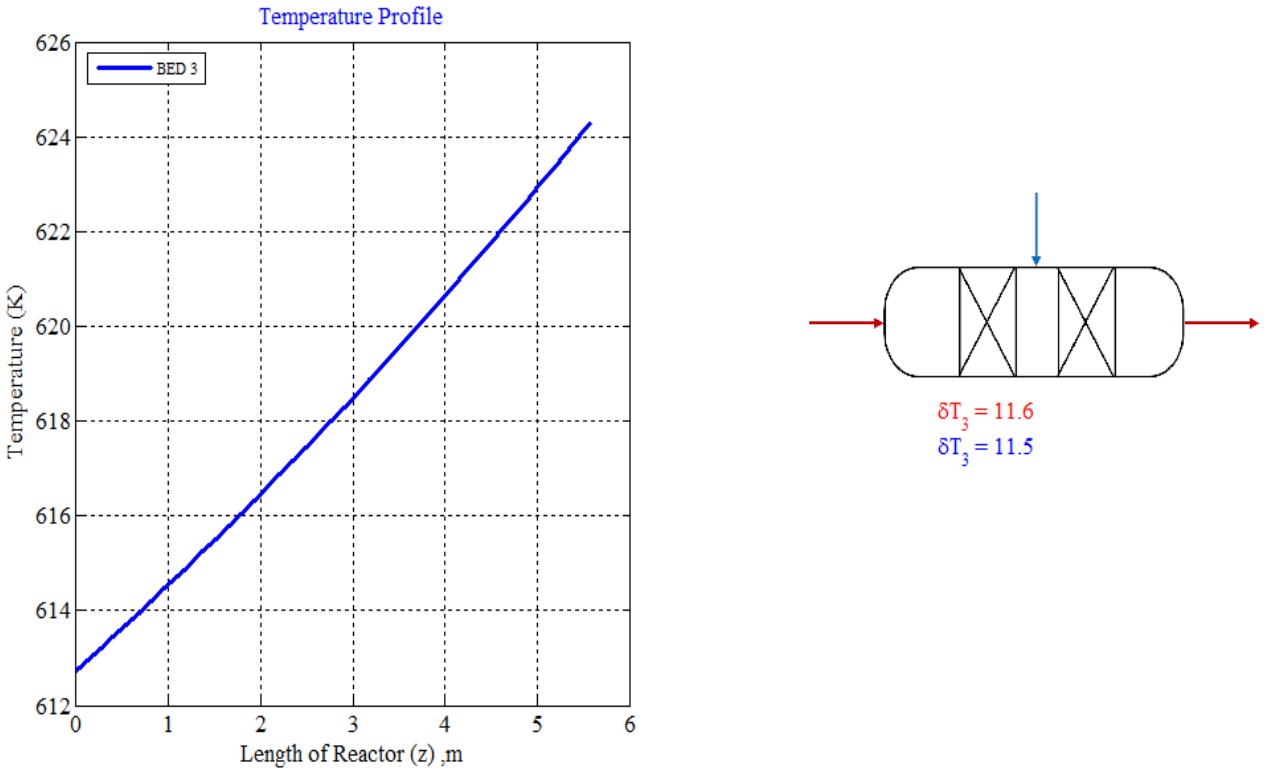

Figure 6.14: Temperature profile for HC reactor

The overall performance of the model can be presented as in the Figure 6.15 for a particular date.

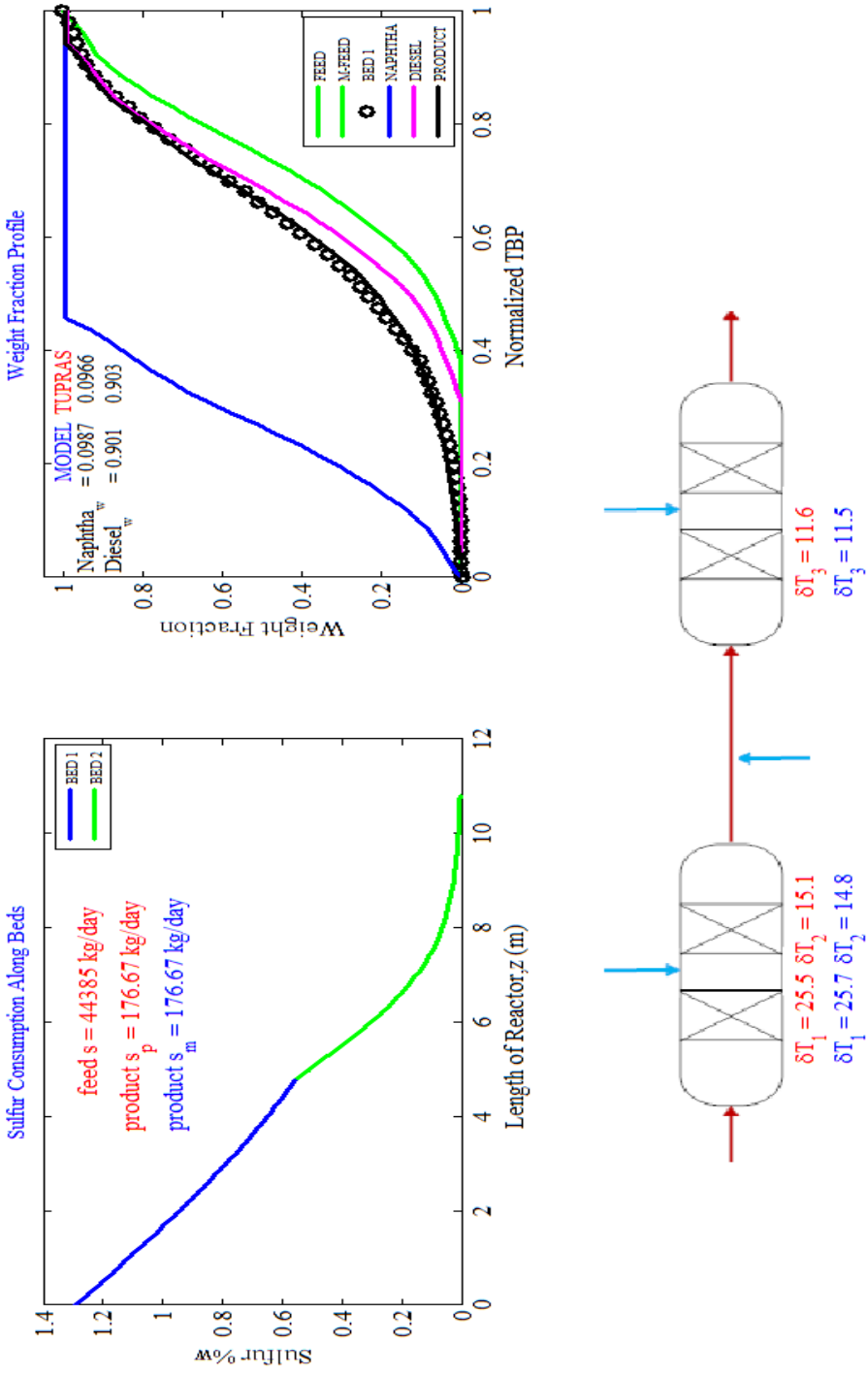

Figure 6.15: Overall performance of the HDS and HC models for 30.01.2014

6.3. Monitoring of Model Parameters

The simulations are done for 18 shifts and the parameters are estimated to monitor the changes in the values of the parameters. After many simulations, it is observed that $k_{min1,HDS}$ and $\Delta H_{2,HDS}$ parameters are more effective to match temperature differences in the hydrodesulfurization reactor and $k_{min2,HDS}$ parameter is more effective to match sulfur content of the product. Hydrocracker simulations are done with another independent parameter $k_{max,HC}$. The parameters of HDS and HC models are estimated simultaneously. Thus, each shift has four parameters ($k_{min1,HDS}$, $k_{min2,HDS}$, $\Delta H_{2,HDS}$, $k_{max,HC}$). The shifts (shift 1) 00:00-08:00 and (shift 3) 16:00-24:00 have only temperature measurements for the HDS reactor, so the parameter estimation for these shifts can be done with two adjustable parameters $k_{min1,HDS}$ and $\Delta H_{2,HDS}$. Since there is only one shift with product sulfur content measurement, this shift requires adjusting parameter $k_{min2,HDS}$ to estimate the sulfur content of the product in addition to parameters $k_{min1,HDS}$ and $\Delta H_{2,HDS}$ which are used to match the temperature differences of the shift. In the meantime, hydrocracking reactor is simulated with adjustable parameter $k_{max,HC}$. These adjustable parameters can be kept constant if the error between model and plant data is relatively small. If the error is not tolerable, some model parameters can be adjusted to match the plant data.

The procedure for the parameter estimation is as follows:

1. Three model parameters ($k_{min1,HDS}$, $\Delta H_{2,HDS}$, $k_{max,HC}$) are estimated for the first shift (00:00-08:00) of the day and $k_{min2,HDS}$ is kept constant. After estimating these three parameters, the model is simulated to see how close the model results to plant data and error between the plant and model data is calculated. An example of this step is given in Figure 6.16 for the shift 1 (00:00-08:00) on 07.01.2014.

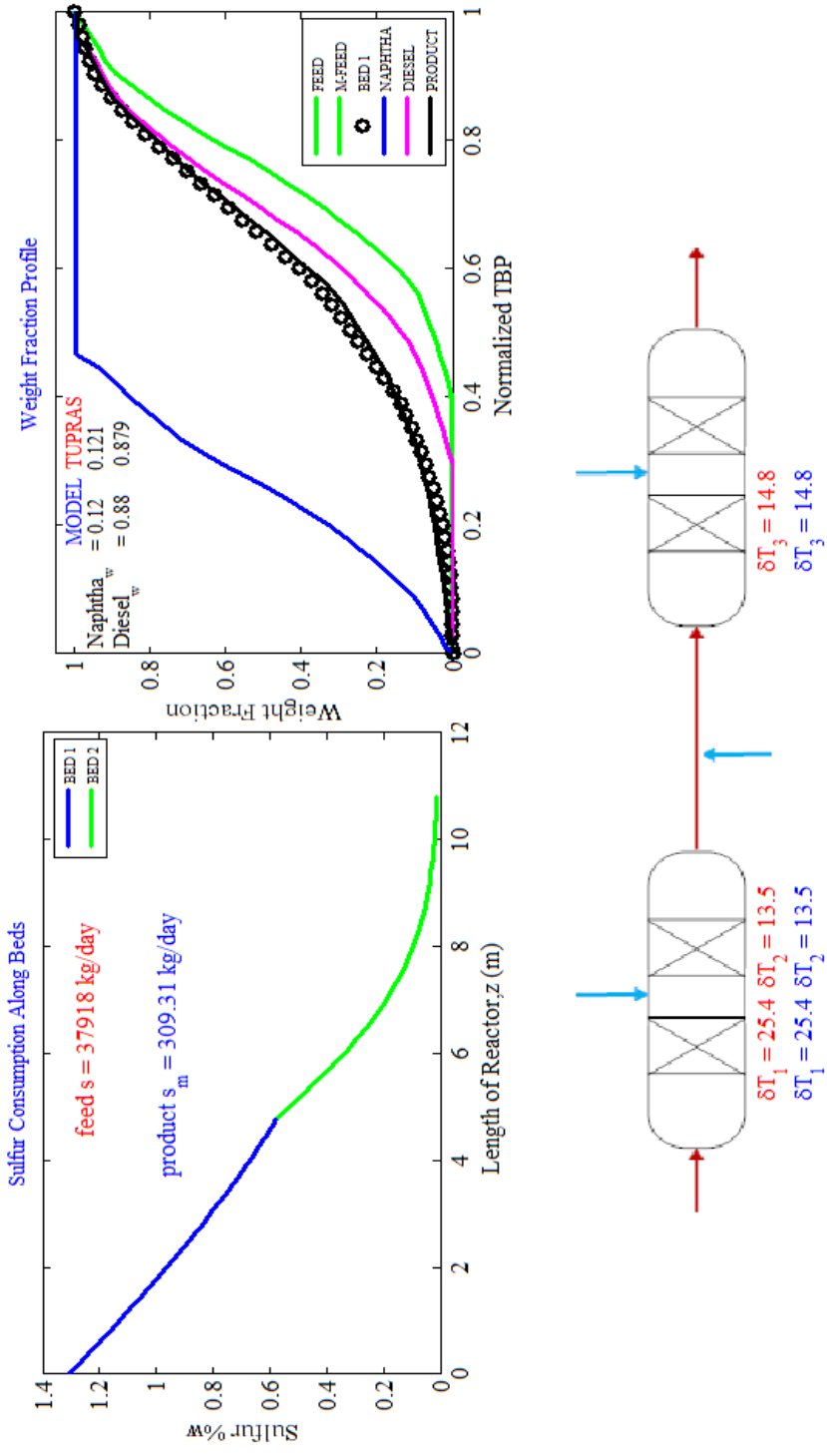

Figure 6.16: Overall performance of the HDS and HC models for shift 1 on 07.01.2014

Table 6.1 gives the values of the percent errors between model outputs and plant data.

Table 6.1: Percent Error of Prediction (07.01.2014 00:00-08:00)

		Products [% wt]		Bed Exit Temperatures [°C]		
	Sulfur [% wt]	Diesel	Naphtha	T_1	T_2	T_3
Error %	-	0.59	4.2	0.00084	0.00022	0.009

Since the units of outputs differ, the values of errors are considered independently. Moreover, plant restrictions have to be considered while evaluating errors such as 0.5 or 1 ˚C deviation is acceptable in the temperature results which mean errors in the bed exit temperature bigger than 0.1 % are not tolerable and requires updating of parameters to reduce the errors. The values of the parameters are as follows:

Table 6.2: Model Parameters for Shift 1 on 07.01.2014

date &shift	$k_{min1,HDS}$	$k_{min2,HDS}$	$\Delta H_{2,HDS}$	$k_{max,HC}$
07.01.2014 00:00-08:00	0.068304	0.141111	-7230.74	0.105604

2. The second shift (08:00-16:00) has product sulfur measurement. First, this shift is simulated with the parameters of shift 1 like in Figure 6.17 for the second shift on 07.01.2014 and the error between the plant and model data is calculated like given in Table 6.3.

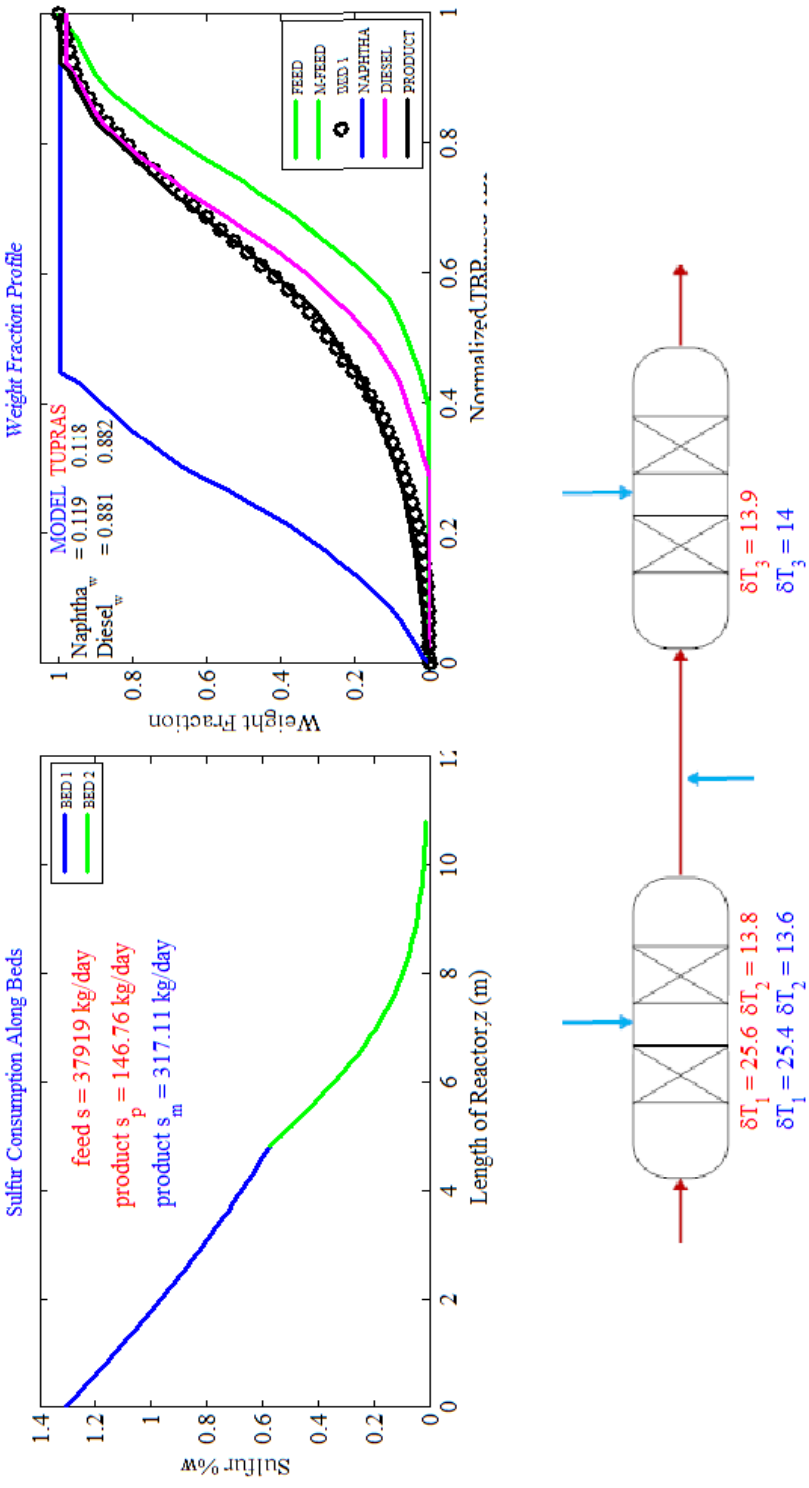

Figure 6.17: Overall performance of the HDS and HC models for shift 2 on 07.01.2014

Table 6.3: Percent Error of Prediction (07.01.2014 08:00-16:00)

		Products [% wt]		Bed Exit Temperatures [°C]		
	Sulfur [% wt]	Diesel	Naphtha	T_1	T_2	T_3
Error %	1.2e+002	0.086	0.64	0.04	0.036	0.028

Table 6.3 shows the error in the product sulfur weight percent is not tolerable. This requires adjusting of the $k_{min2,HDS}$ parameter since it is effective to match the sulfur content. The remaining parameters $k_{min1,HDS}$, $\Delta H_{2,HDS}$, $k_{max,HC}$ are kept constant due to other small errors. They also can be adjusted if necessary. The parameters are as follows:

Table 6.4: Model Parameters for Shift 2 on 07.01.2014

date &shift	$k_{min1,HDS}$	$k_{min2,HDS}$	$\Delta H_{2,HDS}$	$k_{max,HC}$
07.01.2014 08:00-16:00	0.068304	0.16985	-7230.74	0.105604

The model is simulated with the parameters in Table 6.4 and the results are given in Figure 6.18. The prediction errors are small and tolerable after simulating the model with updated parameters;

Table 6.5: Percent Error of Prediction (07.01.2014 08:00-16:00) After Updating the Parameters

		Products [% wt]		Bed Exit Temperatures [°C]		
	Sulfur [% wt]	Diesel	Naphtha	T_1	T_2	T_3
Error %	0.0012	0.085	0.64	0.04	0.013	0.027

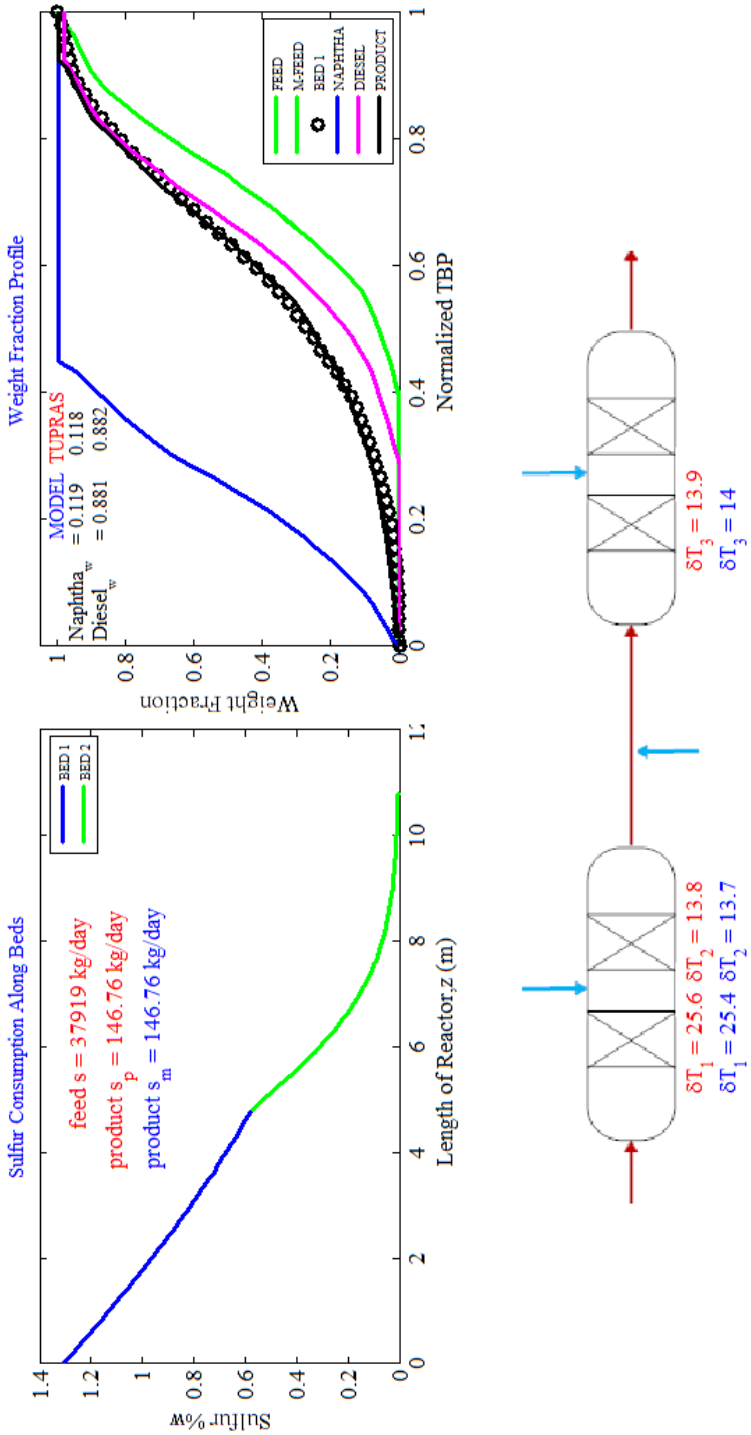

Figure 6.18: Overall performance of the HDS and HC models for shift 2 on 07.01.2014 after udpating parameters

3. The third shift (16:00-24:00) is simulated with the last parameters of the second shift given in Table 6.4 and the errors are checked to see if they are tolerable or not. It is not possible to compare the sulfur content of the product since there is not any plant data related in the third shift.

Table 6.6: Percent Error of Prediction (07.01.2014 16:00-24:00)

		Products [% wt]		Bed Exit Temperatures [°C]		
	Sulfur [% wt]	Diesel	Naphtha	T_1	T_2	T_3
Error %	-	0.37	2.6	0.067	0.014	0.018

As seen from Table 6.5, the errors are relatively small, then the parameters are not updated and same parameters are used with second shift.

Table 6.7: Model Parameters for Shift 3 on 07.01.2014

date &shift	$k_{min1,HDS}$	$k_{min2,HDS}$	$\Delta H_{2,HDS}$	$k_{max,HC}$
07.01.2014 16:00-24:00	0.068304	0.16985	-7230.74	0.105604

The simulation plots are given in Figure 6.19.

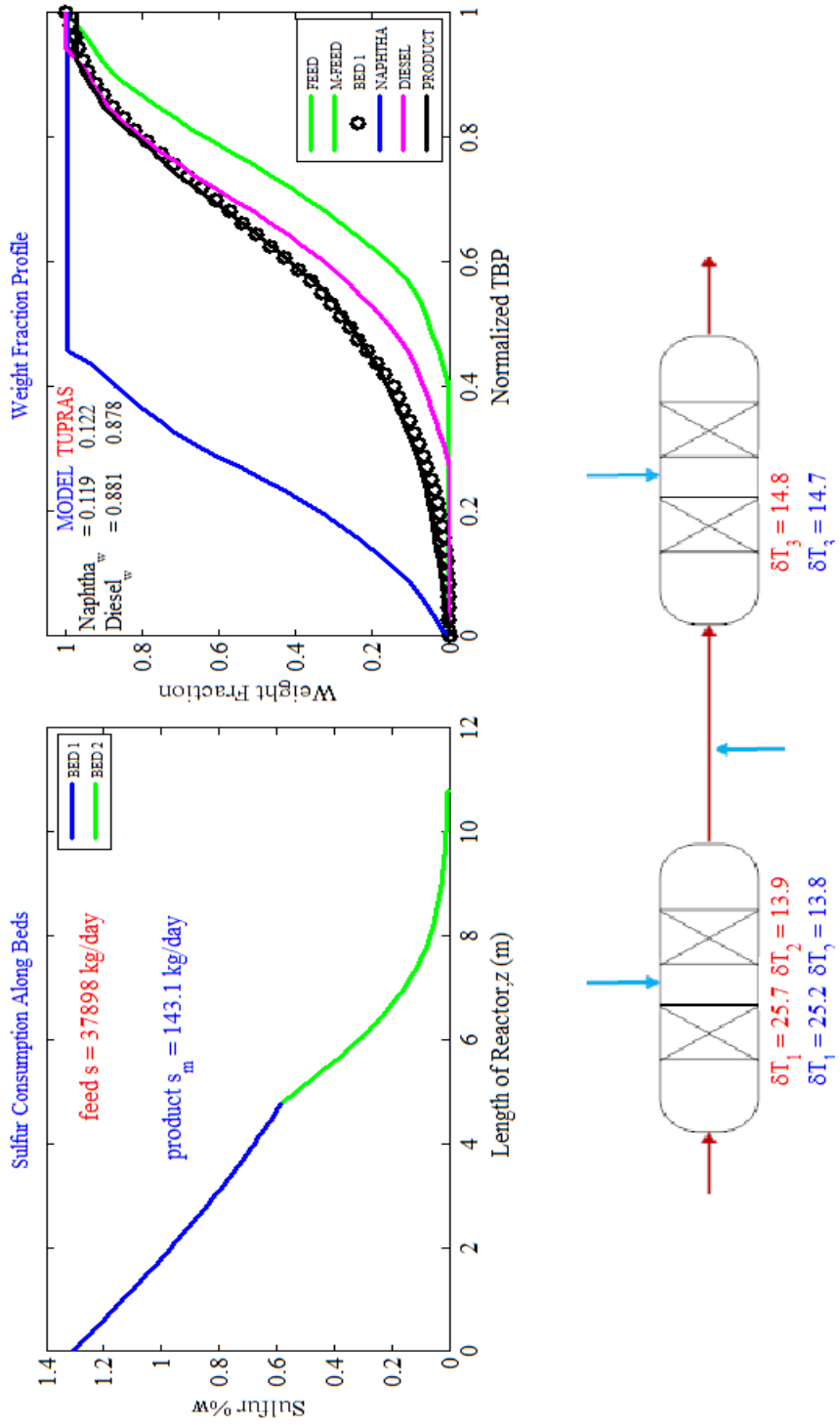

Figure 6.19: Overall performance of the HDS and HC models for shift 3 on 07.01.2014

4. The first shift of the next day is simulated with the last parameters which are the parameters of the third shift of the previous day. Similar to other steps, errors are calculated to see the difference between model and plant data.

Table 6.8: Percent Error of Prediction (09.01.2014 00:00-08:00)

		Products [% wt]		Bed Exit Temperatures [°C]		
	Sulfur [% wt]	Diesel	Naphtha	T_1	T_2	T_3
Error %	-	1.3	8.7	0.57	0.25	0.2

As seen from Table 6.8, the errors in the bed exit temperatures are relatively intolerable due to plant restrictions and the parameters $k_{min1,HDS}$, $\Delta H_{2,HDS}$, $k_{max,HC}$ that are effective to match temperatures are needed to be updated by parameter estimation. Since there is not any plant measurement related to product sulfur content in first shift, $k_{min2,HDS}$ parameter is kept constant at the same value in the previous parameter set. Figure 6.20 shows the plots of this simulation and the errors can be seen on the figure.

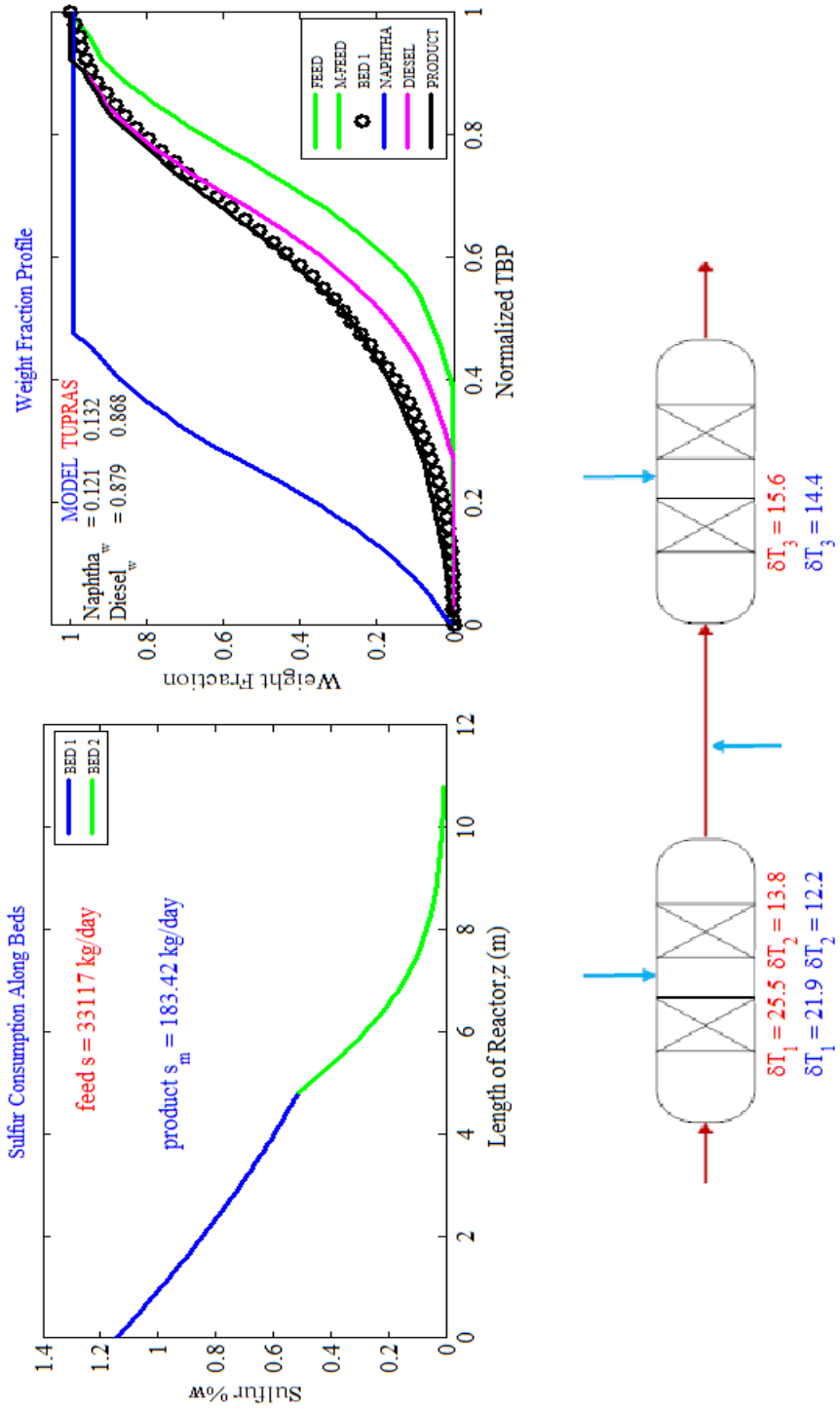

Figure 6.20: Overall performance of the HDS and HC models for shift 1 on 09.01.2014

After parameter estimation, new model parameters are updated as follows:

Table 6.9: Model Parameters for Shift 1 on 09.01.2014

date &shift	$k_{min1,HDS}$	$k_{min2,HDS}$	$\Delta H_{2,HDS}$	$k_{max,HC}$
09.01.2014 00:00-08:00	0.099861	0.16985	-10290.6	0.112982

Prediction errors are given in Table 6.10 and simulation results are given in Figure 6.21 below.

Table 6.10: Percent Error of Prediction (09.01.2014 00:00-08:00) After Updating Parameters

		Products [% wt]		Bed Exit Temperatures [°C]		
	Sulfur [% wt]	Diesel	Naphtha	T_1	T_2	T_3
Error %	-	0.075	0.49	0.0049	0.001	0.00047

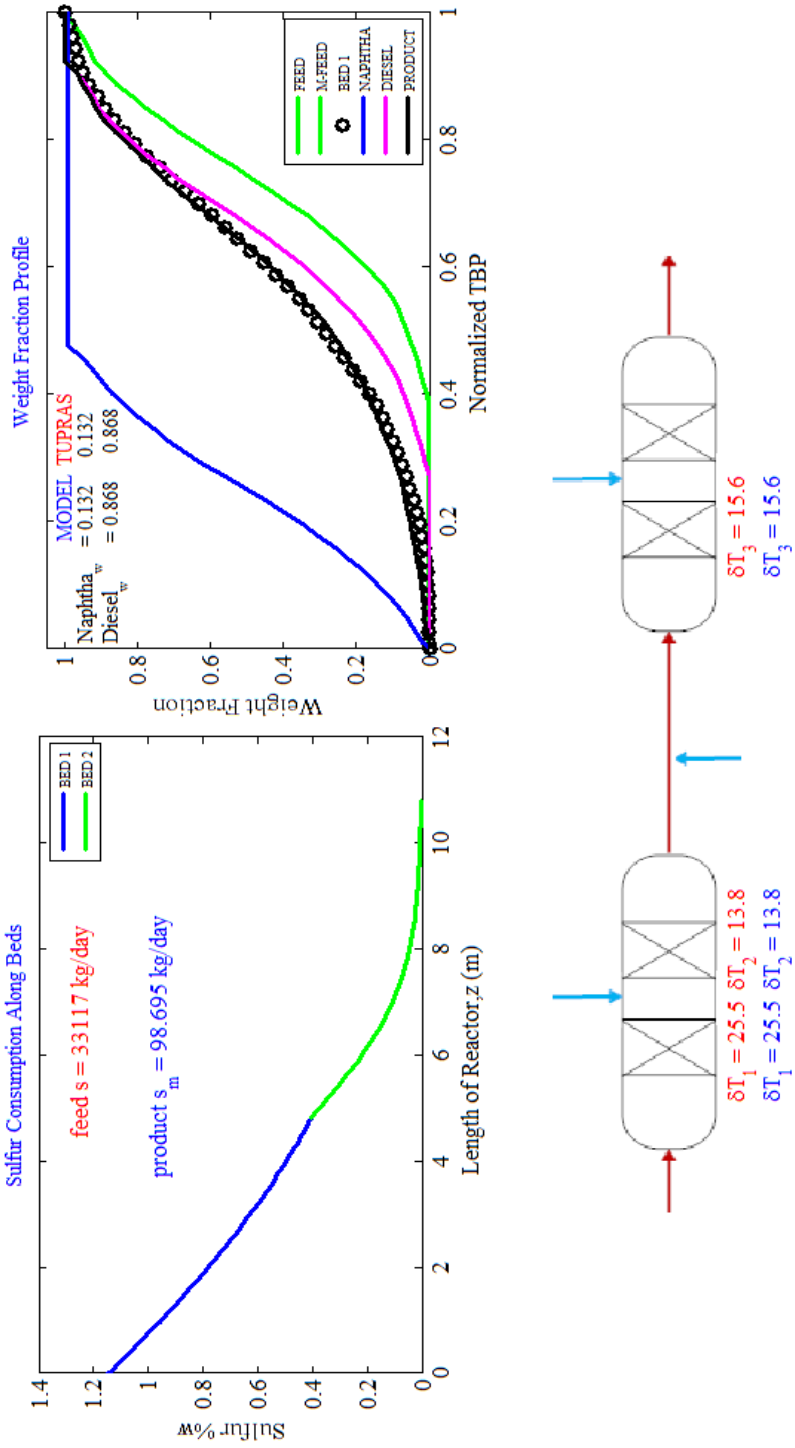

Figure 6.21: Overall performance of the HDS and HC models for shift 1 on 09.01.2014 after updating the parameters

5. The procedure is repeated starting from step 2 for the second shift of the corresponding day.

This procedure is applied to 18 shifts of plant and the values of the parameters are given in Table 6.11.

Table 6.11: Model Parameters for Selected Days

date &shift	$k_{min1,HDS}$	$k_{min2,HDS}$	$\Delta H_{2,HDS}$	$k_{max,HC}$
02.01.2014 00:00-08:00	0.06582	0.174986	-6747.46	0.103779
02.01.2014 08:00-16:00	0.06582	0.141111	-6747.46	0.103779
02.01.2014 16:00-24:00	0.054522	0.141111	-6227.88	0.117343
07.01.2014 00:00-08:00	0.068304	0.141111	-7230.74	0.105604
07.01.2014 08:00-16:00	0.068304	0.16985	-7230.74	0.105604
07.01.2014 16:00-24:00	0.068304	0.16985	-7230.74	0.105604
09.01.2014 00:00-08:00	0.099861	0.16985	-10290.6	0.112982
09.01.2014 08:00-16:00	0.099861	0.176354	-10290.6	0.112982
09.01.2014 16:00-24:00	0.099861	0.176354	-10290.6	0.096581
14.01.2014 00:00-08:00	0.099861	0.176354	-10290.6	0.11239
14.01.2014 08:00-16:00	0.099861	0.15384	-10290.6	0.11239
14.01.2014 16:00-24:00	0.109936	0.15384	-11645.9	0.100777
30.01.2014 00:00-08:00	0.07123	0.15384	-8107.61	0.08833
30.01.2014 08:00-16:00	0.07123	0.135438	-8107.61	0.08833
30.01.2014 16:00-24:00	0.083534	0.135438	-9102.14	0.08833
06.02.2014 00:00-08:00	0.057869	0.135438	-7768.29	0.09813
06.02.2014 08:00-16:00	0.057869	0.1411	-7768.29	0.09813
06.02.2014 16:00-24:00	0.068194	0.1411	-8277.46	0.093975

The changes in the model parameters are plotted to observe the trends of the changes.

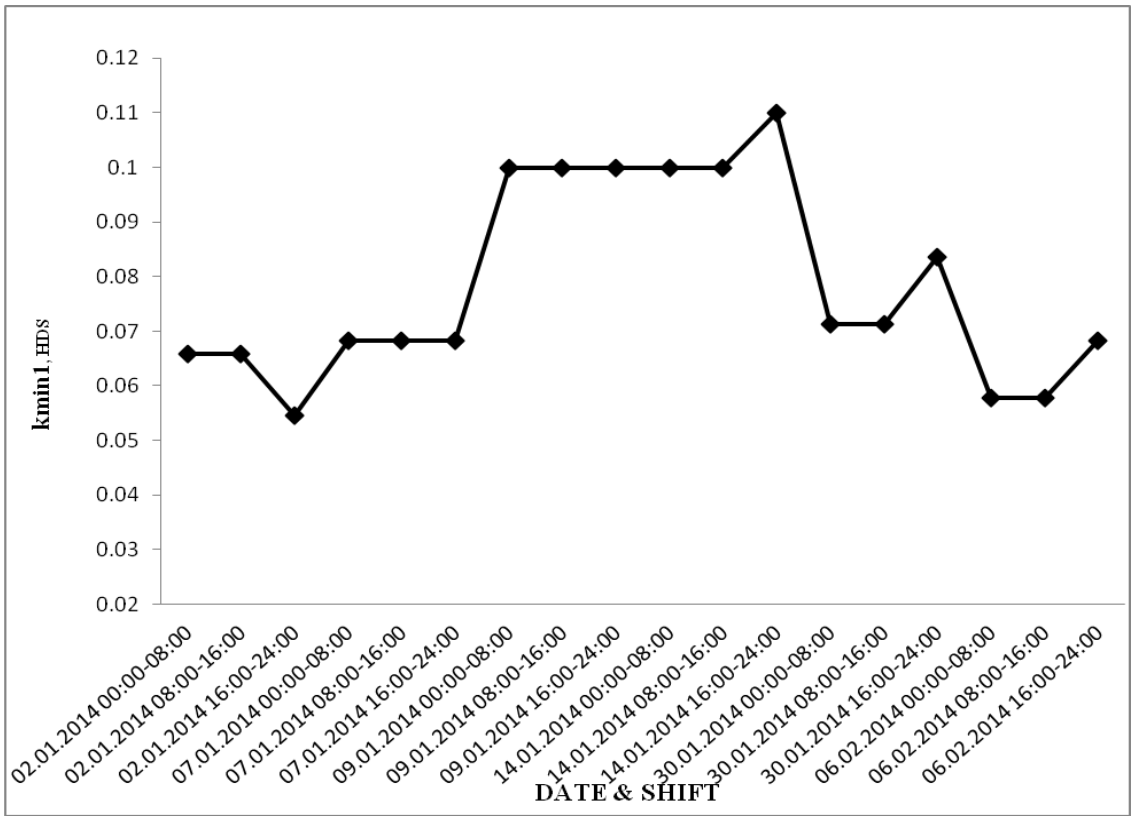

Figure 6.22: Change of $k_{min1,HDS}$ for a period of time

As the reactivity of the sulfur compounds decreases more sulfur is removed during HDS reactions. From Figure 6.22 and Table 6.11, it can be seen that the values of k_{min1} parameter are reasonable when compared with the literature (see Chapter 4).

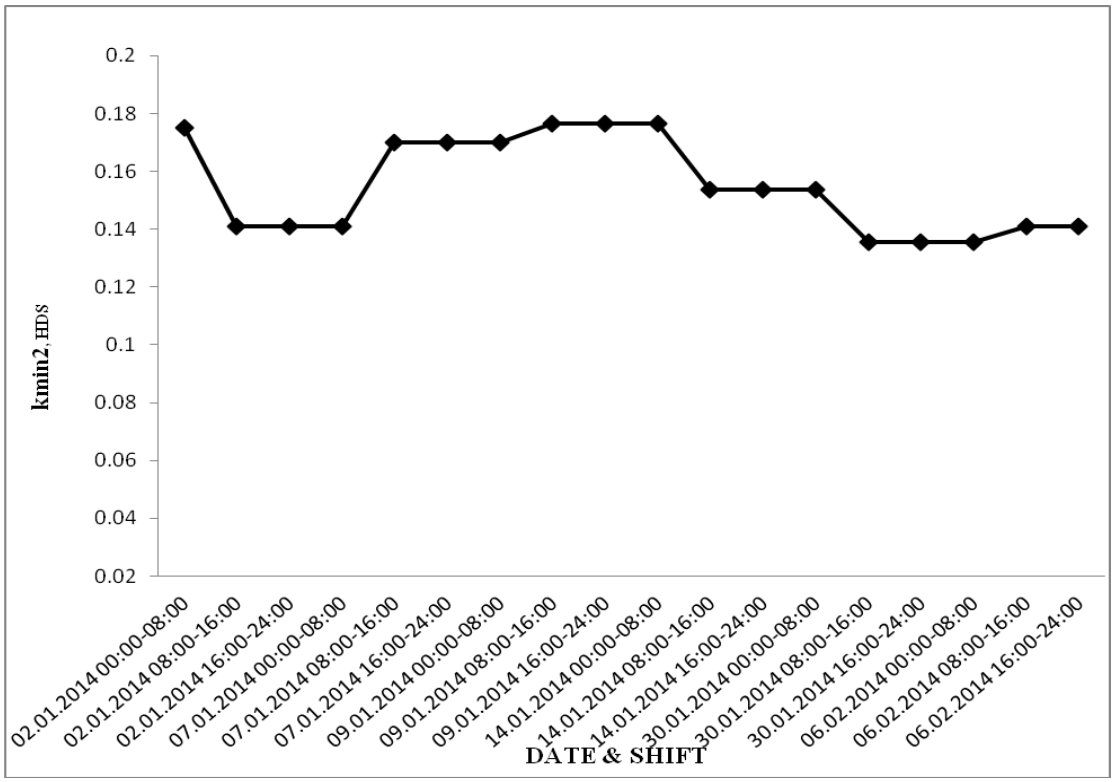

Figure 6.23: Change of $k_{min1,HDS}$ for a period of time

The HDS parameter k_{min2} estimated to match sulfur content of product data in plant and the values are in an acceptable range.

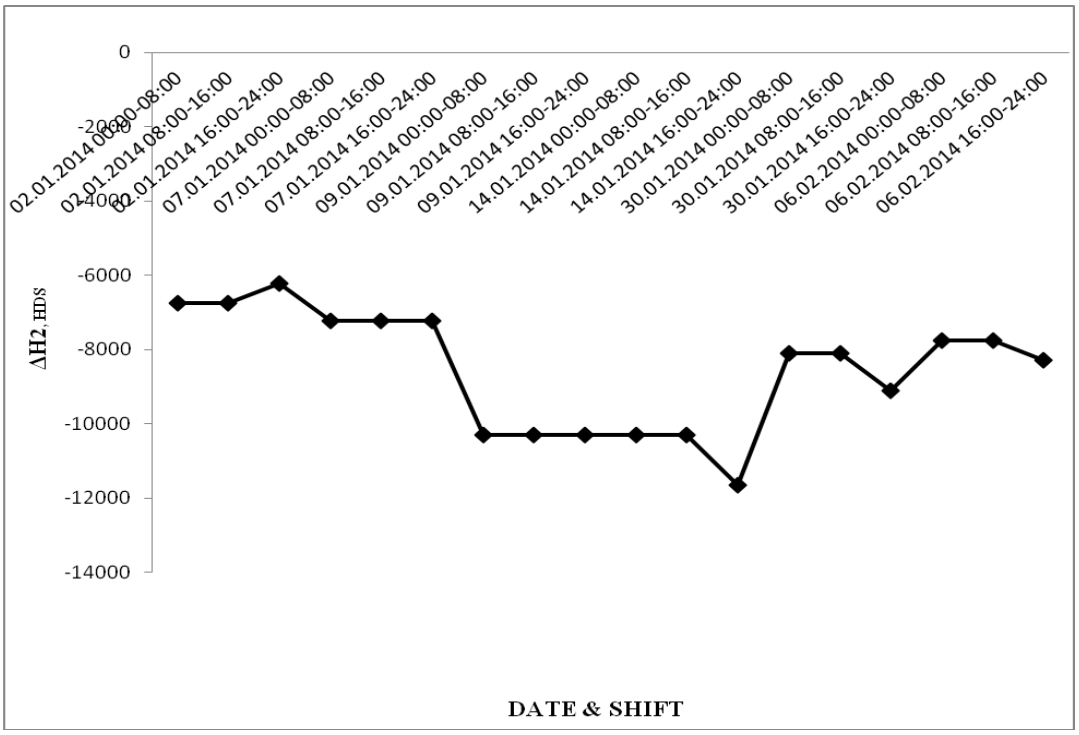

Figure 6.24: Change of $\Delta H_{2,HDS}$ for a period of time

As seen from Figure 6.24, the values of the heat of reaction in bed 2 of hydrodesulfurization reactor is reasonable when compared to literature values. As mentioned before, each sulfur compound has different heat of reaction value due to hydrogenation reaction chemistry and differs too much for different compounds.

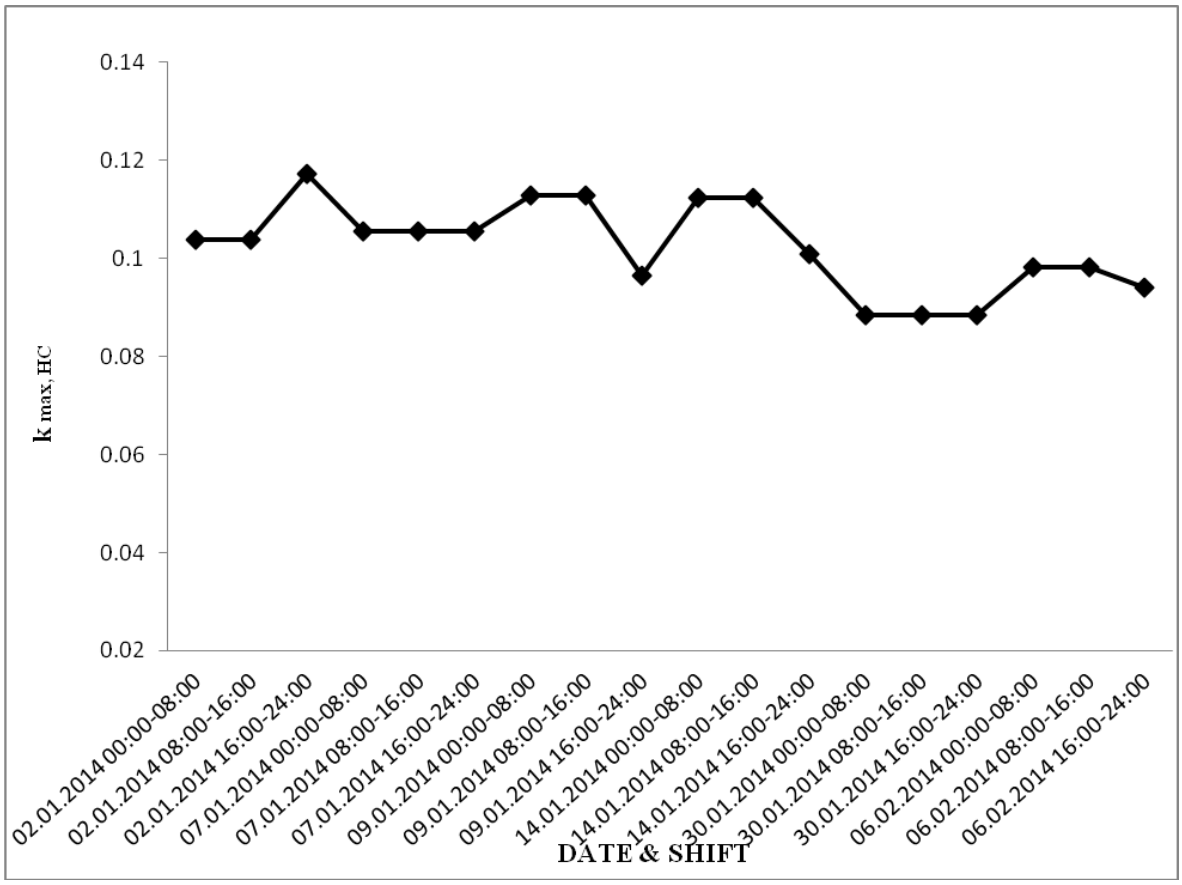

Figure 6.25: Change of $k_{max,HC}$ for a period of time

In the hydrocracker, only $k_{max,HC}$ is an adjustable parameter and the product weight fraction distribution of the products and the temperature difference in the reactor is estimated by adjusting $k_{max,HC}$ for different shifts and days as shown in Figure 6.25.

After estimation of the parameters and simulating the model with these parameters, the plant outputs and model results are compared to see if the parameters are adjusted enough or not. The errors are given in Table 6.12;

Table 6.12: Percent Errors of Prediction

		Products [% wt]		Bed Exit Temperatures [°C]		
	Sulfur [% wt]	Diesel	Naphtha	T_1	T_2	T_3
02.01.2014 00:00-08:00	-	0.59	4.2	0.00084	0.00022	0.009
02.01.2014 08:00-16:00	0.046	0.22	1.6	0.063	0.04	0.015
02.01.2014 16:00-24:00	-	1.5	10	0.0044	0.0018	0.032
07.01.2014 00:00-08:00	-	0.12	0.89	0.0006	0.00054	0.00082
07.01.2014 08:00-16:00	0.0012	0.085	0.64	0.04	0.013	0.027
07.01.2014 16:00-24:00	-	0.37	2.6	0.067	0.014	0.018
09.01.2014 00:00-08:00	-	0.075	0.49	0.0049	0.001	0.00047
09.01.2014 08:00-16:00	0.00068	0.2	1.3	0.038	0.017	0.0075
09.01.2014 16:00-24:00	-	1.8	13	0.087	0.0089	0.0029
14.01.2014 00:00-08:00	-	0.29	1.9	0.061	0.0022	0.0066
14.01.2014 08:00-16:00	0.0056	0.66	4.5	0.094	0.046	0.016
14.01.2014 16:00-24:00	-	1	7.3	6.8e-005	0.0024	0.014
30.01.2014 00:00-08:00	-	0.16	1.5	6.5e-006	0.025	0.0052
30.01.2014 08:00-16:00	0.002	0.23	2.2	0.023	0.054	0.0095
30.01.2014 16:00-24:00	-	0.32	2.9	0.0016	0.00039	0.078
06.02.2014 00:00-08:00	-	0.95	8.2	0.00035	0.0018	0.019
06.02.2014 08:00-16:00	0.011	0.12	0.95	0.11	0.031	0.026
06.02.2014 16:00-24:00	-	0.24	2	1.6e-005	0.0017	0.0054

After these comparisons, it is clear that the parameters are estimated to match the plant data reasonably since the errors are very small and it is shown that the model is able to

accurately predict temperature profiles in each bed, sulfur content of the product and the product distribution in hydrocracker.

Since the model parameters have physical meaning, some parameters are correlated with some feed properties. After many simulations, the mass flow rate of the sulfur in the feedstock is found to be correlated with some model parameters as in Table 6.13.

Table 6.13: Correlated Parameters with Sulfur Mass Flow Rate

date &shift	sulfur mass flow rate (kg/h)	$k_{min2,HDS}$	$\Delta H_{2,HDS}$
14.01.2014 00:00-08:00	1355.849716	0.176353648	-10290.59593
14.01.2014 08:00-16:00	1356.587345	0.15384	-10290.59593
14.01.2014 16:00-24:00	1359.25286	0.15384	-11645.86293
09.01.2014 16:00-24:00	1361.255779	0.176353648	-10290.59593
09.01.2014 08:00-16:00	1378.817224	0.176353648	-10290.59593
09.01.2014 00:00-08:00	1379.855434	0.16984972	-10290.59593
07.01.2014 16:00-24:00	1579.09504	0.16984972	-7230.739548
07.01.2014 00:00-08:00	1579.909278	0.141110574	-7230.739548
07.01.2014 08:00-16:00	1579.962372	0.16984972	-7230.739548
30.01.2014 16:00-24:00	1633.681539	0.135438066	-9102.140406
02.01.2014 16:00-24:00	1645.037415	0.141110574	-6227.878862
02.01.2014 00:00-08:00	1646.347006	0.17498624	-6747.458009
02.01.2014 08:00-16:00	1657.275887	0.141110574	-6747.458009
06.02.2014 08:00-16:00	1814.478408	0.1411	-7768.288314
06.02.2014 00:00-08:00	1817.840994	0.135438066	-7768.288314
06.02.2014 16:00-24:00	1836.627759	0.1411	-8277.458566
30.01.2014 00:00-08:00	1847.101892	0.15384	-8107.609324
30.01.2014 08:00-16:00	1849.38028	0.135438066	-8107.609324

The mass flow rates of sulfur in the feedstock and corresponding parameters are sorted from smallest to largest in Table 6.13 and the relationship between the mass flow rate of the sulfur in the feedstock and $k_{min1,HDS}$ is investigated like below;

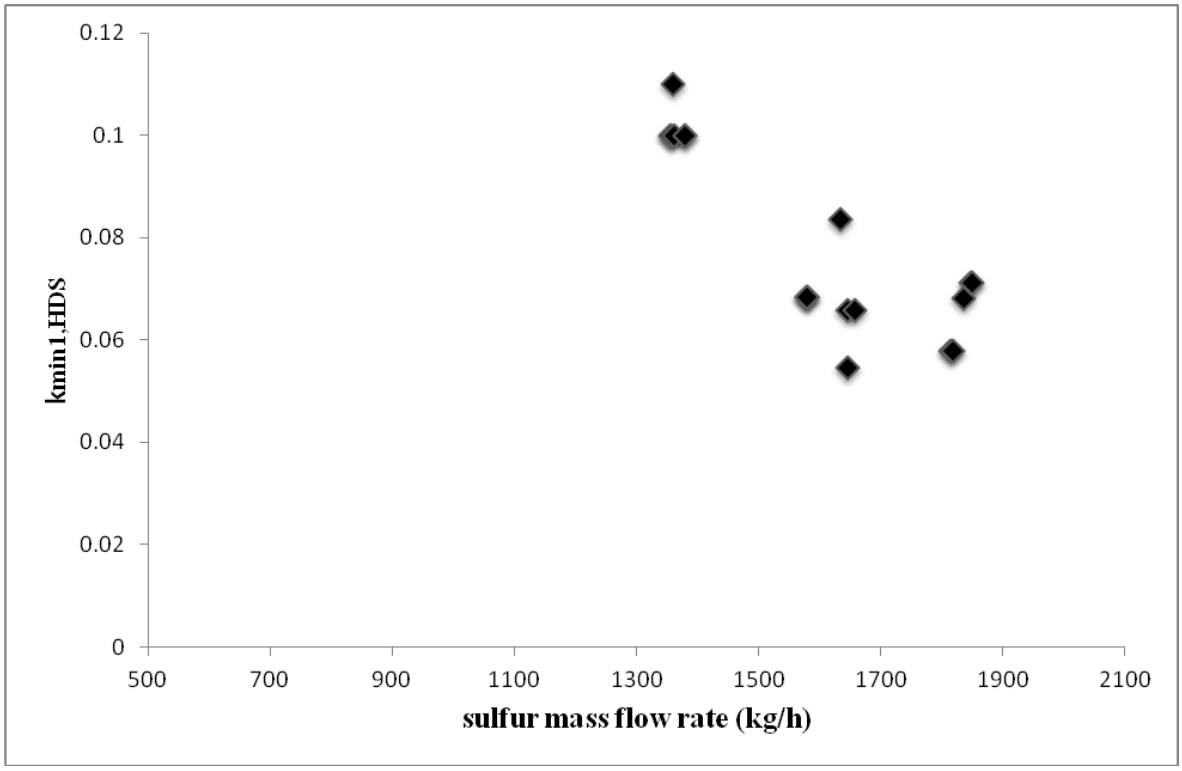

Figure 6.26: Relationship between mass flow rate of sulfur in feed and $k_{min1,HDS}$

As seen from Figure 6.26, the reactivity of the sulfur compounds decreases with increasing sulfur amount in the feed. When more sulfur compounds enter to the reactor, more sulfur is removed during the hydrodesulfurization reactions and more H_2S (hydrogen sulfide) is generated. It is known in the literature that hydrogen sulfide inhibits the hydrodesulfurization reactor. If more H_2S is generated during HDS reactions, these

conpounds inhibit the HDS reaction and reactivity in the reactor decreases. Although, the relationship looks linear, there is not exact correlation between mass flow rate of sulfur in feed and $k_{min1,HDS}$. Investigations on this subject continue. Similar trend is observed for another parameter, $\Delta H_{2,HDS}$ as seen in Figure 6.27 below:

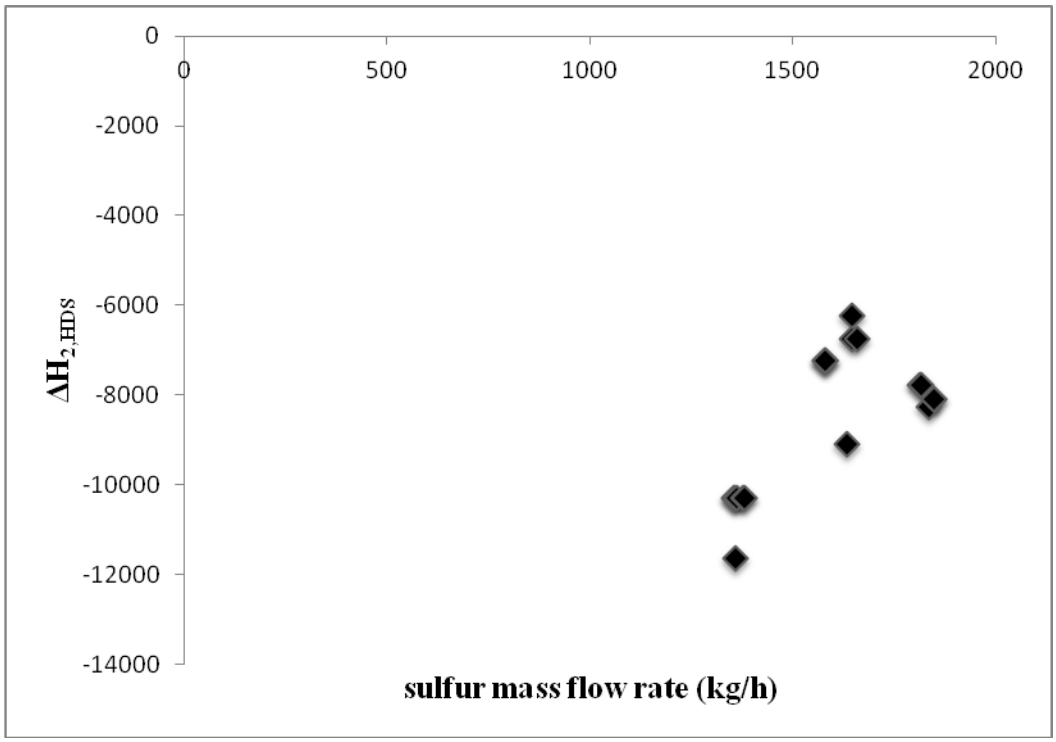

Figure 6.27: Relationship between mass flow rate of sulfur in feed and $\Delta H_{2,HDS}$

Chapter 7

CONCLUSION

This study develops a scheme for pseudo-homogeneous plug flow model to represent the behavior of catalytic hydrodesulfurization and hydrocracking of blended diesel mixture under steady-state non-isothermal conditions.

Since the diesel mixture is a complex mixture due to huge number of hydrocarbons in addition to impurities such as sulfur, continuous lumping technique was employed to treat the diesel mixture as continuum. HDS reactions were described by a continuous model with three adjustable parameters and hydrocracking reactions were described by a continuous model with one adjustable parameter. HDS and HC models were united to construct a model for kinetic analysis of both hydrodesulfurization and hydrocracking reactions. The model consists of a set of integro-differential mass balance and energy balance equations which were to be solved simultaneously and all routines were written in MATLAB software.

The model parameters were estimated by minimizing the sum of the squared errors (SSE) between the plant and model data to find the best kinetic models. The parameters were updated for new data sets online. The feed to the reactors was characterized by some correlations in the literature and the plant product boiling point curve was built in ASPEN HYSYS Oil Manager.

After the simulations, it was shown that the model predictions for temperature profiles in each bed, sulfur weight fraction in the product and the product distribution in

hydrocracker agreed well with the plant data. For the real-time application of the model, a user-friendly interface was developed to evaluate the performance of the reactors used for diesel hydroprocessing.

BIBLIOGRAPHY

1. Chandra Srivastava, V., An evaluation of desulfurization technologies for sulfur removal from liquid fuels. RSC Advances, 2012. 2(3): p. 759-783.
2. Egorova, M., Study of aspects of deep hydrodesulfurization by means of model reactions. 2003.
3. Schmitz, C., L. Datsevitch, and A. Jess, Deep desulfurization of diesel oil: kinetic studies and process-improvement by the use of a two-phase reactor with pre-saturator. Chemical Engineering Science, 2004. 59(14): p. 2821-2829.
4. Rana, M.S., et al., A review of recent advances on process technologies for upgrading of heavy oils and residua. Fuel, 2007. 86(9): p. 1216-1231.
5. Jarullah, A.T., Kinetic modelling simulation and optimal operation of trickle bed reactor for hydrotreating of crude oil: kinetic parameters estimation of hydrotreating reactions in trickle. 2011.
6. Moqadam, S.I. and M. Mahmoudi, Advent of Nanocatalysts in Hydrotreating Process: Benefits and Developements. American Journal of Oil and Chemical Technologies, 2013. 01(02): p. 13-21.
7. Gary, J.H., G.E. Handwerk, and M.J. Kaiser, Petroleum Refining: Technology and Economics. 2007: CRC PressINC.
8. Gruia, A., Hydrotreating, in Handbook of Petroleum Processing, D.J.S. Jones and P. Pujadó, Editors. 2006, Springer Netherlands. p. 321-354.
9. Stanislaus, A., A. Marafi, and M.S. Rana, Recent advances in the science and technology of ultra low sulfur diesel (ULSD) production. Catalysis Today, 2010. 153(1–2): p. 1-68.
10. Gary, J.H. and G.E. Handwerk, Petroleum Refining: Technology and Economics. 1994: M. Dekker.

11. Ancheyta, J., Modeling and Simulation of Catalytic Reactors for Petroleum Refining. 2011: Wiley.
12. Ancheyta, J. and J.G. Speight, Hydroprocessing of Heavy Oils and Residua. 2007: Taylor & Francis.
13. Chung, S.H.K., Thermal Hydroprocessing of Heavy Gas Oils. 2009: Harvard University.
14. Hobson, G.D. and I.o. Petroleum, Modern petroleum technology. 1984: Wiley.
15. Speight, J.G., The Desulfurization of Heavy Oils and Residua. 2000: M. Dekker.
16. Castaneda-Lopez, L.C., T. A, and M. University, Kinetic Modeling of the Hydrotreatment of Light Cycle Oil/diesel. 2006: Texas A&M University.
17. Topsøe, H., B. Clausen, and F. Massoth, Hydrotreating Catalysis, in Catalysis, J. Anderson and M. Boudart, Editors. 1996, Springer Berlin Heidelberg. p. 1-269.
18. Boelhouwer, J.G., Nonsteady Operation of Trickle-bed Reactors: Hydrodynamics, Mass and Heat Transfer. 2001: Technische Universiteit Eindhoven.
19. Mederos, F.S., I. Elizalde, and J. Ancheyta, Steady-State and Dynamic Reactor Models for Hydrotreatment of Oil Fractions: A Review. Catalysis Reviews, 2009. 51(4): p. 485-607.
20. Bhutani, N., A.K. Ray, and G.P. Rangaiah, Modeling, Simulation, and Multi-objective Optimization of an Industrial Hydrocracking Unit. Industrial & Engineering Chemistry Research, 2006. 45(4): p. 1354-1372.
21. Medde, M., Experimental Analysis and Modelling of Gasoil Hydrotreatment Process. 2008, University of Cagliari.
22. Knudsen, K.G., B.H. Cooper, and H. Topsøe, Catalyst and process technologies for ultra low sulfur diesel. Applied Catalysis A: General, 1999. 189(2): p. 205-215.

23. Mochida, I. and K.-H. Choi, An Overview of Hydrodesulfurization and Hydrodenitrogenation. Journal of The Japan Petroleum Institute, 2004. 47(3): p. 145-163.
24. Girgis, M.J. and B.C. Gates, Reactivities, reaction networks, and kinetics in high-pressure catalytic hydroprocessing. Industrial & Engineering Chemistry Research, 1991. 30(9): p. 2021-2058.
25. Sadighi, S., A. Ahmad, and M. Rashidzadeh, 4-Lump kinetic model for vacuum gas oil hydrocracker involving hydrogen consumption. Korean Journal of Chemical Engineering, 2010. 27(4): p. 1099-1108.
26. Jarullah, A.T., I.M. Mujtaba, and A.S. Wood, Kinetic parameter estimation and simulation of trickle-bed reactor for hydrodesulfurization of crude oil. Chemical Engineering Science, 2011. 66(5): p. 859-871.
27. Elizalde, I. and J. Ancheyta, Modeling the Simultaneous Hydrodesulfurization and Hydrocracking of Heavy Residue Oil by using the Continuous Kinetic Lumping Approach. Energy & Fuels, 2012. 26(4): p. 1999-2004.
28. Kuo, J.C.W. and J. Wei, Lumping Analysis in Monomolecular Reaction Systems. Analysis of Approximately Lumpable System. Industrial & Engineering Chemistry Fundamentals, 1969. 8(1): p. 124-133.
29. Basak, K., et al., Industrial hydrocracker model based on novel continuum lumping approach for optimization in petroleum refinery. Catalysis Today, 2004. 98(1–2): p. 253-264.
30. Weekman, V.W. and D.M. Nace, Kinetics of catalytic cracking selectivity in fixed, moving, and fluid bed reactors. AIChE Journal, 1970. 16(3): p. 397-404.
31. Elizalde, I., M.A. Rodríguez, and J. Ancheyta, Application of continuous kinetic lumping modeling to moderate hydrocracking of heavy oil. Applied Catalysis A: General, 2009. 365(2): p. 237-242.

32. Aris, R., Prolegomena to the rational analysis of systems of chemical reactions II. Some addenda. Archive for Rational Mechanics and Analysis, 1968. 27(5): p. 356-364.
33. Aris, R., Reactions in continuous mixtures. AIChE Journal, 1989. 35(4): p. 539-548.
34. Astarita, G., Lumping nonlinear kinetics: Apparent overall order of reaction. AIChE Journal, 1989. 35(4): p. 529-532.
35. Astarita, G. and A. Nigam, Lumping nonlinear kinetics in a CSTR. AIChE Journal, 1989. 35(12): p. 1927-1932.
36. Astarita, G. and R. Ocone, Lumping nonlinear kinetics. AIChE Journal, 1988. 34(8): p. 1299-1309.
37. Chou, M.Y. and T.C. Ho, Continuum theory for lumping nonlinear reactions. AIChE Journal, 1988. 34(9): p. 1519-1527.
38. Ho, T.C., B.S. White, and R. Hu, Lumped kinetics of many parallel nth-order reactions. AIChE Journal, 1990. 36(5): p. 685-700.
39. Ho, T.C., Aggregate behavior and lumped kinetics of many reactions in backmixed and plug-flow reactors. AIChE Journal, 1996. 42(1): p. 214-231.
40. Ho, T.C., Hydroprocessing kinetics for oil fractions, in Studies in Surface Science and Catalysis, G.F.F. B. Delmon and P. Grange, Editors. 1999, Elsevier. p. 179-186.
41. Ho, T.C. and R. Aris, On apparent second-order kinetics. AIChE Journal, 1987. 33(6): p. 1050-1051.
42. Laxminarasimhan, C.S., R.P. Verma, and P.A. Ramachandran, Continuous lumping model for simulation of hydrocracking. AIChE Journal, 1996. 42(9): p. 2645-2653.
43. Prasad, G.N., J.B. Agnew, and T. Sridhar, Modeling of coal liquefaction kinetics based on reactions in continuous mixtures. Part II: Comparison with experiments on

catalyzed and uncatalyzed liquefaction of coals of different rank. AIChE Journal, 1986. 32(8): p. 1288-1300.

44. Quann, R.J. and S.B. Jaffe, Structure-oriented lumping: describing the chemistry of complex hydrocarbon mixtures. Industrial & Engineering Chemistry Research, 1992. 31(11): p. 2483-2497.
45. Froment, G.F., Single Event Kinetic Modeling of Complex Catalytic Processes. Catalysis Reviews, 2005. 47(1): p. 83-124.
46. Chowdhury, R., E. Pedernera, and R. Reimert, Trickle-bed reactor model for desulfurization and dearomatization of diesel. AIChE Journal, 2002. 48(1): p. 126-135.
47. Froment, G.F., G.A. Depauw, and V. Vanrysselberghe, Kinetic Modeling and Reactor Simulation in Hydrodesulfurization of Oil Fractions. Industrial & Engineering Chemistry Research, 1994. 33(12): p. 2975-2988.
48. Korsten, H. and U. Hoffmann, Three-phase reactor model for hydrotreating in pilot trickle-bed reactors. AIChE Journal, 1996. 42(5): p. 1350-1360.
49. Sau, M., C.S.L. Narasimhan, and R.P. Verma, A Kinetic model for hydrodesulfurisation, in Studies in Surface Science and Catalysis, B.D. G.F. Froment and P. Grange, Editors. 1997, Elsevier. p. 421-435.
50. Tsamatsoulis, D. and N. Papayannakos, Investigation of intrinsic hydrodesulphurization kinetics of a VGO in a trickle bed reactor with backmixing effects. Chemical Engineering Science, 1998. 53(19): p. 3449-3458.
51. van Hasselt, B.W., et al., A numerical comparison of alternative three-phase reactors with a conventional trickle-bed reactor. The advantages of countercurrent flow for hydrodesulfurization. Chemical Engineering Science, 1999. 54(21): p. 4791-4799.

52. Cotta, R.M., M.R. Wolf-Maciel, and R.M. Filho, A cape of HDT industrial reactor for middle distillates. Computers & Chemical Engineering, 2000. 24(2–7): p. 1731-1735.
53. Matos, E.M. and R. Guirardello, Modeling and simulation of hydrodemetallation and hydrodesulfurization processes with transient catalytic efficiency. Brazilian Journal of Chemical Engineering, 2000. 17: p. 171-179.
54. Kumar, V.R., et al., PERFORMANCE STUDY OF CERTAIN COMMERCIAL CATALYSTS IN HYDRODESULFURIZATION OF DIESEL OILS. Petroleum Science and Technology, 2001. 19(9-10): p. 1029-1038.
55. Bhaskar, M., et al., APPLICATION OF A THREE PHASE HETEROGENEOUS MODEL TO ANALYSE THE PERFORMANCE OF A PILOT PLANT TRICKLE BED REACTOR. Petroleum Science and Technology, 2002. 20(3-4): p. 251-268.
56. Avraam, D.G. and I.A. Vasalos, HdPro: a mathematical model of trickle-bed reactors for the catalytic hydroprocessing of oil feedstocks. Catalysis Today, 2003. 79–80(0): p. 275-283.
57. Pedernera, E., et al., Deep desulfurization of middle distillates: process adaptation to oil fractions' compositions. Catalysis Today, 2003. 79–80(0): p. 371-381.
58. Bhaskar, M., et al., Three-Phase Reactor Model to Simulate the Performance of Pilot-Plant and Industrial Trickle-Bed Reactors Sustaining Hydrotreating Reactions. Industrial & Engineering Chemistry Research, 2004. 43(21): p. 6654-6669.
59. Rodríguez, M.A. and J. Ancheyta, Modeling of Hydrodesulfurization (HDS), Hydrodenitrogenation (HDN), and the Hydrogenation of Aromatics (HDA) in a Vacuum Gas Oil Hydrotreater. Energy & Fuels, 2004. 18(3): p. 789-794.
60. Yamada, H. and S. Goto, Advantages of counter-current operation for hydrodesulfurization in trickle bed reactors. Korean Journal of Chemical Engineering, 2004. 21(4): p. 773-776.

61. Jiménez, F., M. Núñez, and V. Kafarov, Study and modeling of simultaneous hydrodesulfurization, hydrodenitrogenation and hydrodearomatization on vacuum gas oil hydrotreatment, in Computer Aided Chemical Engineering, P. Luis and E. Antonio, Editors. 2005, Elsevier. p. 619-624.
62. Sertić-Bionda, K., Z. Gomzi, and T. Šarić, Testing of hydrodesulfurization process in small trickle-bed reactor. Chemical Engineering Journal, 2005. 106(2): p. 105-110.
63. Trejo, F. and J. Ancheyta, Kinetics of asphaltenes conversion during hydrotreating of Maya crude. Catalysis Today, 2005. 109(1–4): p. 99-103.
64. Botchwey, C., A.K. Dalai, and J. Adjaye, Simulation of a two-stage micro trickle-bed hydrotreating reactor using Athabasca bitumen-derived heavy gas oil over commercial Ni Mo/Al2O3 catalyst : effect of H2S on hydrodesulfurization and hydrodenitrogenation. 2006. 4(A20).
65. Mederos, F.S., et al., Dynamic Modeling and Simulation of Catalytic Hydrotreating Reactors. Energy & Fuels, 2006. 20(3): p. 936-945.
66. Jiménez, F., V. Kafarov, and M. Nuñez, Modeling of industrial reactor for hydrotreating of vacuum gas oils: Simultaneous hydrodesulfurization, hydrodenitrogenation and hydrodearomatization reactions. Chemical Engineering Journal, 2007. 134(1–3): p. 200-208.
67. Mederos, F.S. and J. Ancheyta, Mathematical modeling and simulation of hydrotreating reactors: Cocurrent versus countercurrent operations. Applied Catalysis A: General, 2007. 332(1): p. 8-21.
68. Shokri, S. and M.A. Marvast, PRODUCTION OF ULTRA LOW SULFUR DIESEL : Saeid Shokri *, Mahdi Ahmadi Marvast , MortezaTajerian. 2007.

69. Vanrysselberghe, V. and G.F. Froment, Hydrodesulfurization of Dibenzothiophene on a CoMo/Al2O3 Catalyst: Reaction Network and Kinetics. Industrial & Engineering Chemistry Research, 1996. 35(10): p. 3311-3318.
70. Alvarez, A. and J. Ancheyta, Modeling residue hydroprocessing in a multi-fixed-bed reactor system. Applied Catalysis A: General, 2008. 351(2): p. 148-158.
71. Alvarez, A. and J. Ancheyta, Simulation and analysis of different quenching alternatives for an industrial vacuum gasoil hydrotreater. Chemical Engineering Science, 2008. 63(3): p. 662-673.
72. Bahzad, D. and E. Kam, Atmospheric Residues of Kuwait Heavy Crude Upgrading: A Pilot Plant and Model Simulation Study. Energy & Fuels, 2009. 23(3): p. 1683-1694.
73. Chen, J., V. Mulgundmath, and N. Wang, Accounting for Vapor−Liquid Equilibrium in the Modeling and Simulation of a Commercial Hydrotreating Reactor. Industrial & Engineering Chemistry Research, 2010. 50(3): p. 1571-1579.
74. Farahani, H.F.a.S.S., Simulation of Hydrodesulfurization Trickle Bed Reactor. Chemical Product and Process Modeling, 2011 6(1): p. 1.
75. Qader, S.A. and G.R. Hill, Hydrocracking of Gas Oil. Industrial & Engineering Chemistry Process Design and Development, 1969. 8(1): p. 98-105.
76. Liguras, D.K. and D.T. Allen, Structural models for catalytic cracking. 1. Model compound reactions. Industrial & Engineering Chemistry Research, 1989. 28(6): p. 665-673.
77. Stangeland, B.E., A Kinetic Model for the Prediction of Hydrocracker Yields. Industrial & Engineering Chemistry Process Design and Development, 1974. 13(1): p. 71-76.
78. Mosby, J.F., et al., Process characterization of expanded-bed reactors in series. Chemical Engineering Science, 1986. 41(4): p. 989-995.

79. Krishna, R. and A.K. Saxena, Use of an axial-dispersion model for kinetic description of hydrocracking. Chemical Engineering Science, 1989. 44(3): p. 703-712.
80. Yui, S.M. and E.C. Sanford, Mild hydrocracking of bitumen-derived coker and hydrocracker heavy gas oils: kinetics, product yields, and product properties. Industrial & Engineering Chemistry Research, 1989. 28(9): p. 1278-1284.
81. Mohanty, S., D.N. Saraf, and D. Kunzru, Modeling of a hydrocracking reactor. Fuel Processing Technology, 1991. 29(1–2): p. 1-17.
82. Callejas, M.A. and M.T. Martínez, Hydrocracking of a Maya Residue. Kinetics and Product Yield Distributions. Industrial & Engineering Chemistry Research, 1999. 38(9): p. 3285-3289.
83. Martens, G.G. and G.B. Marin, Kinetics for hydrocracking based on structural classes: Model development and application. AIChE Journal, 2001. 47(7): p. 1607-1622.
84. Aoyagi, K., W.C. McCaffrey, and M.R. Gray, Kinetics of Hydrocracking and Hydrotreating of Coker and Oilsands Gas Oils. Petroleum Science and Technology, 2003. 21(5-6): p. 997-1015.
85. Sánchez, S., M.A. Rodríguez, and J. Ancheyta, Kinetic Model for Moderate Hydrocracking of Heavy Oils. Industrial & Engineering Chemistry Research, 2005. 44(25): p. 9409-9413.
86. Khorasheh, F., E.C. Chan, and M.R. Gray, Development of a continuous kinetic model for catalytic hydrodesulfurization of bitumen. Petroleum and Coal, 2005.
87. Ashuri, E., F. Khorasheh, and M. Gray, Development of a continuous kinetic model for catalytic hydrodenitrogenation of bitumen. Scientia Iranica, 2007. 14(2): p. 152-160.

88. Sanchez, S. and J. Ancheyta, Effect of Pressure on the Kinetics of Moderate Hydrocracking of Maya Crude Oil. Energy Fuels, 2007. 21(2): p. 653-661.
89. Govindhakannan, J. and J.B. Riggs, On the Construction of a Continuous Concentration−Reactivity Function for the Continuum Lumping Approach. Industrial & Engineering Chemistry Research, 2007. 46(5): p. 1653-1656.
90. Sadighi, S., Ahmad, A. and Irandoukht, A., Kinetic Study on a Commercial Amorphous Hydrocracking Catalyst by Weighted Lumping Strategy. International Journal of Chemical Reactor Engineering 2010. 8(1): p. 1.
91. Sildir, H., et al., A dynamic non-isothermal model for a hydrocracking reactor: Model development by the method of continuous lumping and application to an industrial unit. Journal of Process Control, 2012. 22(10): p. 1956-1965.
92. Chang, A.F., K. Pashikanti, and Y.A. Liu, Refinery Engineering: Integrated Process Modeling and Optimization. 2012: Wiley.
93. Daubert, T.E.D., R. P., API Technical Data Book: Petroleum Refining. 1997, Washington D. C.: American Petroleum Institute.
94. Daubert, T.E., Petroleum Fractions Distillation Interconversion. Hydrocarbon Processing, 1994. 73(9): p. 75-78.
95. Fahim, M.A., T.A. Al-Sahhaf, and A. Elkilani, Fundamentals of Petroleum Refining. 2009: Elsevier Science.
96. De Hemptinne, J.C., J.M. Ledanois, and P. Mougin, Select Thermodynamic Models for Process Simulation: A Practical Guide Using a Three Steps Methodology. 2012: Editions Technip.
97. Song, C., An overview of new approaches to deep desulfurization for ultra-clean gasoline, diesel fuel and jet fuel. Catalysis Today, 2003. 86(1–4): p. 211-263.
98. Natrella, M., NIST/SEMATECH e-Handbook of Statistical Methods, ed. C. Croarkin, et al. 2010: NIST/SEMATECH.

99. Ma, X., et al., Hydrodesulfurization Reactivities of Narrow-Cut Fractions in a Gas Oil. Industrial & Engineering Chemistry Research, 1995. 34(3): p. 748-754.
100. Stratiev, D., et al. Hydrotreating units chemical hydrogen consumption analysis a tool for improving refinery hydrogen management. in 44th International Petroleum Conference. 2009.
101. Beck, J.V. and K.J. Arnold, Parameter estimation in engineering and science. 1977: Wiley.
102. Boukamp, B.A., A Nonlinear Least Squares Fit procedure for analysis of immittance data of electrochemical systems. Solid State Ionics, 1986. 20(1): p. 31-44.
103. Ioslovich, I., P.-O. Gutman, and I. Seginer, Dominant parameter selection in the marginally identifiable case. Mathematics and Computers in Simulation, 2004. 65(1–2): p. 127-136.
104. Hamby, D.M., A review of techniques for parameter sensitivity analysis of environmental models. Environmental Monitoring and Assessment, 1994. 32(2): p. 135-154.
105. Machado, V.C., et al., Systematic identifiability study based on the Fisher Information Matrix for reducing the number of parameters calibration of an activated sludge model. Environ. Model. Softw., 2009. 24(11): p. 1274-1284.
106. Ma, C.G. and H.X. Weng, A Study on the Lumping Kinetic Model for a Residual Oil Hydrodesulfurization Process. Energy Sources, Part A: Recovery, Utilization, and Environmental Effects, 2012. 34(21): p. 1933-1942.
107. Reséndiz, E., et al., Estimation of activation energies during hydrodesulfurization of middle distillates. Fuel, 2007. 86(9): p. 1247-1253.

108. Ueda, S., et al., The Heat of Hydrodesulfurization Reaction of Heavy Oil. Industrial & Engineering Chemistry Process Design and Development, 1975. 14(4): p. 493-499.

109. Ali, S.A., Thermodynamic Aspects of Hydrodesulfurization and Hydrodenitrogenation. Petroleum Science and Technology, 2007. 25(7): p. 841-852.

110. Vrinat, M.L., The kinetics of the hydrodesulfurization process - a review. Applied Catalysis, 1983. 6(2): p. 137-158.

111. Lababidi, H.M.S. and F.S. AlHumaidan, Modeling the Hydrocracking Kinetics of Atmospheric Residue in Hydrotreating Processes by the Continuous Lumping Approach. Energy & Fuels, 2011. 25(5): p. 1939-1949.

112. Li, W., C.-W. Hui, and A. Li, Integrating CDU, FCC and product blending models into refinery planning. Computers & Chemical Engineering, 2005. 29(9): p. 2010-2028.

113. Martinez-Grimaldo, H.J., et al., Prediction of Sulfur Content, API Gravity, and Viscosity Using a Continuous Mixture Kinetic Model for Maya Crude Oil Hydrocracking in a Slurry-Phase Reactor. Energy & Fuels, 2011. 25(8): p. 3605-3614.

114. Ancheyta, J., S. Sánchez, and M.A. Rodríguez, Kinetic modeling of hydrocracking of heavy oil fractions: A review. Catalysis Today, 2005. 109(1–4): p. 76-92.